Efficient option pricing for Rough Bergomi model

1 Introduction

1.1 The goal and outline of the project

The main goal of the project is to design a fast option pricer, based on multi-index stochastic collocation (MISC) as [18], for options whose dynamics follow rBergomi model as in [2]. We may later investigate QMC.

1.2 Review of literature

Extending the Black-Scholes model, in which volatility is assumed to be constant, to the case where the volatility is stochastic has proved to be successful in explaining certain phenomena observed in option price data, in particular the implied volatility smile. The main drawback of such stochastic volatility models, however, is that they are unable to capture the true steepness of the implied volatility smile close to maturity. While choosing to add jumps to stock price models, for example modelling the stock price process as an exponential Lévy process, does indeed produce steeper implied volatility smiles, the issue of the presence of jumps in stock price processes remains controversial[1, 10].

As an alternative to diffusive stochastic volatility models, rough stochastic volatility has emerged as a new paradigm in quantitative finance, motivated by the statistical analysis of realised volatility by Gatheral, Jaisson and Rosenbaum [16] and the theoretical results on implied volatility by Fukasawa [13]. In these models, the trajectories of volatility are less regular than those of the standard Brownian motion. As shown in [16, 2], these models are a family of (continuous-path) stochastic volatility models where the driving noise of the volatility process has Hölder regularity lower than Brownian motion, typically achieved by modeling the fundamental noise innovations of the volatility process as a fractional Brownian motion with Hurst exponent (and hence Hölder regularity)$0 < H < 1/2$. A major advantage of such rough volatility models is the fact that they allow to explain crucial phenomena observed in financial markets both from a statistical [16, 5] and an option-pricing point of view [2]. For instance, it was observed empirically that in equity markets that as time to maturity becomes small the empirical implied volatility skew follows a power law with negative exponent, and thus becomes arbitrarily large near zero. While standard stochastic volatility models with continuous paths struggle to capture this phenomenon, predicting instead a constant at-the-money implied volatility behaviour on he short end [14], fractional stochastic volatility models (and more specifically so-called rough volatility models) constitute alternative models that fit empirical implied volatilities for short dated options. Consequently, they have become the go-to models capable of reproducing stylised facts of financial markets.

Rough volatility models are based on fractional Brownian motion (fBM), which is a centred Gaussian process, whose covariance structure depends on the Hurst parameter $H \in (0,1)$. If $H \in (0,1/2)$, then the fractional Brownian motion has negatively correlated increments and "rough" sample paths, and if $H \in (1/2,1)$ then it has positively correlated increments and "smooth" sample paths, when compared with a standard Brownian motion, which is recovered by taking $H = 1/2$. Gatheral, Jaisson, and Rosenbaum [16] justify empirically the benefits of such models; in particular, they argue that log-volatility in practice behaves essentially as fBM with the Hurst exponent $H \approx 0.1$ at any reasonable time scale (see also [15]). This finding is confirmed by Bennedsen, Lunde and Pakkanen [5], who study over a thousand individual US equities and find that the Hurst parameter H lies in $(0,1/2)$ for each equity.

The rough Bergomi (rBergomi) model is one of the recent rough volatility models, developed by Bayer, Friz and Gatheral [2], that is consistent with the stylised fact of implied volatility surfaces being essentially time-invariant, and are able to capture the term structure of skew observed in equity markets. In [2], the authors constructed the rBergomi model by moving from physical to pricing measure and simulated prices under that model to fit well the implied volatility surface in the case of the S&P 500 index with few parameters-just three!. They claim that the fractional model generates strong skews or "smiles" in the implied volatility even for very short time to maturity so that this modeling provides an alternative to using jumps to model such an effect. In [2] the model is so named because of its relationship with the Bergomi variance curve model [7], and may be seen as a non-Markovian generalisation of the latter.

Due to the non-Markovian nature of the fractional driver, pricing and hedging under rough volatility constitute a significant challenge. In fact, the popularity of asset pricing models hinges on the availability of efficient numerical pricing methods. In the case of diffusions, these include Monte Carlo (MC) estimators, PDE discretization schemes, asymptotic expansions and transform methods. With fractional Brownian motion being the prime example of a process beyond the semi-martingale framework, most currently prevalent option pricing methods -particularly the ones assuming semimartingality or Markovianity - may not easily carry over to the rough setting. In fact, due to the lack of Markovianity or affine structure, conventional analytical pricing methods do not apply. At the moment, the only known method for pricing options under such models is MC simulation. In particular, recent advances in simulation methods for the rough Bergomi model have been achieved in [2, 3, 23, 6, 19]. For isntance, in [23], the authors employ a novel composition of variance reduction methods, immediately applicable to any conditionally log-normal stochastic volatility model. They got a substatantial computation gain in the pricing over the exisiting MC methods. On the other hand, more analytical results of option pricing and implied volatility under this model has been done in [20, 4, 12]. For isntance, in [20], they characterise the small-time behaviour of implied volatility using large deviations theory and related results, concerning the small-time near-the-money skew, have been obtained by Bayer, Friz, Gulisashvili, Horvath and Stemper [4]. However, we should point out that pricing and model calibration under rough volatility models still remains time consuming.

In this paper, we suggest to design a fast option pricer, based on multi-index stochastic collocation (MISC) as in [18], for options whose dynamics follow rBergomi model as in [2]. We may later investigate QMC.

1.3 Background on Gaussian and fBM processes

A zero-mean real-valued Gaussian process $(Z_t)_{t\geq 0}$ is a stochastic process such that on any finite subset $\{t_1, \dots t_n\} \subset \mathbb{R}, (Z_{t_1}, \dots, Z_{t_n})$ has a multivariate normal distribution with mean zero. The law of a Gaussian process is entirely determined by the covariance function $K(s,t) = \mathrm{E}[Z_t Z_s]$ and Z induces a Gaussian probability measure on $(E, \mathcal{B}(E))$, where E denotes the Banach space $C_0([0,1])$ with the usual sup norm topology (see, e.g., section 3.1.1 of [9] for details).

Fractional Brownian motion (fBM) is a natural generalization of standard Brownian motion which preserves the properties of stationary increments, self-similarity, and Gaussian finite-dimensional distributions, but it has a more complex dependence structure. In this section, we recall the definition and summarize the basic properties of fBM.

A zero-mean Gaussian process B_t^H is called standard fractional Brownian motion (fBM) with Hurst parameter $H \in (0,1)$ if it has covariance function

$$R_H = \mathrm{E}\left[B_t^H B_s^H\right] - \mathrm{E}\left[B_t^H\right]\mathrm{E}\left[B_s^H\right] = \frac{1}{2}\left(|t|^{2H} + |s|^{2H} - |t-s|^{2H}\right). \tag{1}$$

In order to specify the distribution of a Gaussian process, it is enough to specify its mean and its covariance function; therefore, for each H, the law of B^H is uniquely determined by $R_H(s,t)$. However, this definition by itself does not guarantee the existence of fBM; to show that fBM exists, one needs to verify that the covariance function is nonnegative definite.

We now recall some fundamental properties of fBM (see also Figure 1):

- fBM is continuous a.s. and H-self-similar (H-ss), i.e., for $a > 0, (B_{at})_{t\geq 0} \overset{(d)}{=} a^H (B_t)_{t\geq 0}$ where $\overset{(d)}{=}$ means both processes have the same finite-dimensional distributions. For $H \neq 1/2$, B^H does not have independent increments; for $H = 1/2, B_t^H$ is the standard Brownian motion.
- From (1), we see that
$$\mathrm{E}\left[(B_t^H - B_s^H)^2\right] = |t-s|^{2H},$$
so $B_t^H - B_s^H \sim \mathcal{N}(0, |t-s|^{2H})$; thus B^H has stationary increments.
- If we set $X_n = B_n^H - B_{n-1}^H$, then X_n is a discrete-time Gaussian process with covariance function
$$\begin{aligned}\rho_n &= \mathrm{E}[X_{k+n} X_n] = \mathrm{E}\left[\left(B_{k+n}^H - B_{k+n-1}^H\right)\left(B_k^H - B_{k-1}^H\right)\right] \\ &\sim H(2H-1)n^{2H-2} \quad (n \to \infty),\end{aligned}$$
and thus (by convexity of the function $g(n) = n^{2H}$), we see that two increments the form $B_k - B_{k-1}$ and $B_{k+n} - B_{k+n-1}$ are positively correlated if $H \in (1/2, 1)$ and negatively correlated if $H \in (0, 1/2)$. Thus B^H is persistent (i.e., it is more likely to keep a trend than to break it) when $H > 1/2$, the relatively stronger positive correlation for the consecutive increments of the associated fBm process with increasing H values gives a relatively smoother process whose correlations decay relatively slowly.On the other hand, it is antipersistent when $H < 1/2$ (i.e., if B^H was increasing in the past, it is more likely to decrease in the future, and vice versa). The enhanced negative correlation with smaller Hurst exponent gives a relatively rougher process.

- If $H \in (1/2, 1)$, we can show that $\sum_{n=1}^{\infty} \rho_n = \infty$, which means that the process exhibits long-range dependence, but if $H \in (0, 1/2)$, then $\sum_{n=1}^{\infty} \rho_n < \infty$.
- Using that $\mathrm{E}\left[(B_t^H - B_s^H)^2\right] = (t-s)^{2H}$, we can show that sample paths of B^H are α-H older continuous for all $\alpha \in (0, H)$.
- fBM is the only self-similar Gaussian process with stationary increments (see, e.g., [22]), and for $H \neq 1/2$, B_t^H is neither a Markov process nor a semimartingale (see, e.g., [24]).

For more details regarding the fBm processes we refer to [8, 11, 21].

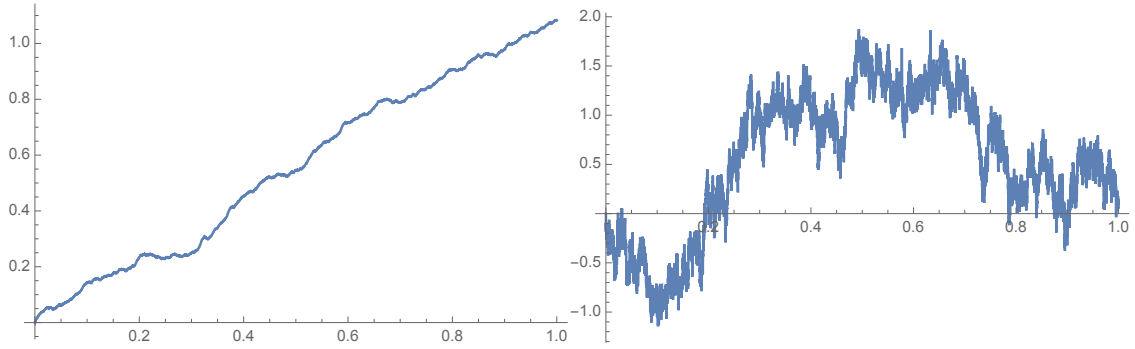

(a) (b)

Figure 1: Monte Carlo simulation of fBM for $H = 0.9$ (left) and $H = 0.3$ (right).

2 Problem setting

2.1 The rBergomi model

We use the rBergomi model for the price process S_t as defined in [2], normalized to $r = 0$, which is defined by

$$dS_t = \sqrt{v_t(\tilde{W}^H)} S_t dZ_t, \tag{2}$$

$$v_t = \xi_0(t) \exp\left(\eta \tilde{W}_t^H - \frac{1}{2}\eta^2 t^{2H}\right), \tag{3}$$

where for $0 < H < 1$ and $\eta > 0$. We have $\tilde{W}^H$ is a certain Volterra process (Riemann-Liouville process), defined by

$$\tilde{W}_t^H = \int_0^t K^H(t, s) dW_s^1, \quad t \geq 0 \tag{4}$$

where the kernel $K^H : \mathbb{R}_+ \times \mathbb{R}_+ \to \mathbb{R}_+$ reads

$$K^H(t, s) = \sqrt{2H}(t-s)^{H-1/2}, \quad \forall\, 0 \leq s \leq t. \tag{5}$$

We note that the map $s \to K^H(s,t)$ belongs to L^2, so that the stochastic integral (4) is well defined.

W^1, Z denote two *correlated* standard Brownian motions with correlation $\rho \in [-1,1]$, so that

$$Z := \rho W^1 + \overline{\rho} W^{\perp} \equiv \rho W^1 + \sqrt{1-\rho^2} W^{\perp}, \tag{6}$$

where $(W^1, W^{\perp})$ are two independent standard Brownian motions, Therefore, Eq 2 can be written as

$$\begin{aligned} S_t &= S_0 \exp\left(\int_0^t \sqrt{v(s)} dZ(s) - \frac{1}{2}\int_0^t v(s) ds\right), \quad S_0 > 0 \\ v(u) &= \xi_0(u) \exp\left(\eta \tilde{W}_u^H - \frac{\eta^2}{2} u^H\right), \quad \xi_0 > 0 \end{aligned} \tag{7}$$

The filtration $(\mathcal{F}_t)_{t\geq 0}$ can here be taken as the one generated by the two-dimensional Brownian motion $(W^1, W^{\perp})$ under the risk neutral measure $\mathbb{Q}$, resulting in a filtered probability space $(\Omega, \mathcal{F}; \mathcal{F}_t, \mathbb{Q})$. The stock price process S is clearly then a local $(\mathcal{F}_t)_{t\geq 0}$-martingale and a super-martingale, therefore integrable. We shall henceforth use the notation $\mathrm{E}[.] = E^{\mathbb{Q}}[. \mid \mathcal{F}_0]$ unless we state otherwise.

We refer to v_u as the variance process, where $\xi_0(u) = \mathrm{E}[v_u] \in \mathcal{F}_0$ a.s. the forward variance curve. $\tilde{W}^H$ is a centered, locally $(H-\epsilon)$- Hölder continuous, Gaussian process with $\mathrm{var}[\tilde{W}_t^H] = t^{2H}$.

We note that the model parameters (η, ρ, H) may have an intuitive interpretation of their influence over implied volatilities. In fact, η might seen as smile, ρ as skew, $H - 1/2$ as the explosion(smile and skew).

2.2 Option pricing under rBergomi model

Assuming $S_0 = 1$, and using the conditioning argument on the σ-algebra generated by W^1 (argument first used by [25] in the context of Markovian SV models), we can show that the call price is given by

$$\begin{aligned} C_{RB}(T,K) &= E\left[(S_T - K)^+\right] \\ &= \mathrm{E}\left[\mathrm{E}\left[(S_T - K)^+ \mid \sigma(W^1(t), t \leq T)\right]\right] \\ &= E\left[C_{BS}\left(S_0 = \exp\left(\rho\int_0^T \sqrt{v_t} dW_t^1 - \frac{1}{2}\rho^2 \int_0^T v_t dt\right),\ K = K,\ T = 1,\ \sigma^2 = (1-\rho^2)\int_0^T v_t dt\right)\right], \end{aligned} \tag{8}$$

where C_{BS} denotes the Black-Scholes price.

In fact, if we use the orthogonal decomposition of S_t into S_t^1 and S_t^2, where

$$S_t^1 := \mathcal{E}\{\rho \int_0^t \sqrt{v_s} dW_s^1\},\ S_t^2 := \mathcal{E}\{\sqrt{1-\rho^2} \int_0^t \sqrt{v_s} dW_s^{\perp}\}, \tag{9}$$

where $\mathcal{E}()$ denotes the stochastic exponential, then, we obtain by conditional log-normality

$$\log S_t \mid \mathcal{F}_t^1 \sim \mathcal{N}\left(\log S_t^1 - \frac{1}{2}(1-\rho^2)\int_0^t v_s ds, (1-\rho^2)\int_0^t v_s ds\right), \tag{10}$$

where $\mathcal{F}_t^1 = \sigma\{W_s^1 : s \leq t\}$. Therefore, we obtain (8).

We insist that the smoothing trick, based on conditionning, performed in Eq (8) enable us to get a smooth term inside the expectation. Therefore, applying sparse quadrature techniques becomes an adequate option for computing the call price as we shall see later.

2.3 Simulation of the rBergomi model

The main challenge is the computation of $S = \int_0^T \sqrt{v_t} dW_t^1$ and $V = \int_0^T v_t dt$. As was mentioned in [3], we may try to avoid any sampling related to W^2 by a brute-force approach that consists in simulating a scalar Brownian motion W^1, followed by computing $\tilde{W}^H = \int K dW^1$ by Itô/Riemann Stieltjes approximations of (S, V). However, this is not advisable given the singularity of the Volterra kernel $K(s,t)$ at the diagonal $s = t$. Therefore, one needs to jointly simulate the two-dimensional Gaussian process $(W_t^1, \tilde{W}_t^H : 0 \leq t \leq T)$, resulting in $W_{t_1}^1, \ldots, W_{t_N}$ and $\tilde{W}_{t_1}^H, \ldots, \tilde{W}_{t_N}^H$ along a given grid $t_1 < \cdots < t_N$. There are essentially three possible ways to achieve this:

1. Euler discretization of the integral defining $\tilde{W}^H$ together with classical simulation of increments of W^1. This is horribly inefficient because the integral is singular and adaptivity probably does not help, as the singularity moves with time. For this method, we need an N-dimensional random Gaussian input vector to produce one (approximate, inaccurate) sample of $W_{t_1}^1, \ldots, W_{t_N}^1, \tilde{W}_{t_1}^H, \ldots, \tilde{W}_{t_N}$.

2. Given that $W_{t_1}^1, \ldots, W_{t_N}^1, \tilde{W}_{t_1}^H, \ldots, \tilde{W}_{t_N}$ together forms a $(2N)$-dimensional Gaussian random vector with computable covariance matrix. We can use Cholesky decomposition of the covariance matrix to produce exact samples of $W_{t_1}^1, \ldots, W_{t_N}^1, \tilde{W}_{t_1}^H, \ldots, \tilde{W}_{t_N}$, but unlike the first way, we need $2N$-dimensional Gaussian random vectors as input. This method is exact but slow (See [2] and Section 4 in [4]). The simulation requires $\mathcal{O}\left(N^3\right)$. flops.

3. The hybrid scheme of [6] uses a different approach, which is essentially based on Euler discretization as the first way but crucially improved by moment matching for the singular term in the left point rule. It is also inexact in the sense that samples produced here do not exactly have the distribution of $W_{t_1}^1, \ldots, W_{t_N}^1, \tilde{W}_{t_1}^H, \ldots, \tilde{W}_{t_N}$, however they are much more accurate then samples produced from method 1), but much faster than method 2). As in method 2), in this case we need a $2N$-dimensional Gaussian random input vector to produce one sample of $W_{t_1}^1, \ldots, W_{t_N}^1, \tilde{W}_{t_1}^H, \ldots, \tilde{W}_{t_N}$.

In this project, we adopt the last approach for the simulation of the rBergomi model. We utilise the first order variant ($\kappa = 1$) of the hybrid scheme [6], which is based on the approximation

$$\tilde{W}_{\frac{i}{N}}^H \approx \overline{W}_{\frac{i}{N}} := \sqrt{2H}\left(\int_{\frac{i-1}{N}}^{\frac{i}{N}} \left(\frac{i}{N} - s\right)^{H-\frac{1}{2}} dW_u^1 + \sum_{k=2}^{i} \left(\frac{b_k}{N}\right)^{H-\frac{1}{2}} \left(W_{\frac{i-(k-1)}{N}}^1 - W_{\frac{i-k}{N}}^1\right)\right) \tag{11}$$

where N is the number of time steps and

$$b_k := \left(\frac{k^{H+\frac{1}{2}} - (k-1)^{H+\frac{1}{2}}}{H+\frac{1}{2}} \right)^{\frac{1}{H-\frac{1}{2}}}$$

Employing the fast Fourier transform to evaluate the sum in (11), which is a discrete convolution, a skeleton $\overline{W}_0^H, \overline{W}_1^H, \ldots, \overline{W}_{\frac{[Nt]}{N}}^H$ can be generated in $\mathcal{O}(N \log N)$ foating point operations.

The variates $\overline{W}_0^H, \overline{W}_1^H, \ldots, \overline{W}_{\frac{[Nt]}{N}}^H$ can be generated by sampling $[nt]$ iid draws from a $\kappa + 1$-dimensional Gaussian distribution and computing a discrete convolution. We call these pairs of Gaussian random variables from now on as (W^1, W^2).

3 Details our approach and error bounds

Our approach of computing the expectation in (8) is based on multi-index stochastic collocation (MISC), suggested in [18]. We describe the general strategy for the multi-index construction in Section 3.1. Recall that there are two N dimensional Gaussian inputs for the used hybrid approach (N is the number of time steps in the time grid) , namely

- $\{W^1\}_{i=1}^N$: The N Gaussian random parameters that are defined in Section 2.1.
- $\{W^2\}_{i=1}^N$: An artificial introduced N Gaussian random parameters that are used for left-rule points in the hybrid scheme, explained in Section 2.3.

We have a natural error decomposition for the total error of computing the the expectation in (8), namely, $\mathcal{E}$

$$\mathcal{E} \leq \mathcal{E}_Q(TOL_{\text{MISC}}, N) + \mathcal{E}_B(N), \tag{12}$$

where $\mathcal{E}_Q$ is the quadrature error, function of MISC tolerance TOL_{MISC} and N (the number of time steps) and $\mathcal{E}_B$ is the bias, function of N (the number of time steps) or $\Delta_t = \frac{T}{N}$ (size of the time grid).

We note that sampling the Brownian motion can be constructed either sequentially using a standard random walk construction or hierarchically using Brownian bridge (BB) construction. To make an effective use of MISC, which is badly affected by isotropy, we use the BB construnction since it produces dimensions with different importance for MISC (creates anisotropy), contrary to random walk procedure for which all the dimension of the stochastic space have equal importance (isotropic). We explain the BB construction in Section 3.3. This transformation plays a role of dimension reduction of the problem and as a consquence accelerating the MISC procedure by reducing the compotational cost.

Another way to reduce the dimension of the problem is by using Richardson extrapolation, explained in Section 3.4. In fact, Richardson extrapolation acts on both the bias (by reducing it) and MISC procedure by redcing the number of needed time steps ,N, neeeded to achive a certain tolerance, resulting in a lower dimensional problem.

Motivated by some numerical observations regarding the behavior of the MISC solver with respect to the standard Gaussian hermite quadrature (See Section 4), We build a more robust MISC solver by incorporating a change of measure with respect to W^1 as described in Section 3.2.

We also discuss the error bounds in Section 3.5

3.1 Details of the MISC

We focus on solving the problem of approximating the expected value of $\mathrm{E}[f(y)]$ on a tensorization of quadrature formulae over the stochastic domain, Γ. Assuming that $f(y)$ is a continuous function (analytic) over Γ. A quadrature approach is very adequate.

Let us define $\beta \leq 1$ be an integer positive value referred to as a "stochastic discretization level", and $m : \mathbb{N} \to \mathbb{N}$ be a strictly increasing function with $m(0) = 0$ and $m(1) = 1$, that we call a "level-to-nodes function". At level β, we consider a set of $m(\beta)$ distinct quadrature points in $(-\infty; \infty)$, $\mathcal{H}^{m(\beta)} = \{y_\beta^1, y_\beta^2, \ldots, y_\beta^{m(\beta)}\} \subset [-\infty, \infty]$, and a set of quadrature weights, $\mathcal{W}^{m(\beta)} = \{\omega_\beta^1, \omega_\beta^2, \ldots, \omega_\beta^{m(\beta)}\}$. We also let $C^0((-\infty, \infty))$ be the set of real-valued continuous functions over $(-\infty, \infty)$. We then define the quadrature operator as

$$Q(m(\beta)) : C^0((-\infty, \infty)) \to \mathbb{R}, \quad Q(m(\beta))[f] = \sum_{j=1}^{m(\beta)} f(y_\beta^j)\omega_\beta^j. \tag{13}$$

In the multi-variate case Γ is defined as a countable tensor product of intervals. Therefore, we define, for any definitely supported multi-index $\boldsymbol{\beta} \in \mathcal{L}_+$

$$Q^{m(\boldsymbol{\beta})} : \Gamma \to \mathbb{R}, \quad Q^{m(\boldsymbol{\beta})} = \bigotimes_{n \geq 1} Q^{m(\beta_n)}$$

where the n-th quadrature operator is understood to act only on the n-th variable of f. Practically, we obtain the value of $Q^{m(\boldsymbol{\beta})}[f]$ by considering the tensor grid $\mathcal{T}^{m(\boldsymbol{\beta})} = \times_{n \geq 1} \mathcal{H}^{m(\beta_n)}$ with cardinality $\#\mathcal{T}^{m(\boldsymbol{\beta})} = \prod_{n \geq 1} m(\beta_n)$ and computing

$$Q^{\mathcal{T}^{m(\boldsymbol{\beta})}}[f] = \sum_{j=1}^{\#\mathcal{T}^{m(\boldsymbol{\beta})}} f(\widehat{y}_j)\overline{\omega}_j$$

where $\widehat{y}_j \in \mathcal{T}^{m(\boldsymbol{\beta})}$ amd $\overline{\omega}_j$ are (infinite) products of weights of the univariate quadrature rules. We Note that it is essential in this construction that $m(1) = 1$ so that the cardinality of $\mathcal{T}^{m(\boldsymbol{\beta})}$ is finite for any $\boldsymbol{\beta} \in \mathcal{L}_+$ and $\omega_{\beta_n}^1 = 1$ whenever $n = 1$, so that all weights, $\overline{\omega}_j$, are bounded.

We mention that the quadrature points are chosen to optimize the convergence properties of the quadrature error.

A direct approximation $\mathrm{E}[f] \approx Q^{m(\boldsymbol{\beta})}[f]$ is not an appropriate option due to the well-known "curse of dimensionality" effect. We use multi-index stochastic collocation (MISC) as it was suggested in [18]. MISC as a hierarchical adaptive quadrature strategy that uses stochastic discretizations and classic sparsification approach to obtain an effective approximation scheme for $\mathrm{E}[f]$.

In our setting, we are left with a $2N$- dimensional Gaussian random inputs, which are chosen independently, resulting in $2N$ numerical parameters, which we use as the basis of the multi-index construction, reflecting the fact that W_i^1 and W_j^2 can vary independently of each other regardless of $i \neq j$ or $i = j$. For the sake of concreteness, let $l \in \{1, \ldots, 2N\}$ and set

$$m_l \coloneqq \begin{cases} W_l^1, & 1 \leq l \leq N, \\ W_{l-N}^2, & N+1 \leq l \leq 2N. \end{cases} \tag{14}$$

For a multi-index $\ell = (l_i)_{i=1}^{2N} \in \mathbb{N}^{2N}$ we denote by $Q_\ell^N \coloneqq Q^N(m_\ell)$ the result of a discretized integral, using N time steps , with parameters $m_\ell \coloneqq (m_{l_i})_{i=1}^{2N}$. We further define the set of differences ΔQ_ℓ^N as follows: for a single index $1 \le i \le 2N$, let

$$\Delta_i Q_\ell^N \coloneqq \begin{cases} Q^N(m_\ell) - Q^N(m'_\ell) \text{ with } m'_\ell = m_{\ell - e_i}, \text{ if } \ell_i > 0 \\ Q^N(m_\ell) \text{ otherwise} \end{cases} \tag{15}$$

where e_i denotes the ith $2N$-dimensional unit vector. Then, ΔQ_ℓ^N is defined as

$$\Delta Q_\ell^N \coloneqq \left(\prod_{i=1}^{2N} \Delta_i \right) Q_\ell^N. \tag{16}$$

For instance, when $N = 1$, then

$$\begin{aligned} \Delta Q_\ell^1 = \Delta_2 \Delta_1 Q_{(l_1,l_2)}^1 = \Delta_2 \left(Q_{(l_1,l_2)}^1 - Q_{(l_1-1,l_2)}^1 \right) &= \Delta_2 Q_{(l_1,l_2)}^1 - \Delta_2 Q_{(l_1-1,l_2)}^1 \\ &= Q_{(l_1,l_2)}^1 - Q_{(l_1,l_2-1)}^1 - Q_{(l_1-1,l_2)}^1 + Q_{(l_1-1,l_2-1)}^1. \end{aligned}$$

Note that $Q^N(m)$ converges to the biased option price (denoted by $Q^N(\infty)$ as $m \to \infty$. Hence, we have the telescoping property

$$Q^N(\infty) = \sum_{l_1=0}^{\infty} \cdots \sum_{l_{2N}=0}^{\infty} \Delta Q_{(l_1,\ldots,l_{2N})}^N = \sum_{\ell \in \mathbb{N}^{2N}} \Delta Q_\ell^N, \tag{17}$$

provided that $m_{l_1} \xrightarrow{l_1 \to \infty} \infty$, $\ldots$, $m_{l_{2N}} \xrightarrow{l_{2N} \to \infty} \infty$. The telescoping property is accompanied by a corresponding error factorization, i.e., the size of the increment ΔQ_ℓ^N can be bounded by a product of error terms depending on m_i and m_{i+N}.

We denote the computational work at level $\ell = (l_1, \ldots, l_{2N})$ for adding an increment ΔQ_ℓ^N in the telescoping sum by W_ℓ^N, and define the actual estimator for the quantity of interest $Q^N(\infty)$: given a set of multi-indices $\mathcal{I} \subset \mathbb{N}^{2N}$, let

$$Q^N(\mathcal{I}) \coloneqq \sum_{\ell \in \mathcal{I}} \Delta Q_\ell^N.$$

Then the error is given by

$$\left| Q^N(\infty) - Q^N(\mathcal{I}) \right| \le \sum_{\ell \in \mathbb{N}^{2N} \setminus \mathcal{I}} \left| \Delta Q_\ell^N \right|,$$

The construction of $\mathcal{I}$ will be done by profit thresholding, i.e., for a certain threshold value T, we add a multi-index ℓ to $\mathcal{I}$ provided that

$$\log \left(\frac{\left| \Delta Q_\ell^N \right|}{W_\ell^N} \right) \le T.$$

(Actually, we take the error estimate instead of the true error.)

3.2 Gaussian Hermite Quadrature with importance sampling

Let us call the integrand that we feed to MISC by $I(W^1, W^2)$, then

$$C_{RB}(T,K) = \int_{\mathbb{R}_+^{2N}} I(\mathbf{W}^1, \mathbf{W}^2)\rho(\mathbf{W}^1)\rho(\mathbf{W}^2)d\mathbf{W}^1 d\mathbf{W}^2, \tag{18}$$

where N is the number of time steps. We can rewrite the previous expression as

$$C_{RB}(T,K) = \int_{\mathbb{R}_+^{2N}} \frac{I(\mathbf{W}^1, \mathbf{W}^2)\rho(\mathbf{W}^1)}{h(\mathbf{W}^1; \widehat{\mathbf{W}}^1, \Psi)} h(\mathbf{W}^1; \widehat{\mathbf{W}}^1, \Psi)\rho(\mathbf{W}^2)d\mathbf{W}^1 d\mathbf{W}^2, \tag{19}$$

where $h(\mathbf{W}^1; \widehat{\mathbf{W}}^1, \Psi)$ is a multivariate normal density with first and second order moments given by

$$\widehat{\mathbf{W}}^1 = \arg\max_{\mathbf{W}^1 \in \mathbb{R}^N} [\log I(\mathbf{W}^1; \mathbf{W}^2 = \mathbf{0})] \tag{20}$$

$$\Psi = \left(-\frac{\partial^2 [\log I(\mathbf{W}^1; \mathbf{W}^2 = \mathbf{0})]}{\partial (\mathbf{W}^1)^T \mathbf{W}^1} \right)^{-1}_{\mathbf{W}^1 = \widehat{\mathbf{W}}^1} \tag{21}$$

Let us define $\tilde{\mathbf{W}}^1$ as uncorrelated varaibles and the Cholesky factorization of Ψ is given by $\Psi = LL^T$, and $\overline{\mathbf{W}}^1 = \sqrt{2} L \tilde{\mathbf{W}}^1 + \widehat{\mathbf{W}}^1$ then Eq 19 becomes

(22)

$$C_{RB}(T,K) = 2^{N/2}.|L| \int_{\mathbb{R}_+^{2N}} \left(I(\overline{\mathbf{W}}^1, \mathbf{W}^2) \exp(-\frac{1}{2}(\overline{\mathbf{W}}^1)^T \overline{\mathbf{W}}^1) \exp(\frac{1}{2}\tilde{\mathbf{W}}^T \tilde{\mathbf{W}}) \right) \rho(\tilde{\mathbf{W}}^1)\rho(\mathbf{W}^2) d\tilde{\mathbf{W}}^1 d\mathbf{W}^2$$

3.3 Brownian bridge construction

Let us denote $\{t_i\}_{i=0}^N$ the grid of time steps, then the BB construction [17] consists of the following: given a past value B_{t_i} and a future value B_{t_k}, the value B_{t_j} (with $t_i < t_j < t_k$) can be generated according to the formula:

$$B_{t_j} = (1-\rho)B_{t_i} + \rho B_{t_k} + \sqrt{\rho(1-\rho)(k-i)\Delta t} z, \; z \sim \mathcal{N}(0,1), \tag{23}$$

where $\rho = \frac{j-i}{k-i}$. In particular, if N is a power of 2, then given $B_0 = 0$, BB generates the Brownian motion at times $T, T/2, T/4, 3T/4, \ldots$ according

$$\begin{aligned}
B_T &= \sqrt{T} z_1 \\
B_{T/2} &= \frac{1}{2}(B_0 + B_T) + \sqrt{T/4} z_2 = \frac{\sqrt{T}}{2} z_1 + \frac{\sqrt{T}}{2} z_2 \\
B_{T/4} &= \frac{1}{2}(B_0 + B_{T/2}) + \sqrt{T/8} z_3 = \frac{\sqrt{T}}{4} z_1 + \frac{\sqrt{T}}{4} z_2 + \sqrt{T/8} z_3 \\
&\vdots
\end{aligned} \tag{24}$$

where $\{z_j\}_{j=1}^N$ are independent standard normal variables. In BB construction given by (24), the most important values that determine the large scale structure of Brownian motion are the first components of $\mathbf{z} = (z_1, \ldots, z_N)$.

3.4 Richardson extrapolation

We recall that the Euler (often) scheme has weak order 1 so that

$$\left|\mathrm{E}\left[f(\widehat{X}_T^h)\right] - \mathrm{E}\left[f(X_T)\right]\right| \leq Ch \tag{25}$$

for some constant C, all sufficiently small h and suitably smooth f. It was shown that 25 can be improved to

$$\mathrm{E}\left[f(\widehat{X}_T^h)\right] = \mathrm{E}\left[f(X_T)\right] + ch + \mathcal{O}\left(h^2\right), \tag{26}$$

where c depends on f.

Applying 26 with discretization step $2h$, we obtain

$$\mathrm{E}\left[f(\widehat{X}_T^{2h})\right] = \mathrm{E}\left[f(X_T)\right] + 2ch + \mathcal{O}\left(h^2\right), \tag{27}$$

implying

$$2\mathrm{E}\left[f(\widehat{X}_T^{2h})\right] - \mathrm{E}\left[f(\widehat{X}_T^h)\right] = \mathrm{E}\left[f(X_T)\right] + \mathcal{O}\left(h^2\right), \tag{28}$$

For higher levels extrapolations, we use the following: Let us denote by $h_J = h_0.2^{-J}$ the grid sizes (where h_0 is the coarsest grid size), by K the level of the Richardson extrapolation, and by $I(J,K)$ the approximation of $\mathrm{E}\left[f(\widehat{X}_T^{h_J})\right]$ by terms up to level K (leading to a weak error of order K), then we have

$$I(J,K) = \frac{2^K\left[I(J,K-1) - I(J-1,K-1)\right]}{2^K - 1} + \mathcal{O}\left(h^{K+1}\right), \quad J = 1,2,\ldots, K = 1,2,\ldots \tag{29}$$

3.5 Discussion about error bounds

TO-DO: In this Section, we discuss each term in Eq 12 seperatly.

3.5.1 Discussion about the Bias error

3.5.2 Discussion about the quadrature error

4 Numerical tests

In this Section, the default paramters values of the rBergomi model (unless stated), defined in Section 2.1, are: $S_0 = 1$, $\eta = 1.9$, $\xi = 0.235^2$, $\rho = -0.9$, $T = 1$.

4.1 Summary of the numerical results

We started the numerical results with the case where we use the Hermite quadrature without change of measure (See Section 4.2). We first estimate the weak error (Bias) for 3 scenarios involving Richardson extrapolation (leve 1 and 2) (see Section 4.2.1) for the plots and Section 4.2.2 for the observed values along with the tolerances needed by MISC to achieve those biases (We still need a robust way to link the MISC tolerance with the quadrature error). We observed that Richardson extrapolation along with hierarchical representation bring an important improvement for MISC in terms of dimension reduction and weak error, which makes this method highly competitive to MC (see results in tables in Section 4.2.2 which show the gained advantage in terms of bias reduction, as well in terms of computational time, for the case $H = 0.07$). Therefore the only step there is to have a robust way to link MISC tolerance with the quadrature error. We also observed some bad behavior of the mixed differences that may provide a potential reason of some instability observed when running MISC. We try to investigate that in Section 4.2.3. Therefore I guess the two main steps that we are left now for this part are:

- Understand the reasons of the bad behavior observed for mixed differences.
- Design a robust way to link the MISC tolerance with the quadrature error

In a second part, we tried to investigate if a change of measure could be a good option to accelerate MISC and have a more robust MISC solver(avoiding the bad behaviors observed in the mixed difference). We motivate in Section 4.3 the reasons why a change of measure could be a good option as a pre-processing step before applying MISC. In section 4.4, we report the results of weak rates observed with and without Richardson extrapolation. Compared to those observed without change of measure, we observed almost same results without Richardson extrapolation and worser results when using Richardson extrapolation. The investigation of the latter behavior was carried in Section 4.4.2 and we may explain this by the fact that applying the change of measure to the extrapolated formula is not very appropriate since we have a more complex function (bi-modal functions or higher as we go deeper for the levels of Richardson extrapolation).

As a result, we think it is better to focus on the case without applying a change of measure.

4.2 Numerical results for the case without change of measure

4.2.1 Weak error plots

In this section, I include the results of weak error rates for the case without change of measure for both cases without and with Richardson extrapolation (level 1 and 2), for $H \in \{0.43, 0.07\}$. The reference solution was computed with $N = 500$ time steps (which is equal to 0.0712073 for $H = 0.43$ and 0.0792047 for $H = 0.07$). We note that the weak errors plotted here corresponds to relative errors.

Without Richardson extrapolation

From figures (2 and 3), we see that for both cases $H \in \{0.43, 0.07\}$, we get a weak error of order Δt. The upper and lower bounds are 95% confidence interval.

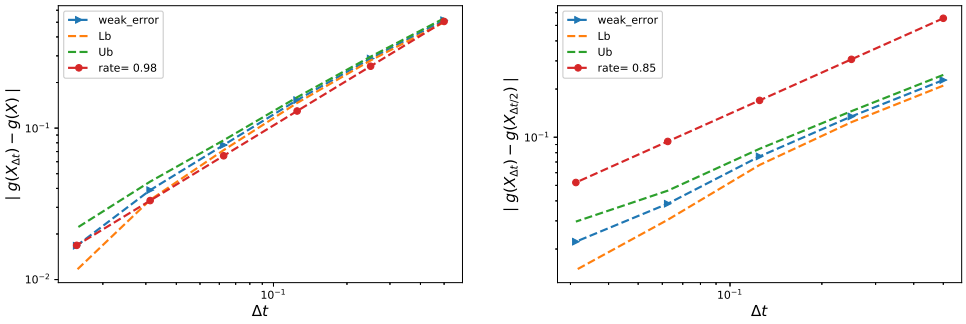

(a) (b)

Figure 2: The rate of convergence of the weak error for $H = 0.43$ $K = 1$, without Richardson extraploation, using MC with $M = 10^5$: a) $|\mathrm{E}\left[g(X_{\Delta t})\right] - g(X)|$ b) $\left|\mathrm{E}\left[g(X_{\Delta t}) - g(X_{\Delta t/2})\right]\right|$

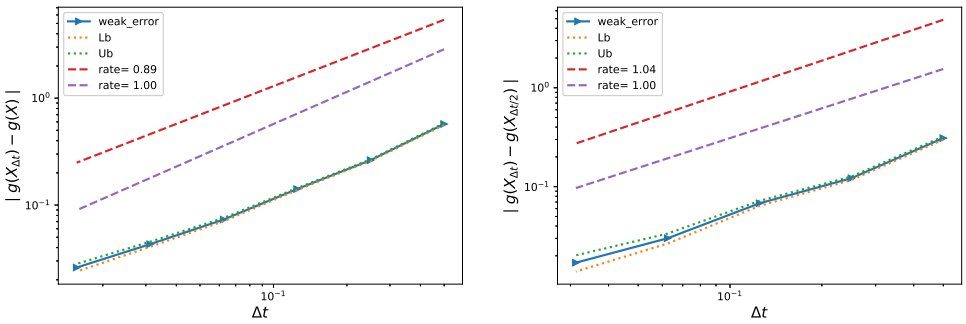

(a) (b)

Figure 3: The rate of convergence of the weak error for $H = 0.07$ $K = 1$, without Richardson extraploation, using MC with $M = 10^6$: a) $|\mathrm{E}\left[g(X_{\Delta t})\right] - g(X)|$ b) $\left|\mathrm{E}\left[g(X_{\Delta t}) - g(X_{\Delta t/2})\right]\right|$

With Richardson extrapolation (level 1)

From figures (4 and 5), we see that for both cases $H \in \{0.43, 0.07\}$, we get a weak error of order higher than Δt^2 (We expect to have order of Δt^2 in the asymptotic regime). The upper and lower bounds are 95% confidence interval.

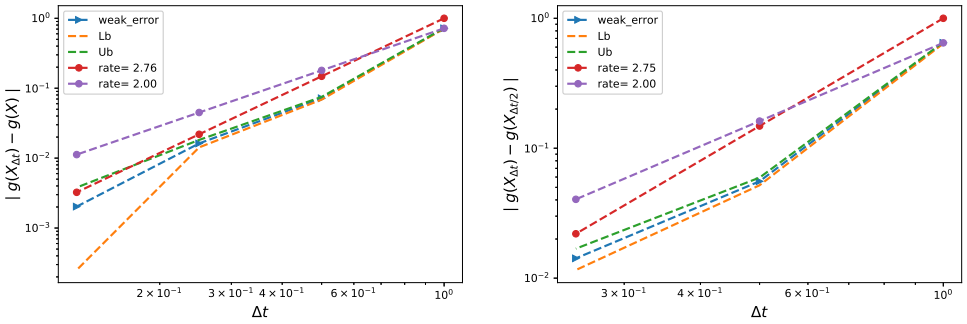

(a) (b)

Figure 4: The rate of convergence of the weak error for $H = 0.43$ $K = 1$, with Richardson extraploation, using MC with $M = 10^6$: a) $\left|\mathrm{E}\left[2g(X_{\Delta t/2}) - g(X_{\Delta t})\right] - g(X)\right|$ b) $\left|\mathrm{E}\left[3g(X_{\Delta t/2}) - g(X_{\Delta t}) - 2g(X_{\Delta t/4})\right]\right|$

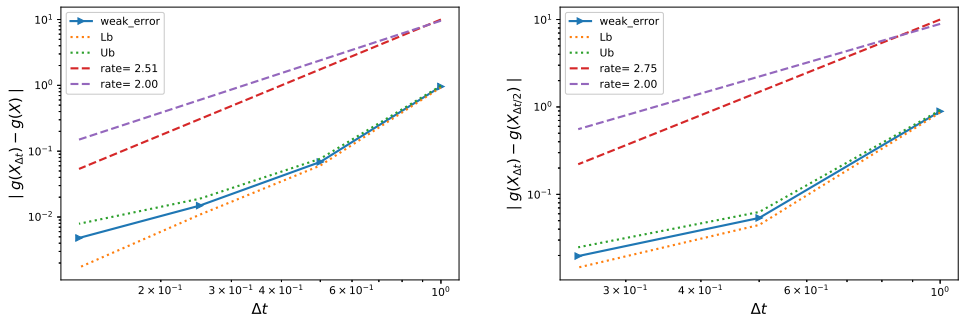

(a) (b)

Figure 5: The rate of convergence of the weak error for $H = 0.07$ $K = 1$, with Richardson extraploation, using MC with $M = 10^6$: a) $\left|\mathrm{E}\left[2g(X_{\Delta t/2}) - g(X_{\Delta t})\right] - g(X)\right|$ b) $\left|\mathrm{E}\left[3g(X_{\Delta t/2}) - g(X_{\Delta t}) - 2g(X_{\Delta t/4})\right]\right|$

With Richardson extrapolation (level 2)

From figures (6 and 7), we see that for both cases $H \in \{0.43, 0.07\}$, we get a non precise estimate of weak error, even with $M = 10^6$ samples, due to the high statistical error. The upper and lower bounds are 95% confidence interval. For later reported values in Section 4.2.2, we extrapolate the first estimated value, with 1 time step at the coarse level, assuming a rate of weak error of order Δt^3.

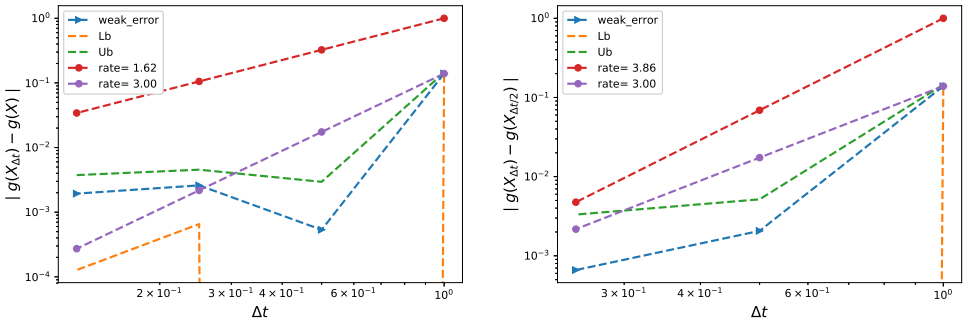

(a) (b)

Figure 6: The rate of convergence of the weak error for $H = 0.43$ $K = 1$, with Richardson extraploation, using MC with $M = 10^6$: a) $\left|\frac{1}{3}\mathrm{E}\left[8g(X_{\Delta t/4}) - 6g(X_{\Delta t/2}) + g(X_{\Delta t})\right] - g(X)\right|$ b) $\left|\frac{1}{3}\mathrm{E}\left[-8g(X_{\Delta t/8}) + 14g(X_{\Delta t/4}) - 7(X_{\Delta t/2}) + g(X_{\Delta t})\right]\right|$

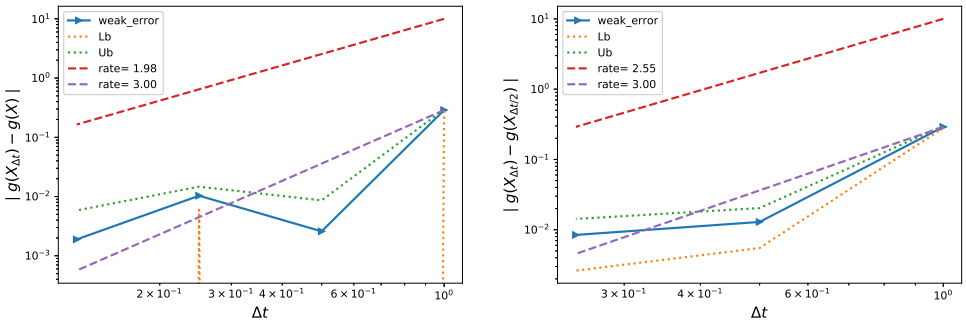

(a) (b)

Figure 7: The rate of convergence of the weak error for $H = 0.07$ $K = 1$, with Richardson extraploation (level 2), using MC with $M = 10^6$: a) $\left|\frac{1}{3}\mathrm{E}\left[8g(X_{\Delta t/4}) - 6g(X_{\Delta t/2}) + g(X_{\Delta t})\right] - g(X)\right|$ b) $\left|\frac{1}{3}\mathrm{E}\left[-8g(X_{\Delta t/8}) + 14g(X_{\Delta t/4}) - 7(X_{\Delta t/2}) + g(X_{\Delta t})\right]\right|$

4.2.2 Comparing relative errors

We note that the below results are preliminary since we observed an over-estimated tolerance for MISC solver. We need to figure out a way to define the adequate procedure to use the right MISC tolerance. However, as for now, we think that these results are very promising and could be even improved if we solve the issue of mixed difference.

The results were reported for $H \in \{0.43, 0.07\}$, and number of time steps $N \in \{2, 4, 8, 16\}$. Also, we use $S_0 = 1$, so the options will be prices in terms of the moneyness K, where K is the strike price.

In the following, we compare the relative errors for H $\in \{0.43, 0.07\}$ (see appendices A.1 and A.2 for the values of Call option prices). We note that for each case the reference solution was computed for $N = 500$ (number of time steps) using MC with 10^6 samples (which is equal to

0.0712073 for $H = 0.43$ and 0.0792047 for $H = 0.07$). In each case we report the results for 3 scenarios: i) Without using Richardson extrapolation, ii) Using level 1 Richardson extrapoaltion and iii) Using level 2 Richardson extrapoaltion. Tables (1, 2, 3) correspond to $H = 0.43$ and tables (4, 6, 8) correspond to $H = 0.07$.

Given the normalized bias computed by MC method (reported as bold values in the tables) (we also report the absolute error between parentheses for $H = 0.07$), we report in red in each table the smallest tolerance that MISC required to get below that relative bias (I do not put values for smaller tolerances, once the required bias is reached).

From the tables below, we have the following observations:

Using Richardson extrapoaltion, we got a significant improvement for the relative error with the use of minimal time steps.

- For instance, for $H = 0.43$, we achieved around 8% of relative error, with 16 time steps when not using Richardson extrapolation (see table 1). However, When using level 1 of Richardson extrapolation (see table 2), we achieved around 6% of relative error, with only 2 time steps in the coarse level, and we got around 1% of relative error, with 4 time steps in the coarse level. A more significant improvement is seen with level 2 of Richardson extrapolation, in fact, with just 1 step in the coarse level, we got around 3% percent of relative error.

- For $H = 0.07$, we achieved around 7% of relative error, with 16 time steps when not using Richardson extrapolation (see table 4). However, When using level 1 of Richardson extrapolation (see table 6), we achieved around 7% of relative error, with only 2 time steps in the coarse level, and we got below 1% of relative error, with 4 time steps in the coarse level. We observed a less significant improvement when using levle 2 of Richardson extrapolation, compared to the case of $H = 0.43$.

We also report in tables (5,7,9), the comparison of CPU time needed for MC and MISC, for $H = 0.07$, for different cases. We mention that we just put the computational time of MISC method for the cases where we acheieve the required bias (marked in red in relative error tables). From those tables, we see that MISC when coupled with Richardson extrapolation, is very competitive compared to MC, in the low dimension regime.

Case $H = 0.43$, Relative error for different methods

Method \Steps	2	4	8	16
MISC ($TOl = 2.10^{-1}$)	0.6011	0.3497	0.1910	0.0801
MISC ($TOl = 10^{-1}$)	0.6011	0.3497	0.2233	–
MISC ($TOl = 10^{-2}$)	0.5126	0.3258	0.1770	–
MISC ($TOl = 10^{-3}$)	–	0.2935	0.1503	–
MC method ($M = 10^6$)	**0.5154**	**0.2935**	**0.1545**	**0.0801**

Table 1: Relative error of Call option price of the different tolerances for different number of time steps. Case $K = 1$, $H = 0.43$, without Richardson extrapolation

Method \Steps	$1-2$	$2-4$	$4-8$	$8-16$
MISC ($TOl = 5.10^{-1}$)	0.9059	0.0997	0.0323	0.0028
MISC ($TOl = 10^{-1}$)	0.9059	0.0997	0.1025	–
MISC ($TOl = 10^{-2}$)	0.7374	0.0969	0.0463	–
MISC ($TOl = 10^{-3}$)	0.7191	0.0758	0.0112	–
MISC ($TOl = 5.10^{-4}$)	0.7129	0.0609	–	–
MC method ($M = 10^6$)	**0.7133**	**0.0698**	**0.0160**	**0.0035**

Table 2: Relative error of Call option price of the different tolerances for different number of time steps. Case $K = 1$, $H = 0.43$, using Richardson extrapolation (level 1)

Method \Steps	$1-2-4$	$2-4-8$	$4-8-16$
MISC ($TOl = 5.10^{-1}$)	0.1699	0.0098	0.0056
MISC ($TOl = 2.10^{-1}$)	0.1699	–	0.0014
MISC ($TOl = 10^{-1}$)	0.2037	–	–
MISC ($TOl = 5.10^{-2}$)	0.0295	–	–
MC method ($M = 10^6$)	**0.1440**	**0.0180**	**0.0023**

Table 3: Relative error of Call option price of the different tolerances for different number of time steps. Case $K = 1$, $H = 0.43$, using Richardson extrapolation (level 2)

Case $H = 0.07$, Relative error for different methods

Method \Steps	2	4	8	16	32	64
MISC ($TOl = 5.10^{-1}$)	0.3662	0.1578	0.1010	0.0758	–	–
MC method ($M = 10^6$)	**0.5727** (0.0454)	**0.2629** (0.0208)	**0.1411** (0.0112)	**0.0731** (0.0058)	**0.0431** (0.0034)	**0.0260** (0.0021)

Table 4: Relative error of Call option price of the different tolerances for different number of time steps. Case $K = 1$, $H = 0.07$, without Richardson extrapolation. The numbers between parentheses are the corresponding absolute errors.

Method \Steps	2	4	8	16
MISC	0.08	0.13	0.20	0.41
MC method ($M = 10^6$)	30	32	37	52

Table 5: Comparsion of the computational time of MC and MISC, used to compute Call option price of rBergomi model for different number of time steps. Case $K = 1, H = 0.07$

Method \Steps	$1-2$	$2-4$	$4-8$	$8-16$
MISC ($TOl = 5.10^{-1}$)	0.5682	0.0505	0.1389	0.1604
MISC ($TOl = 16.10^{-2}$)	–	–	0.1389	0.0038
MISC ($TOl = 10^{-1}$)	–	–	0.1692	–
MISC ($TOl = 5.10^{-2}$)	–	–	0.0088	–
MISC ($TOl = 10^{-2}$)	–	–	–	–
MC method ($M = 10^6$)	**0.9594** (0.0760)	**0.0686** (0.0054)	**0.0149** (0.0012)	**0.0048** (0.0004)

Table 6: Relative error of Call option price of the different tolerances for different number of time steps. Case $K = 1$, $H = 0.07$, using Richardson extrapolation (level 1). The numbers between parentheses are the corresponding absolute errors.

Method \Steps	$1-2$	$2-4$	$4-8$	$8-16$
MISC + Richardson (level 1)	0.1	0.14	34	92
MC method + Richardson (level 1) ($M = 10^6$)	43	46	54	71

Table 7: Comparsion of the computational time of MC and MISC, coupled with Richardson extrapolation (level 1), used to compute Call option price of rBergomi model for different number of time steps. Case $K = 1, H = 0.07$

Method \Steps	$1-2-4$	$2-4-8$	$4-8-16$
MISC ($TOl = 10^{-1}$)	0.2563	0.1566	0.0025
MISC ($TOl = 7.10^{-2}$)	0.3005	0.0227	–
MISC ($TOl = 5.10^{-2}$)	0.4874	–	–
MISC ($TOl = 10^{-2}$)	0.1742	–	–
MC method ($M = 10^6$)	**0.2231**	**0.0279**	**0.0035**

Table 8: Relative error of Call option price of the different tolerances for different number of time steps. Case $K = 1$, $H = 0.07$, using Richardson extrapolation (level 2)

Method \Steps	$1-2-4$	$2-4-8$	$4-8-16$
MISC +Richardson (level 2)	19	33	–
MC method+Richardson (level 2) ($M = 10^6$)	66	74	95

Table 9: Comparsion of the computational time of MC and MISC, coupled with Richardson extrapolation (level 2), used to compute Call option price of rBergomi model for different number of time steps. Case $K = 1, H = 0.07$

4.2.3 First and mixed differences rates

In this section, we plot the first and second order differences for the case without change of measure. These plots are important because they provide an indication about the efficiency and speed of MISC. We show the plots for the case of $H = 0.07$ and $N = 4$ time steps (we observed similar behaviors for other scenarios of number of time steps). From figures (8,9), we have the following observations:

- i) As was expected, the slowest directions are those corresponding to W^1, compared to those of W^2.
- ii) We face a bad behavior for the second differences, for the case without change of measure, which may explain the potential instability observed by MISC as well its bad convergence behavior for high number of time steps.

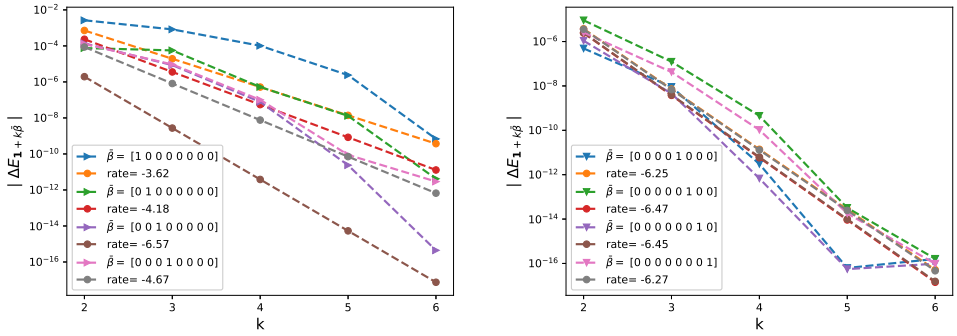

(a) (b)

Figure 8: The rate of convergence of first order differences $|\Delta E_\beta|$ ($\beta = \mathbf{1}+k\bar{\beta}$), for $K = 1$, $H = 0.07$: a) for W^1 b) for W^2

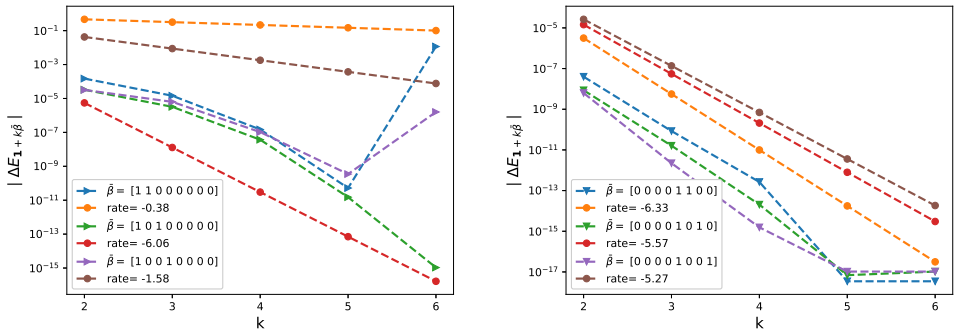

(a) (b)

Figure 9: The rate of convergence of second order differences $|\Delta E_\beta|$ ($\beta = \mathbf{1} + k\bar{\beta}$), for $K = 1$, $H = 0.07$: a) for W^1 b) for W^2

We tried to investigate the reason of the bad behavior observed for the mixed differences. From our experiments, we observed that whenever the mixed differences is diverging the maximum value of the integrand evaluated at quadrature points seems to blow up. We plot in figures (10,11) the function evaluated with quadrature points without the gaussian weights. The integrand behavior without weights seems to blow up maybe with faster rate than how the weights of the Hermite quadrature is decaying. In order to solve the issue of the divergence of mixed difference, we need to understand the interplay between the weights and the function values.

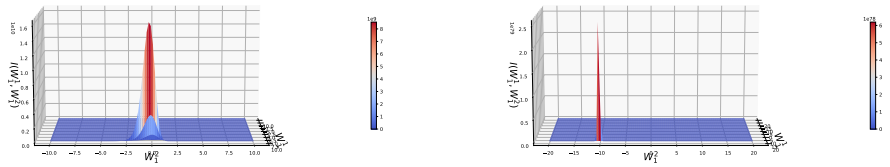

(a) (b)

Figure 10: Two dimensional Plotting of the integrand I (in (8)) without the Gaussian weight for $H = 0.07$ and $N = 4$, function of W_1 coordinates (W_1^1, W_1^2)

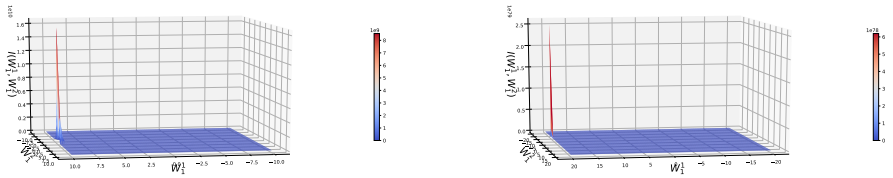

(a) (b)

Figure 11: Two dimensional Plotting of the integrand I (in (8)) without the Gaussian weight for $H = 0.07$ and $N = 4$, function of W_1 coordinates (W_1^1, W_1^2)

4.3 Motivation for the need of measure change

In this Section, we motivate the need of measure change as a pre-processing step before applying the MISC solver.

4.3.1 Integrand plotting wrt different random inputs

In this section, we plot the integrand, given by the term inside the expectation in (8)(including the Gaussian density), wrt different random inputs (W^1, W^2). This is important to check if we need a measure change and if needed for which variables. We show the results for $H = 0.07$ and for two scenarios of number of time steps $N \in \{2, 4\}$ (similar plots are produced for $H = 0.43$ in Appendices (B.1,B.2). We also show the two dimensional plots (See figures 14,17,19,18). As it seems from the plots, we just need change of measure wrt to W^1 coordinates and we do not need a measure chnage for W^2 coordinates.

N=2, H=0.07

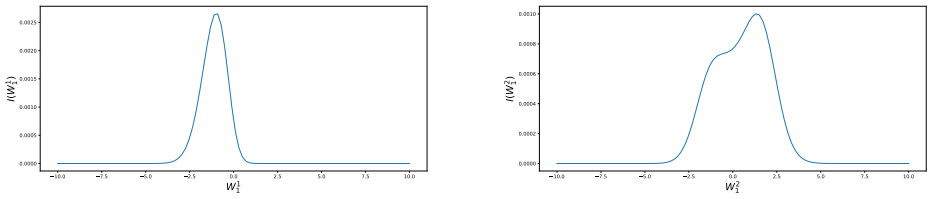

(a) (b)

Figure 12: Plotting the integrand I (in (8)) as a function of W^1 coordinates for $H = 0.07$ and $N = 2$.

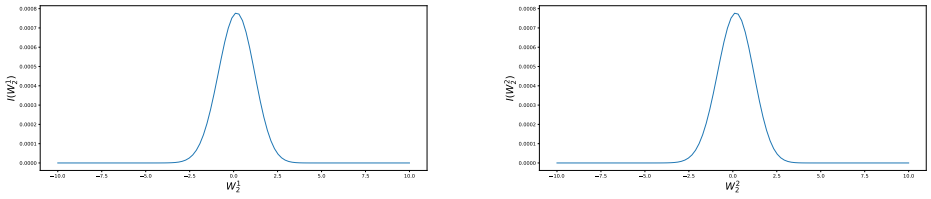

(a) (b)

Figure 13: Plotting the integrand I (in (8)) as a function of W^2 coordinates for $H = 0.07$ and $N = 2$.

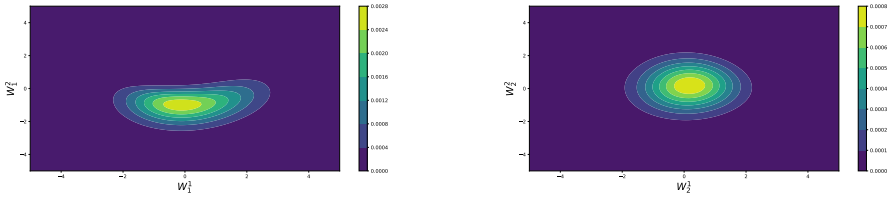

(a) (b)

Figure 14: Two dimensional Plotting of the integrand I (in (8)) for $H = 0.07$ and $N = 2$, a) function of W_1 coordinates, b) function of W^2 coordinates

N=4, H=0.07

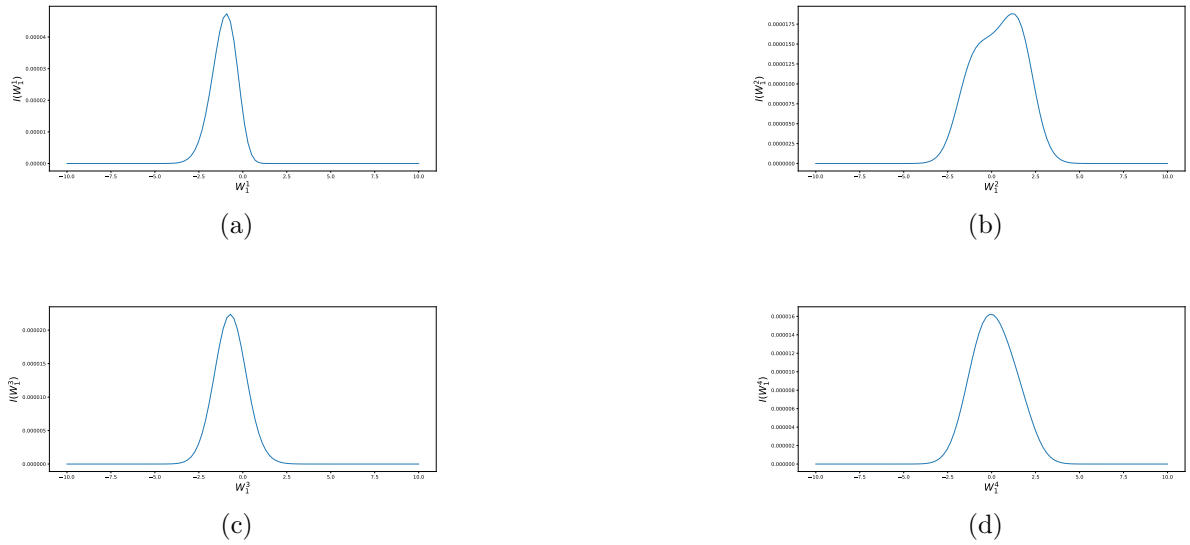

(a) (b)

(c) (d)

Figure 15: Plotting the integrand I (in (8)) as a function of W_1 coordinates for $H = 0.07$ and $N = 4$.

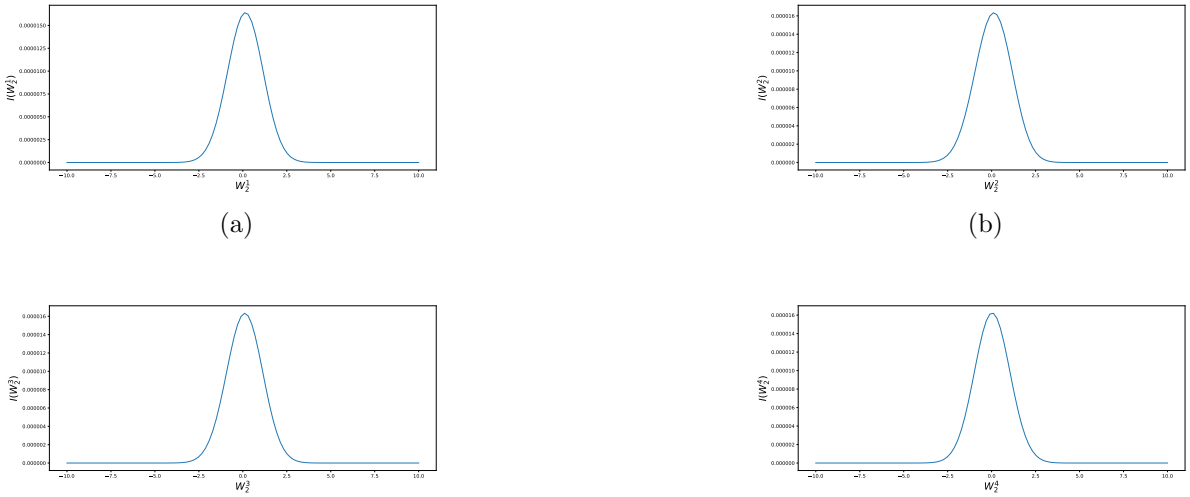

(a) (b)

(c) (d)

Figure 16: Plotting the integrand I (in (8)) as a function of W_2 coordinates for $H = 0.07$ and $N = 4$.

4.3.2 Comparing the mixed differences rates

In this section, we compare the mixed differences (first and second differences) rates for the standard case against the case where we do a partial change of measure wrt W_1 coordinates (see Section 3.2), for the case of $H = 0.07$ and $N = 4$ time steps. From figures (20,22,21,23), we may notice that we face a bad behavior for the second differences, for the case without change of measure, which may

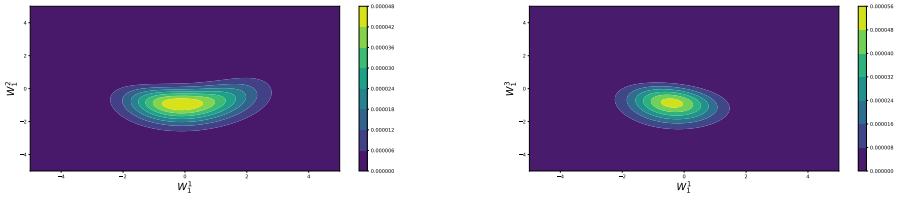

(a) (b)

Figure 17: Two dimensional Plotting of the integrand I (in (8)) for $H = 0.07$ and $N = 4$, a) function of W_1^1 and W_1^2 , b) function of W_1^1 and W_1^3

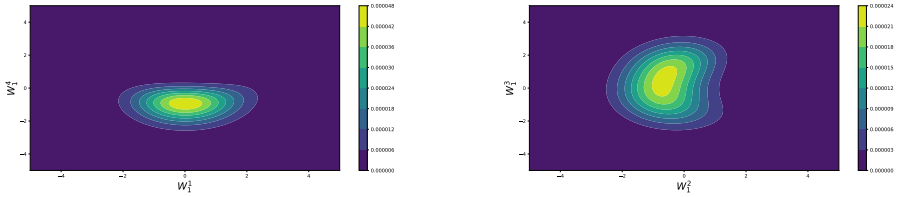

(a) (b)

Figure 18: Two dimensional Plotting of the integrand I (in (8)) for $H = 0.07$ and $N = 4$, a) function of W_1^1 and W_1^4 , b) function of W_1^2 and W_1^3

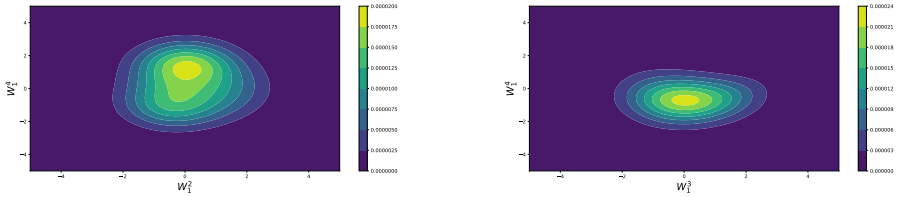

(a) (b)

Figure 19: Two dimensional Plotting of the integrand I (in (8)) for $H = 0.07$ and $N = 4$, a) function of W_1^2 and W_1^4 , b) function of W_1^3 and W_1^4

explain the observed instability by MISC. This bad behavior is resolved when doing the partial change of measure. We obtained better results when using a measure change based on spectral decomposition rather than Cholesky decomposition. therefore by doing the change of measure, we expect to obtain a more robust MISC solver.

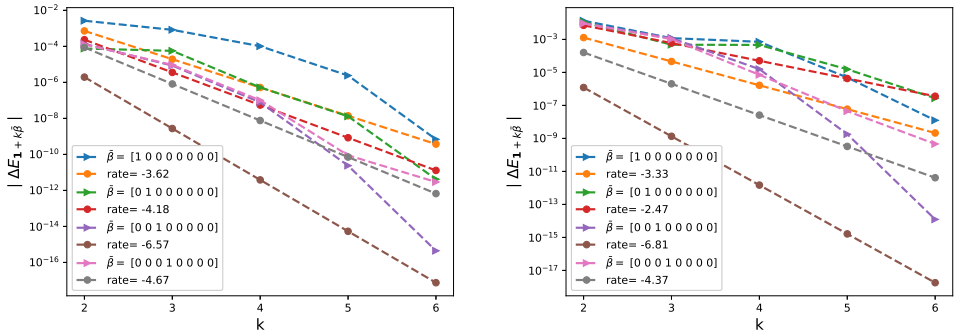

(a) (b)

Figure 20: The rate of convergence of first order differences $|\Delta E_\beta|$ $(\beta = \mathbf{1} + k\overline{\beta}))$, for W^1, for $K = 1$, $H = 0.07$: a) Without measure change b) With measure change

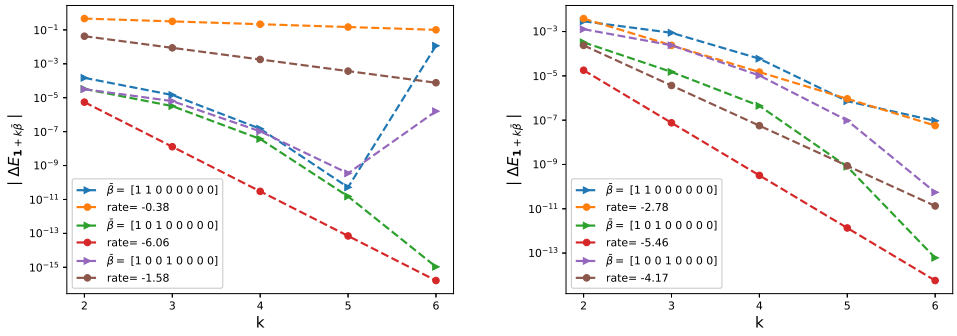

(a) (b)

Figure 21: The rate of convergence of second order differences $|\Delta E_\beta|$ $(\beta = \mathbf{1} + k\overline{\beta}))$, for W^1, for $K = 1$, $H = 0.07$: a) Without measure change b) With measure change

4.4 Numerical results for the case with change of measure

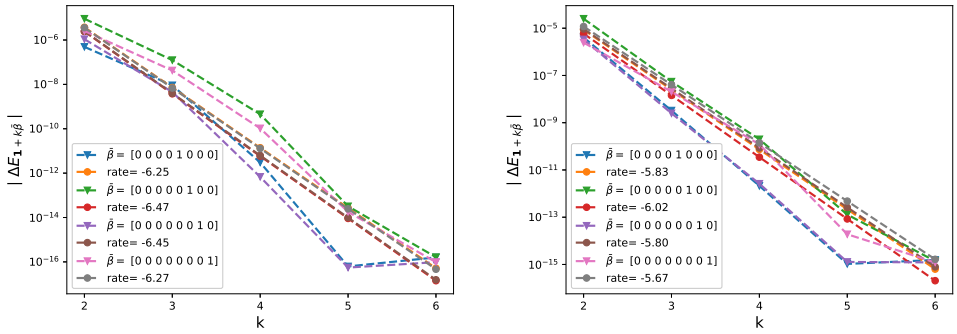

(a) (b)

Figure 22: The rate of convergence of first order differences $|\Delta E_\beta|$ ($\beta = \mathbf{1} + k\overline{\beta}$)), for W^2, for $K = 1$, $H = 0.07$: a) Without measure change b) With measure change

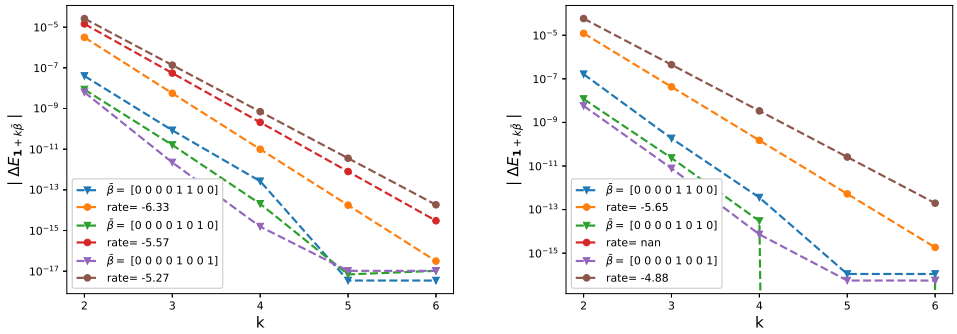

(a) (b)

Figure 23: The rate of convergence of second order differences $|\Delta E_\beta|$ ($\beta = \mathbf{1} + k\overline{\beta}$)), for W^2, for $K = 1$, $H = 0.07$: a) Without measure change b) With measure change

4.4.1 Weak error plots

In this section, I include the results of weak error rates for the case with change of measure for both cases without and with Richardson extrapolation, for $H = 0.07$. The reference solution was computed with $N = 500$ time steps. We note that we limit the maximum number of changed coordinates up to 4, due to practical purposes related to the optimization procedure. We note that the weak errors plotted here corresponds to relative errors.

Without Richardson extrapolation

From figure 24), we see that for $H = 0.07$, we get a weak error of order Δt. The upper and lower bounds are 95% confidence interval. In table 10, we show the values of relative weak error. it is clear that compared to the values observed in table 4, we almost observe the same behavior, which may tell us that the change of measure procedure maybe not needed to improve results since we are adding complexity without observing gains in terms of the weak error.

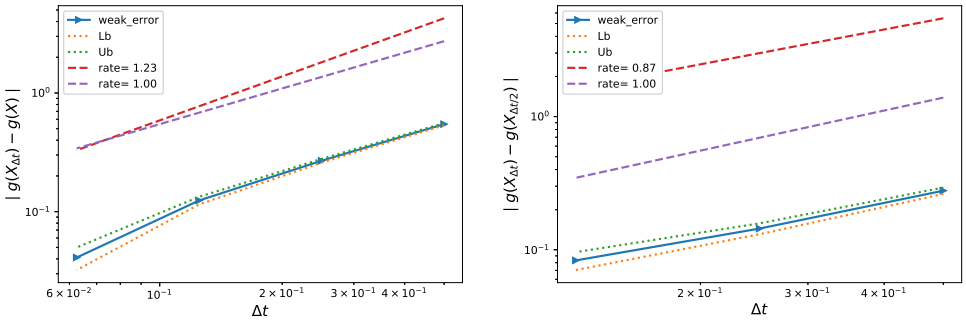

(a) (b)

Figure 24: The rate of convergence of the weak error for $H = 0.07$ $K = 1$, without Richardson extraploation, using MC with $M = 10^5$: a) $|\mathrm{E}\left[g(X_{\Delta t})\right] - g(X)|$ b) $\left|\mathrm{E}\left[g(X_{\Delta t}) - g(X_{\Delta t/2})\right]\right|$

Method \Steps	2	4	8	16
MC method ($M = 10^6$)	**0.5462**	**0.2686**	**0.1243**	**0.0411**

Table 10: Relative error of Call option price of the different tolerances for different number of time steps. Case $K = 1$, $H = 0.07$, without Richardson extrapolation

With Richardson extrapolation (level 1)

From figure 25 , we see that for $H = 0.07$, we get a weak error of order Δt^2. The upper and lower bounds are 95% confidence interval. In table 11, we show the corresponding results. Comparing to the results without change of measure (see figure 5 and table 6), we got worser weak error values after the change of measure. We provide a potential explanation of the possible cause of this in Section 4.4.2.

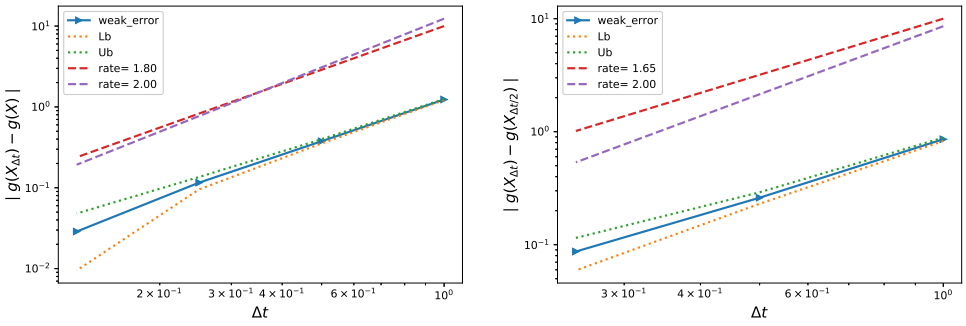

(a) (b)

Figure 25: The rate of convergence of the weak error for $H = 0.07$ $K = 1$, with Richardson extraploation, using MC with $M = 10^6$: a) $\left|\mathrm{E}\left[2g(X_{\Delta t/2}) - g(X_{\Delta t})\right] - g(X)\right|$ b) $\left|\mathrm{E}\left[3g(X_{\Delta t/2}) - g(X_{\Delta t}) - 2g(X_{\Delta t/4})\right]\right|$

Method \Steps	$1-2$	$2-4$	$4-8$	$8-16$
MC method ($M = 10^6$)	**1.2339**	**0.3763**	**0.1158**	**0.0288**

Table 11: Relative error of Call option price of the different tolerances for different number of time steps. Case $K = 1$, $H = 0.07$, using Richardson extrapolation (level 1)

4.4.2 Plotting the Richardson integrand for the change of measure

In this section, We try to investigate the reason of having worse weak rates than the case without change of measure. We plot the Richardson integrand used for the change of measure, for $H = 0.07$ and for two cases of time steps in the coarse level of Richardson extrapolation ($N \in \{1, 2\}$) . We conclude from those plots that the extrapolated formula is not very appropriate since we have a more complex function (bi-modal functions or higher as we go deeper for the levels of Richardson extrapolation). As a result, we think it is better to focus on the case without applying a change of measure.

N=1, H=0.07

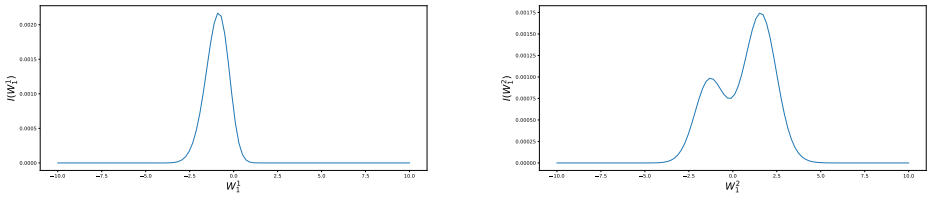

(a) (b)

Figure 26: Plotting the integrand I (in (8)) when using Richardson extrapolation(level 1) as a function of W^1 coordinates for $H = 0.07$ and $N = 1$ in the coarser level.

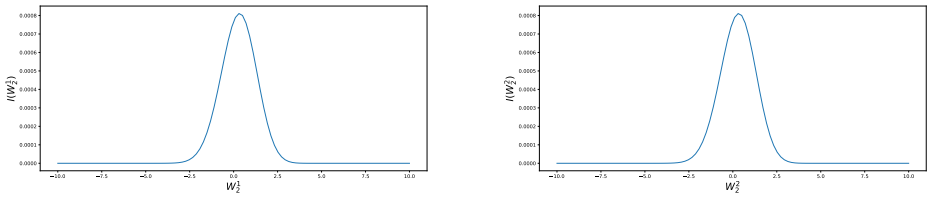

(a) (b)

Figure 27: Plotting the integrand I (in (8)) when using Richardson extrapolation(level 1) as a function of W^2 coordinates for $H = 0.07$ and $N = 1$ in the coarser level.

N=2, H=0.07

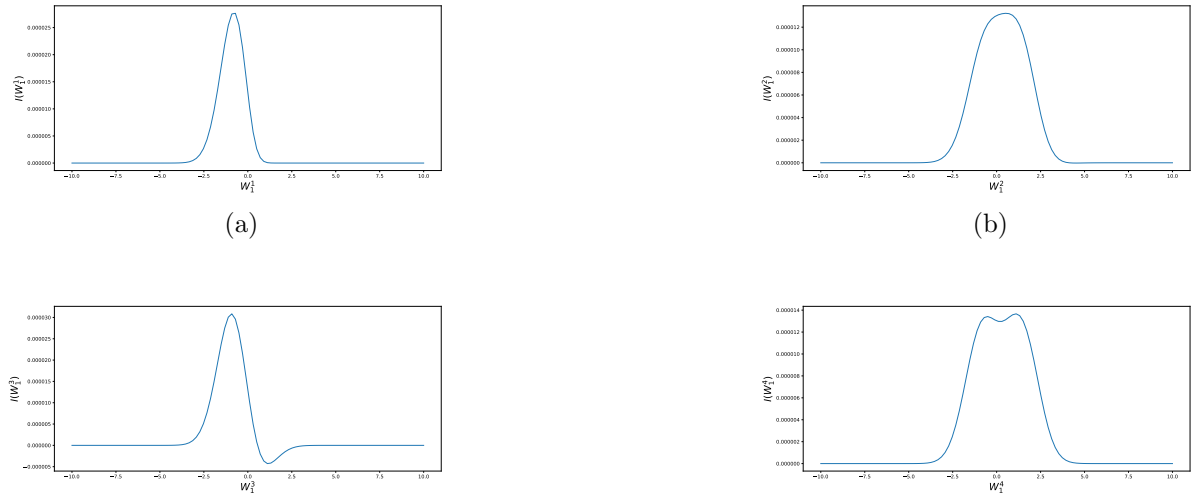

(a) (b)

(c) (d)

Figure 28: Plotting the integrand I (in (8)) when using Richardson extrapolation(level 1) as a function of W^1 coordinates for $H = 0.07$ and $N = 2$ in the coarser level.

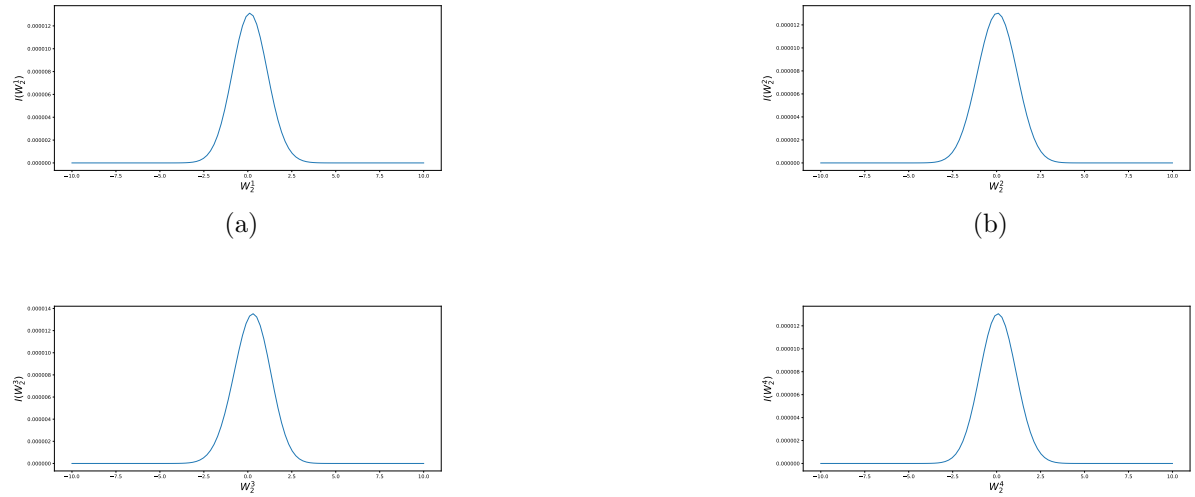

(a) (b)

(c) (d)

Figure 29: Plotting the integrand I (in (8)) when using Richardson extrapolation(level 1) as a function of W^2 coordinates for $H = 0.07$ and $N = 2$ in the coarser level.

References Cited

[1] Pierre Bajgrowicz, Olivier Scaillet, and Adrien Treccani. Jumps in high-frequency data: Spurious detections, dynamics, and news. *Management Science*, 62(8):2198–2217, 2015.

[2] Christian Bayer, Peter Friz, and Jim Gatheral. Pricing under rough volatility. *Quantitative Finance*, 16(6):887–904, 2016.

[3] Christian Bayer, Peter K Friz, Paul Gassiat, Joerg Martin, and Benjamin Stemper. A regularity structure for rough volatility. *arXiv preprint arXiv:1710.07481*, 2017.

[4] Christian Bayer, Peter K Friz, Archil Gulisashvili, Blanka Horvath, and Benjamin Stemper. Short-time near-the-money skew in rough fractional volatility models. *arXiv preprint arXiv:1703.05132*, 2017.

[5] Mikkel Bennedsen, Asger Lunde, and Mikko S Pakkanen. Decoupling the short-and long-term behavior of stochastic volatility. *arXiv preprint arXiv:1610.00332*, 2016.

[6] Mikkel Bennedsen, Asger Lunde, and Mikko S Pakkanen. Hybrid scheme for brownian semistationary processes. *Finance and Stochastics*, 21(4):931–965, 2017.

[7] Lorenzo Bergomi. Smile dynamics ii. 2005.

[8] F. Biagini, Y. Hu, B. Øksendal, and T. Zhang. *Stochastic Calculus for Fractional Brownian Motion and Applications*. Probability and Its Applications. Springer London, 2008.

[9] R. Carmona and M.R. Tehranchi. *Interest Rate Models: an Infinite Dimensional Stochastic Analysis Perspective*. Springer Finance. Springer Berlin Heidelberg, 2007.

[10] Kim Christensen, Roel CA Oomen, and Mark Podolskij. Fact or friction: Jumps at ultra high frequency. *Journal of Financial Economics*, 114(3):576–599, 2014.

[11] Laure Coutin. An introduction to (stochastic) calculus with respect to fractional brownian motion. In *Séminaire de Probabilités XL*, pages 3–65. Springer, 2007.

[12] Martin Forde and Hongzhong Zhang. Asymptotics for rough stochastic volatility models. *SIAM Journal on Financial Mathematics*, 8(1):114–145, 2017.

[13] Masaaki Fukasawa. Asymptotic analysis for stochastic volatility: martingale expansion. *Finance and Stochastics*, 15(4):635–654, 2011.

[14] Jim Gatheral. *The volatility surface: a practitioner's guide*, volume 357. John Wiley & Sons, 2011.

[15] Jim Gatheral, Thibault Jaisson, Andrew Lesniewski, and Mathieu Rosenbaum. Volatility is rough, part 2: Pricing.

[16] Jim Gatheral, Thibault Jaisson, and Mathieu Rosenbaum. Volatility is rough. *arXiv preprint arXiv:1410.3394*, 2014.

[17] Paul Glasserman. *Monte Carlo methods in financial engineering*. Springer, New York, 2004.

[18] Abdul-Lateef Haji-Ali, Fabio Nobile, Lorenzo Tamellini, and Raul Tempone. Multi-index stochastic collocation for random pdes. *Computer Methods in Applied Mechanics and Engineering*, 306:95–122, 2016.

[19] Antoine Jacquier, Claude Martini, and Aitor Muguruza. On vix futures in the rough bergomi model. *Quantitative Finance*, 18(1):45–61, 2018.

[20] Antoine Jacquier, Mikko S Pakkanen, and Henry Stone. Pathwise large deviations for the rough bergomi model. *arXiv preprint arXiv:1706.05291*, 2017.

[21] Benoit B Mandelbrot and John W Van Ness. Fractional brownian motions, fractional noises and applications. *SIAM review*, 10(4):422–437, 1968.

[22] Tina Marquardt et al. Fractional lévy processes with an application to long memory moving average processes. *Bernoulli*, 12(6):1099–1126, 2006.

[23] Ryan McCrickerd and Mikko S Pakkanen. Turbocharging monte carlo pricing for the rough bergomi model. *arXiv preprint arXiv:1708.02563*, 2017.

[24] David Nualart. *The Malliavin calculus and related topics*, volume 1995. Springer, 2006.

[25] Marc Romano and Nizar Touzi. Contingent claims and market completeness in a stochastic volatility model. *Mathematical Finance*, 7(4):399–412, 1997.

A additional results for Call prices under rBergomi for different

A.1 Case $H = 0.43$, Call prices for different methods

Method \Steps	2	4	8	16
MISC ($TOl = 2.10^{-1}$)	0.1140	0.0961	0.0848	0.0769
MISC ($TOl = 10^{-1}$)	0.1140	0.0961	0.0871	–
MISC ($TOl = 10^{-2}$)	0.1077	0.0944	0.0838	–
MISC ($TOl = 10^{-3}$)	–	0.0921	0.0819	–
MC method ($M = 10^6$)	0.1079 (1.55e−04)	0.0921 (9.65e−05)	0.0822 (7.61e−05)	0.0769 (6.65e−05)

Table 12: Call option price of the different methods for different number of time steps. Case $K = 1$, $H = 0.43$, without Richardson extrapolation. The values between parentheses in the tables are the standard errors for MC method

Method \Steps	$1-2$	$2-4$	$4-8$	$8-16$
MISC ($TOl = 5.10^{-1}$)	0.1357	0.0783	0.0735	0.0714
MISC ($TOl = 10^{-1}$)	0.1357	0.0783	0.0785	–
MISC ($TOl = 10^{-2}$)	0.1237	0.0781	0.0745	–
MISC ($TOl = 10^{-3}$)	0.1224	0.0766	0.0720	–
MISC ($TOl = 5.10^{-4}$)	0.1221	0.0763	–	–

Table 13: Call option price of the different methods for different number of time steps. Case $K = 1$, $H = 0.43$, using Richardson extrapolation (level 1)

Method \Steps	$1-2-4$	$2-4-8$	$4-8-16$
MISC ($TOl = 5.10^{-1}$)	0.0591	0.0719	0.0708
MISC ($TOl = 2.10^{-1}$)	0.0591	–	0.0711
MISC ($TOl = 10^{-1}$)	0.0567	–	–
MISC ($TOl = 5.10^{-2}$)	0.0733	–	–

Table 14: Call option price of the different methods for different number of time steps. Case $K = 1$, $H = 0.43$, using Richardson extrapolation (level 2)

A.2 Case $H = 0.07$, Call prices for different methods

Method \Steps	2	4	8	16
MISC ($TOl = 5.10^{-1}$)	0.1082	0.0917	0.0872	0.0732
MC method ($M = 10^6$)	0.1246 (1.05e−03)	0.1000 (1.86e−04)	0.0904 (1.35e−04)	0.0850 (1.08e−04)

Table 15: Call option price of the different methods for different number of time steps. Case $K = 1$, without Richardson extrapolation. The values between parentheses in the tables are the standard errors for MC method

Method \Steps	$1-2$	$2-4$	$4-8$	$8-16$
MISC ($TOl = 5.10^{-1}$)	0.1242	0.0752	0.0682	0.0665
MISC ($TOl = 16.10^{-2}$)	–	–	0.0682	0.0795
MISC ($TOl = 10^{-1}$)	–	–	0.0658	–
MISC ($TOl = 5.10^{-2}$)	–	–	0.0799	–
MISC ($TOl = 10^{-2}$)	–	–	–	–

Table 16: Call option price of the different methods for different number of time steps. Case $K = 1$, $H = 0.07$, using Richardson extrapolation (level 1)

Method \Steps	$1-2-4$	$2-4-8$	$4-8-16$
MISC ($TOl = 10^{-1}$)	0.0589	0.0668	0.079
MISC ($TOl = 7.10^{-2}$)	0.0554	0.0810	–
MISC ($TOl = 5.10^{-2}$)	0.0406	–	–
MISC ($TOl = 10^{-2}$)	0.0654	–	–

Table 17: Call option price of the different methods for different number of time steps. Case $K = 1$, $H = 0.07$, using Richardson extrapolation (level 2)

B additional results

B.1 Integrand plotting wrt different random inputs N=2, H=0.43

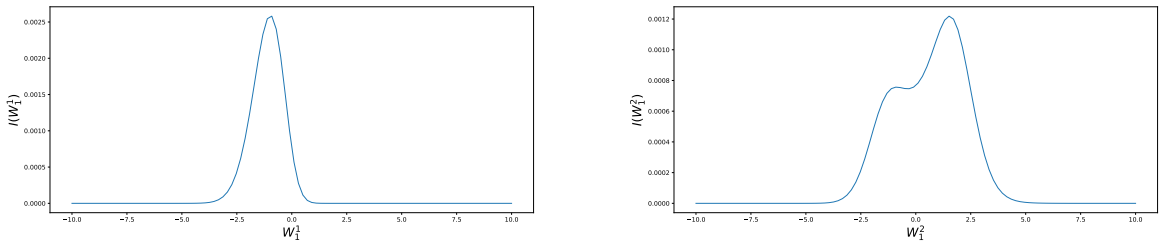

(a) (b)

Figure 30: Plotting the integrand I (in (8)) as a function of W^1 coordinates for $H = 0.43$ and $N = 2$.

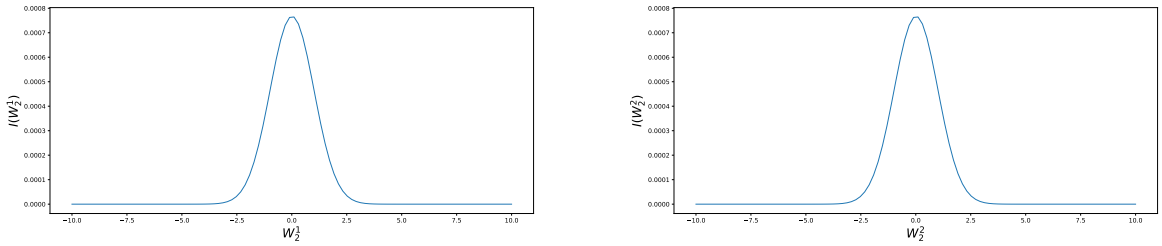

(a) (b)

Figure 31: Plotting the integrand I (in (8)) as a function of W^2 coordinates for $H = 0.43$ and $N = 2$.

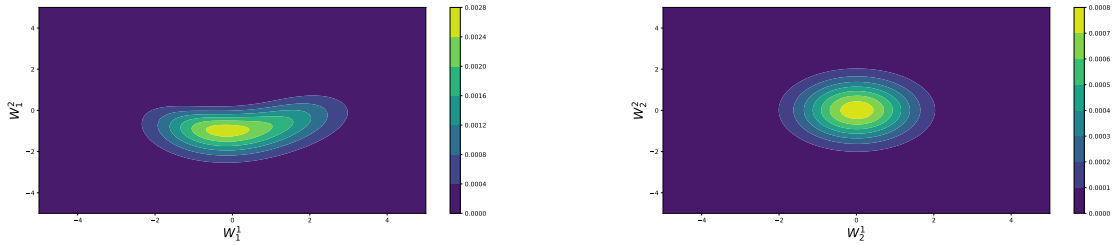

(a) (b)

Figure 32: Two dimensional Plotting of the integrand I (in (8)) for $H = 0.43$ and $N = 2$, a) function of W^1 coordinates, b) function of W^2 coordinates

B.2 Integrand plotting wrt different random inputs: N=4, H=0.43

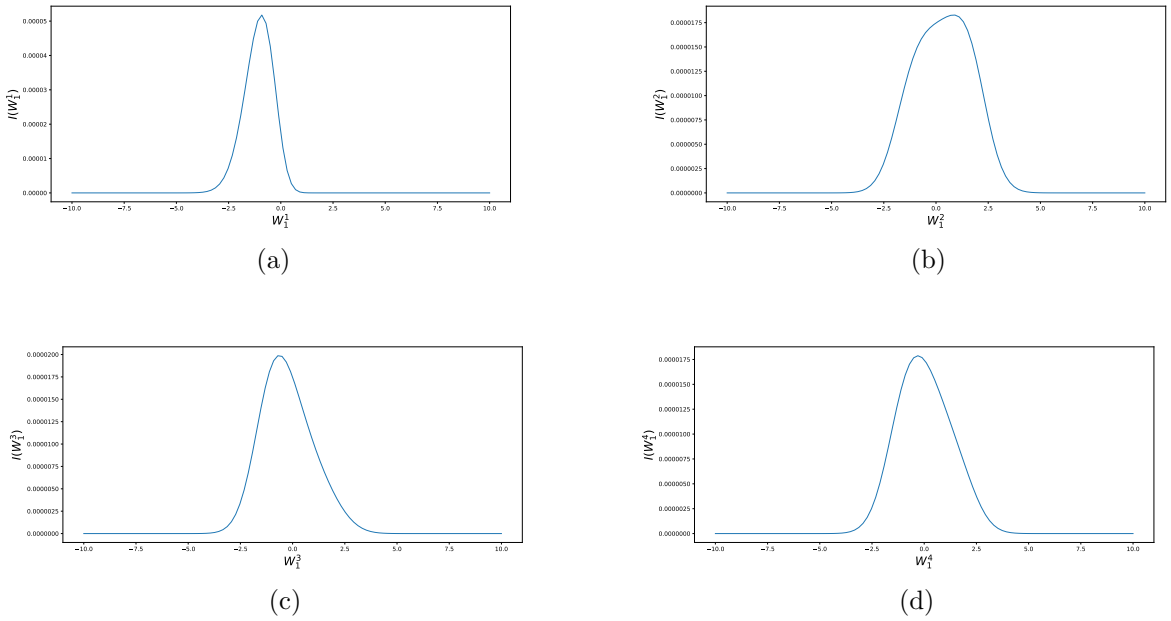

(a) (b)

(c) (d)

Figure 33: Plotting the integrand I (in (8)) as a function of W^1 coordinates for $H = 0.43$ and $N = 4$.

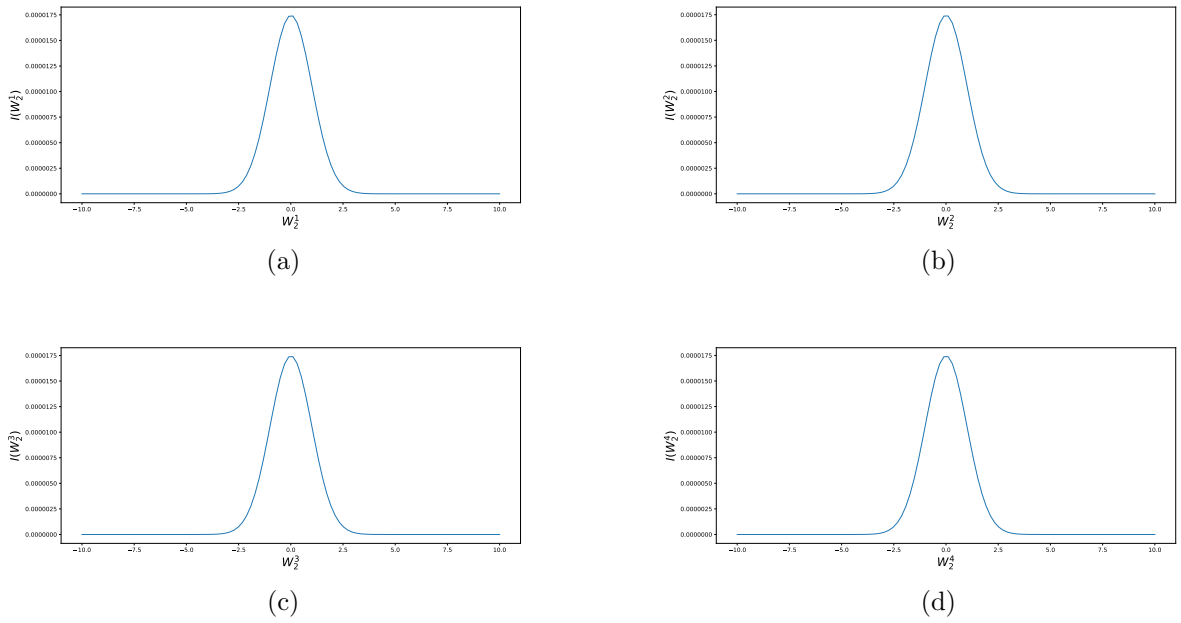

(a) (b)

(c) (d)

Figure 34: Plotting the integrand I (in (8)) as a function of W^2 coordinates for $H = 0.43$ and $N = 4$.

B.3 Motivation of the hierarchical representation and investigating the effect with respect to H

In this section, we motivate the idea of using hierarchical representation (Brownian bridge construction) for buiding W^1 and W^2.

B.3.1 Totally Hierarchical

In this section, we do both hierarchical transformation, based on brownian bridges, for both directions W^1 and W^2. We see clearly from figures (35,36) the advantage of buiding W^2 in a hierarchical fashion as W^1

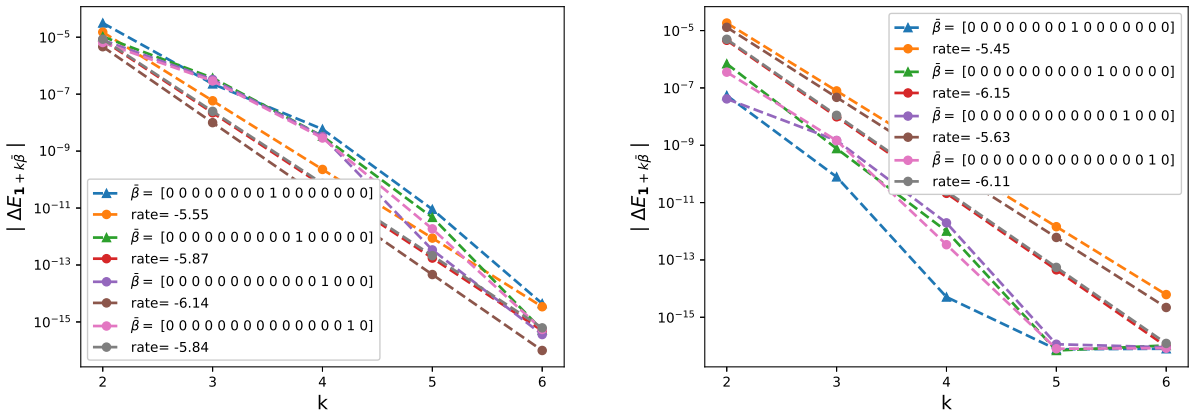

(a) (b)

Figure 35: The rate of convergence of first order differences $|\Delta E_\beta|$ $(\beta = \mathbf{1} + k\bar{\beta})$ for $K = 1$: a) Without hierarchical for W_2 b) With hierarchical for W_2

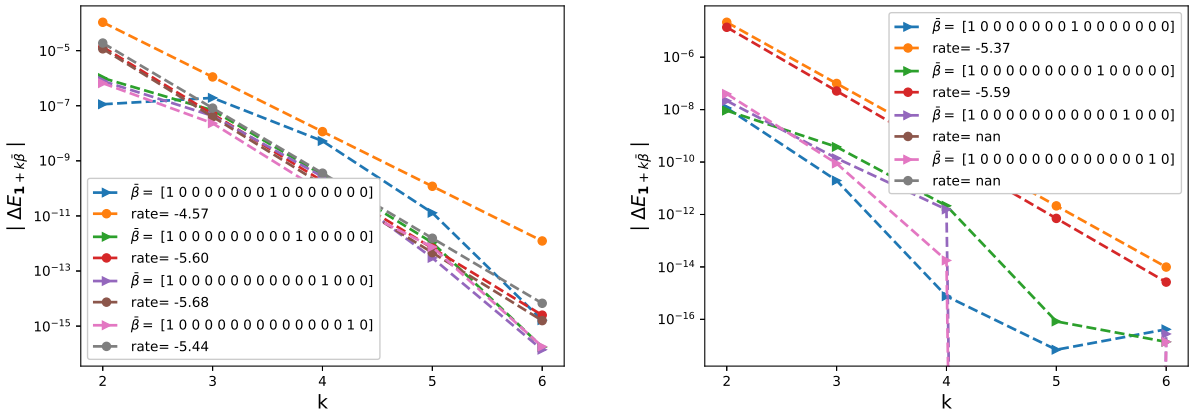

(a) (b)

Figure 36: The rate of convergence of second order differences $|\Delta E_\beta|$ $(\beta = \mathbf{1} + k\bar{\beta})$ for $K = 1$: a) Without hierarchical for W_2 b) With hierarchical for W_2

B.3.2 Hierarchical

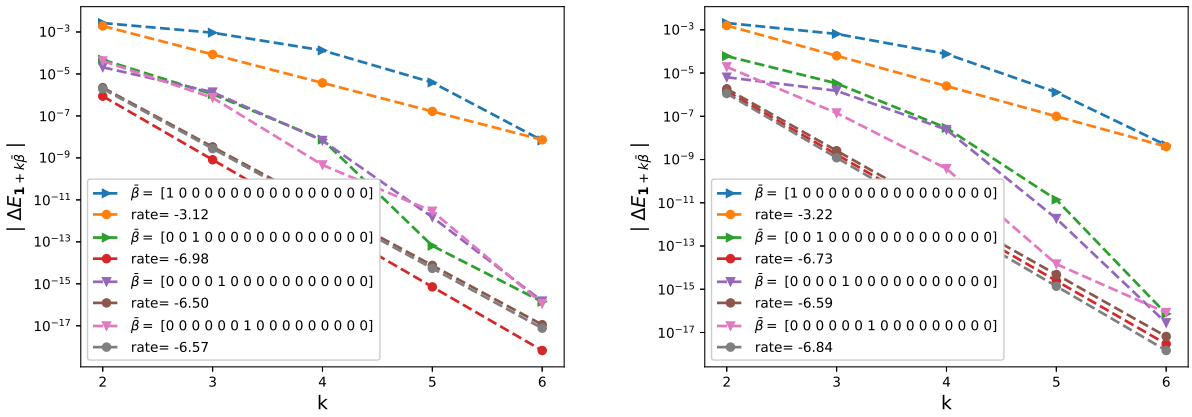

(a) (b)

Figure 37: The rate of convergence of first order differences $|\Delta E_\beta|$ $(\beta = \mathbf{1} + k\bar{\beta}))$ for $K = 1$: a) $H = 0.43$ b) $H = 0.07$

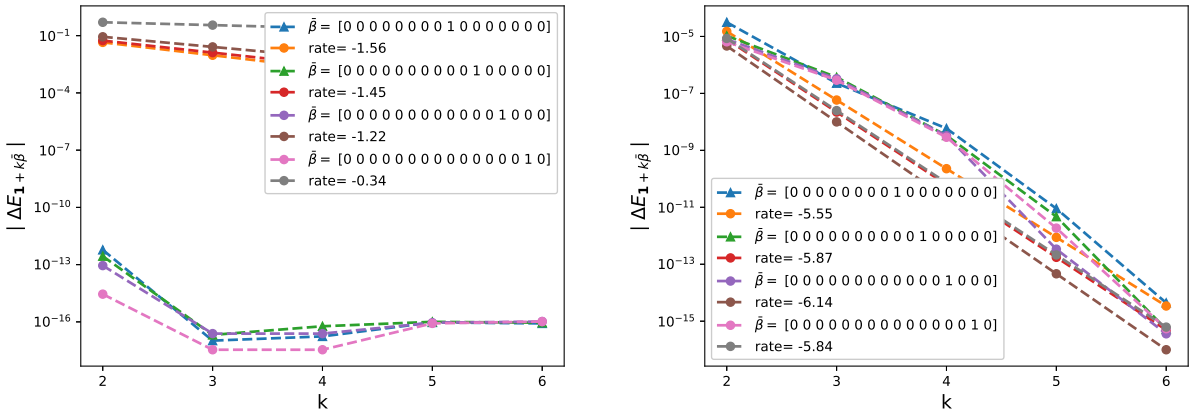

(a) (b)

Figure 38: The rate of convergence of first order differences $|\Delta E_\beta|$ $(\beta = \mathbf{1} + k\bar{\beta}))$ for $K = 1$: a) $H = 0.43$ b) $H = 0.07$

B.3.3 Non Hierarchical

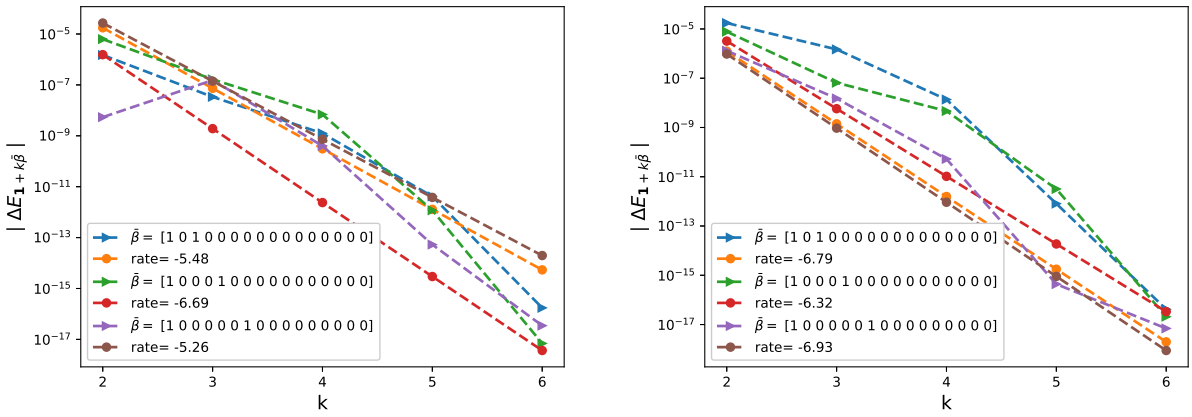

(a) (b)

Figure 39: The rate of convergence of mixed order differences $|\Delta E_\beta|$ $(\beta = \mathbf{1} + k\bar{\beta})$ for $K = 1$: a) $H = 0.43$ b) $H = 0.07$

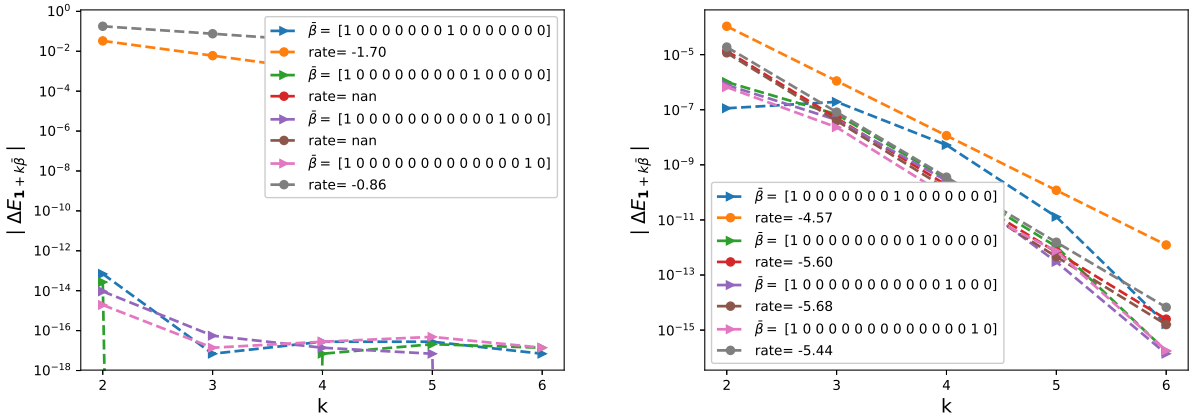

(a) (b)

Figure 40: The rate of convergence of mixed order differences $|\Delta E_\beta|$ $(\beta = \mathbf{1} + k\bar{\beta})$ for $K = 1$: a) $H = 0.43$ b) $H = 0.07$

B.4 Investigating mixed differences wrt ρ

N=4, K=1

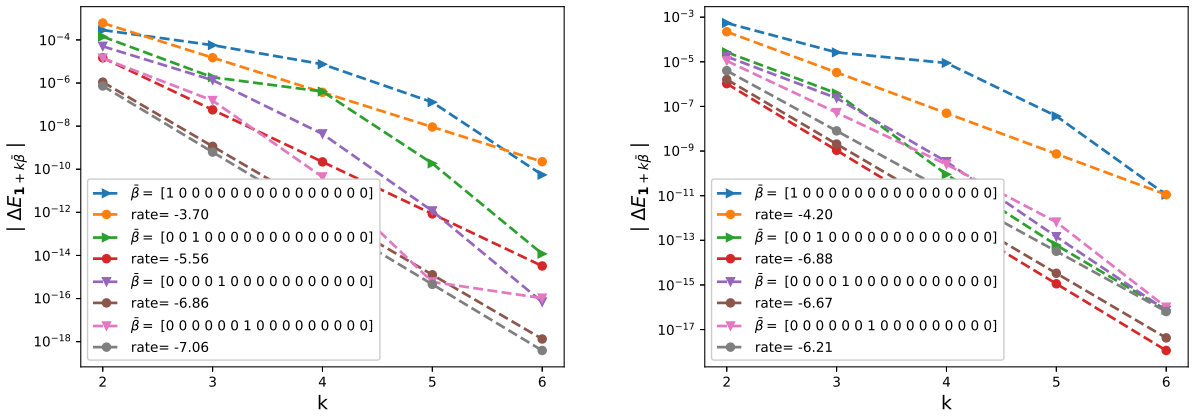

(a) (b)

Figure 41: The rate of convergence of first order differences $|\Delta E_\beta|$ $(\beta = \mathbf{1} + k\bar{\beta}))$ for $K = 1$: a) $H = 0.43$ b) $H = 0.07$

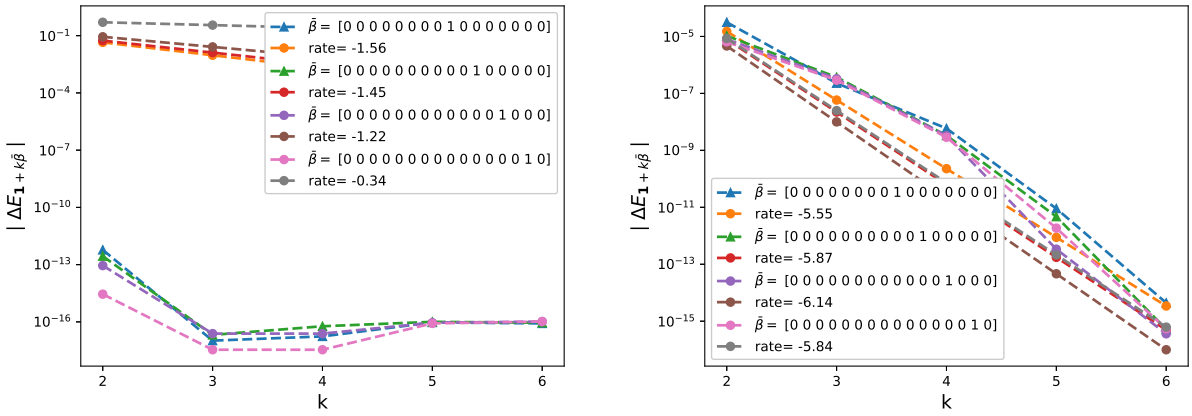

(a) (b)

Figure 42: The rate of convergence of first order differences $|\Delta E_\beta|$ $(\beta = \mathbf{1} + k\bar{\beta}))$ for $K = 1$: a) $H = 0.43$ b) $H = 0.07$

N=8, K=1

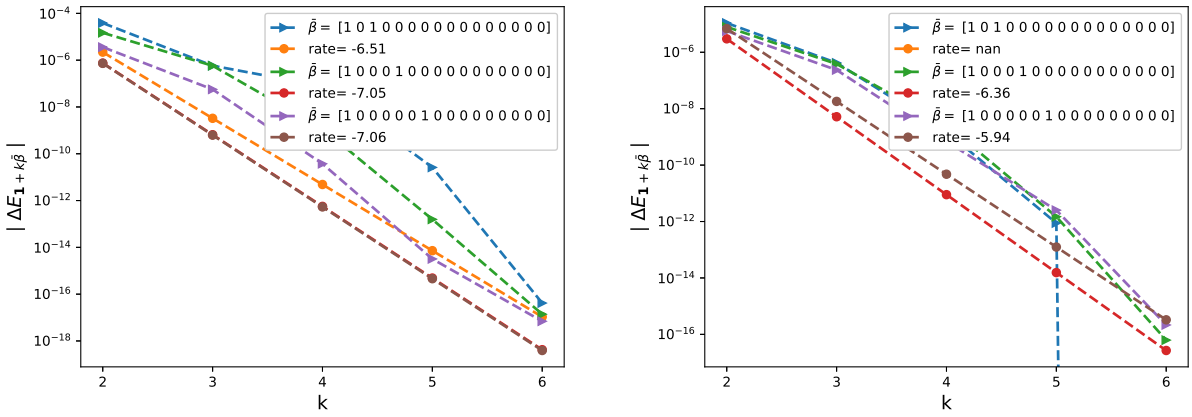

(a) (b)

Figure 43: The rate of convergence of mixed order differences $|\Delta E_\beta|$ $(\beta = \mathbf{1} + k\overline{\beta})$ for $K = 1$: a) $H = 0.43$ b) $H = 0.07$

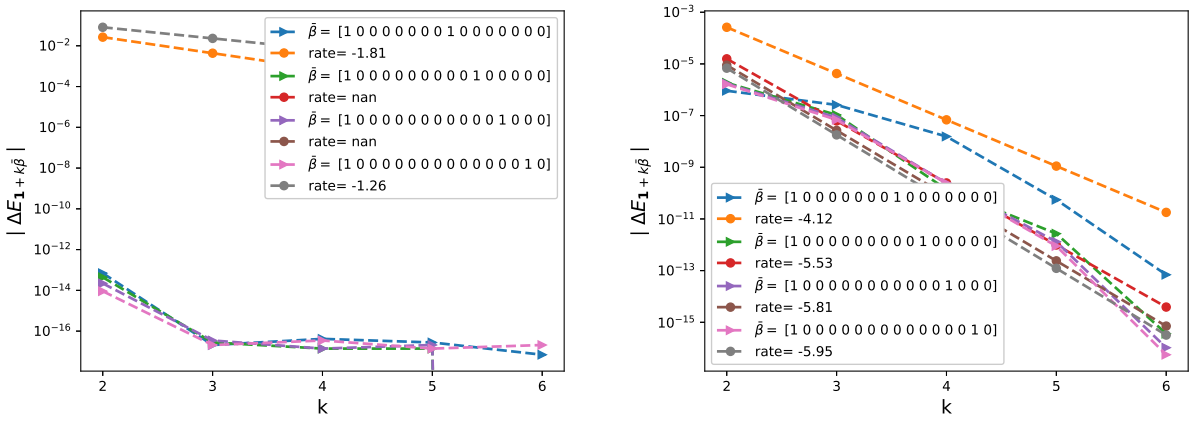

(a) (b)

Figure 44: The rate of convergence of mixed order differences $|\Delta E_\beta|$ $(\beta = \mathbf{1} + k\overline{\beta})$ for $K = 1$: a) $H = 0.43$ b) $H = 0.07$

N=4, K=0.8

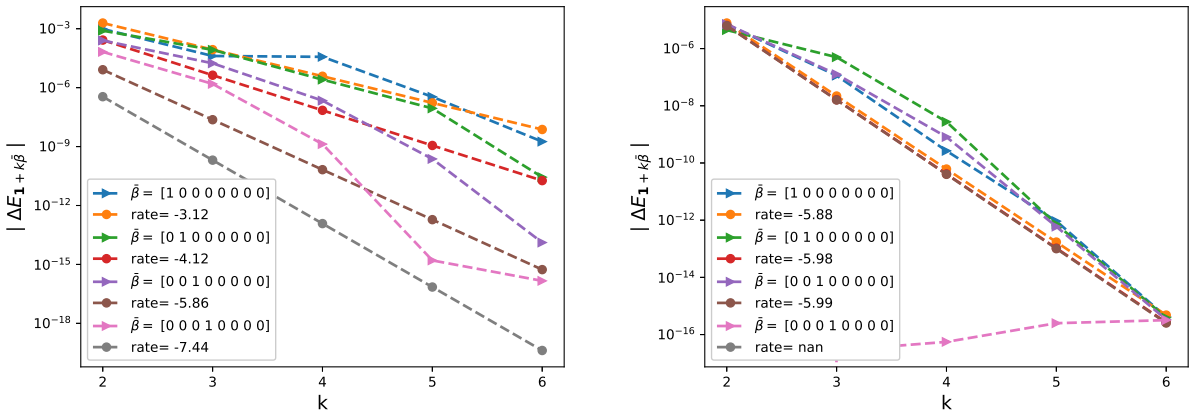

(a) (b)

Figure 45: The rate of convergence of first order differences $|\Delta E_\beta|$ $(\beta = \mathbf{1} + k\bar{\beta})$ for $K = 1$: a) $\rho = -0.9$ b) $\rho = 0$.

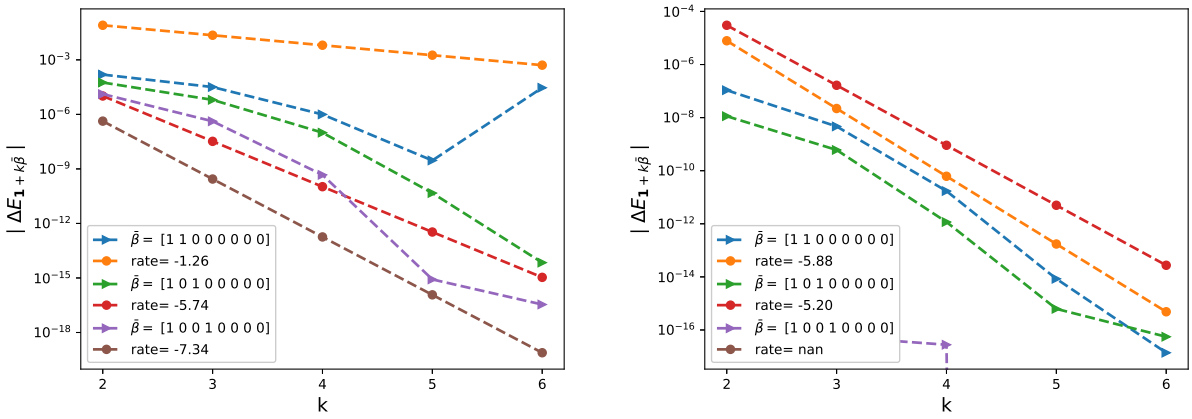

(a) (b)

Figure 46: The rate of convergence of mixed order differences $|\Delta E_\beta|$ $(\beta = \mathbf{1} + k\bar{\beta})$): a) $\rho = -0.9$ b) $\rho = 0$.

N=8, K=0.8

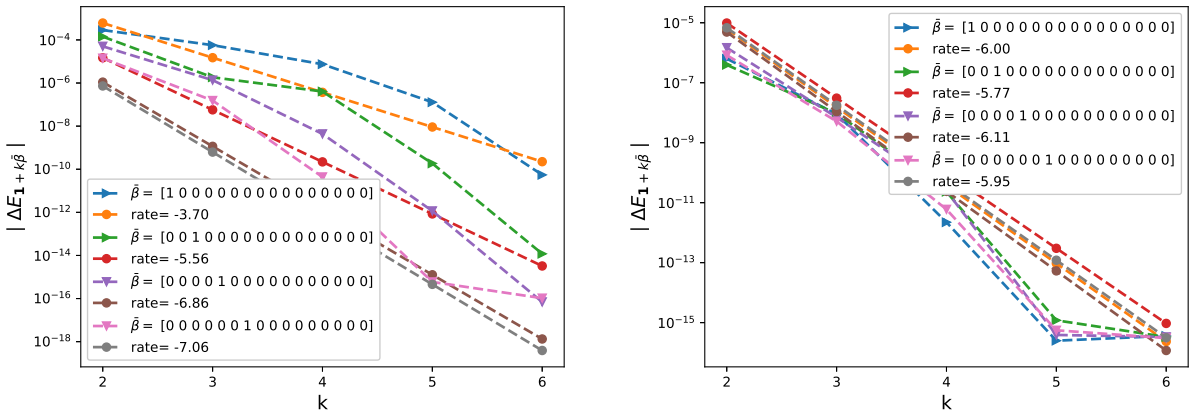

(a) (b)

Figure 47: The rate of convergence of first order differences $|\Delta E_\beta|$ $(\beta = \mathbf{1} + k\bar{\beta})$): a) $\rho = -0.9$ b) $\rho = 0$.

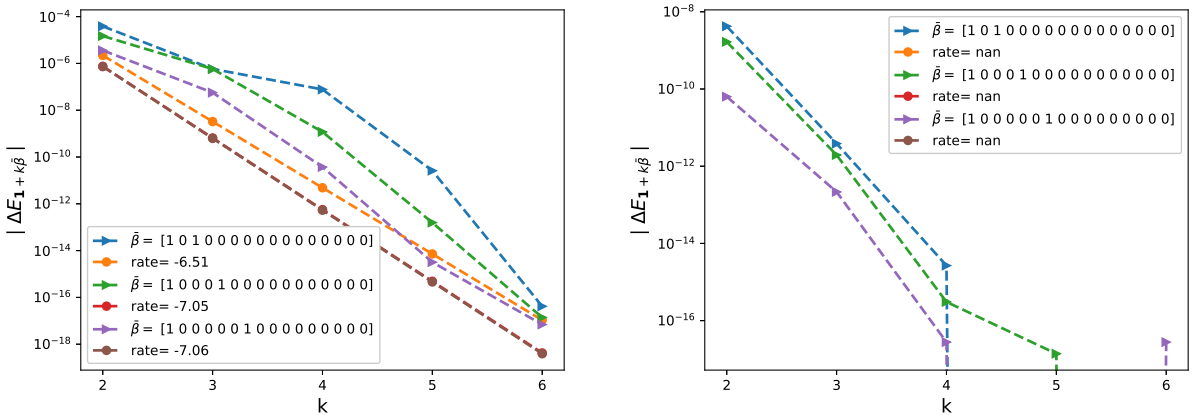

(a) (b)

Figure 48: The rate of convergence of mixed order differences $|\Delta E_\beta|$ $(\beta = \mathbf{1} + k\bar{\beta})$): a) $\rho = -0.9$ b) $\rho = 0$.

B.5 Investigating mixed differences wrt ξ

N=4, K=1

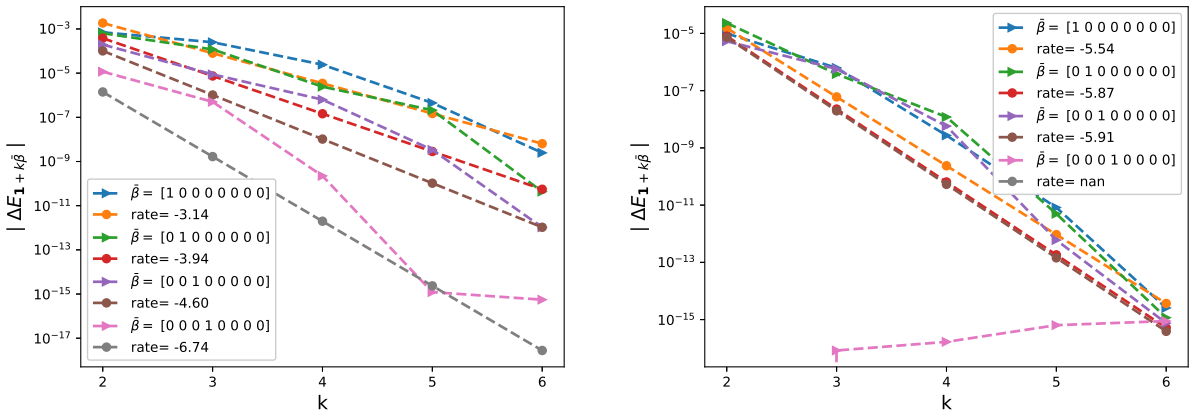

(a) (b)

Figure 49: The rate of convergence of first order differences $|\Delta E_\beta|$ ($\beta = \mathbf{1} + k\bar{\beta}$)): a) $\rho = -0.9$ b) $\rho = 0$.

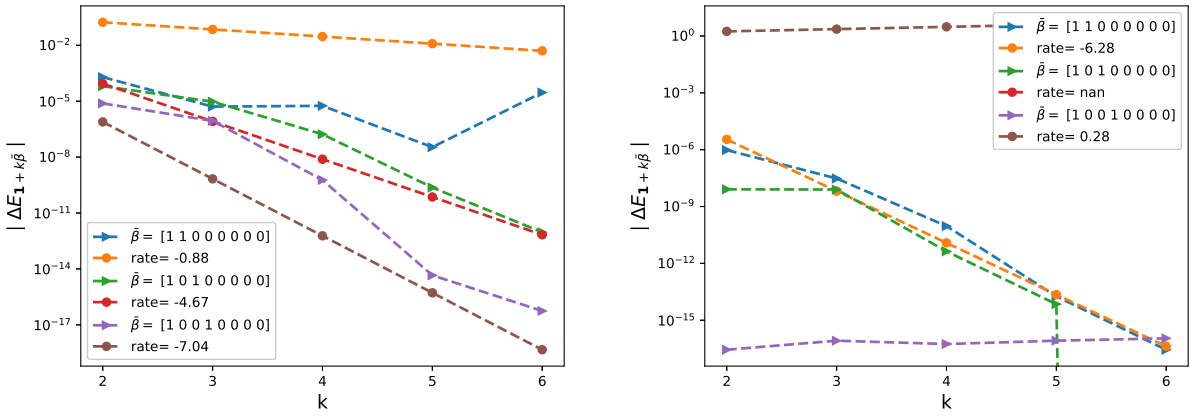

(a) (b)

Figure 50: The rate of convergence of mixed order differences $|\Delta E_\beta|$ ($\beta = \mathbf{1} + k\bar{\beta}$)): a) $\rho = -0.9$ b) $\rho = 0$.

N=8, K=1

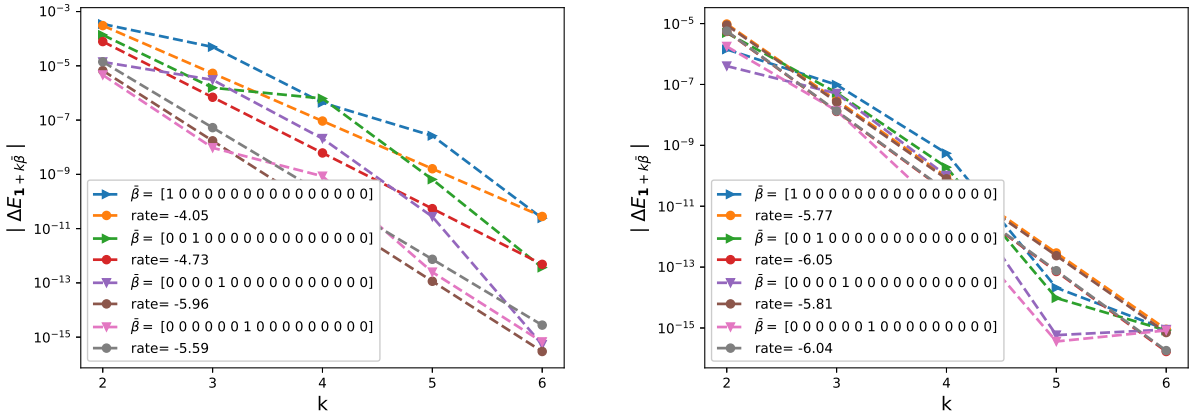

(a) (b)

Figure 51: The rate of convergence of first order differences $|\Delta E_\beta|$ $(\beta = \mathbf{1} + k\bar{\beta})$): a) $\rho = -0.9$ b) $\rho = 0$.

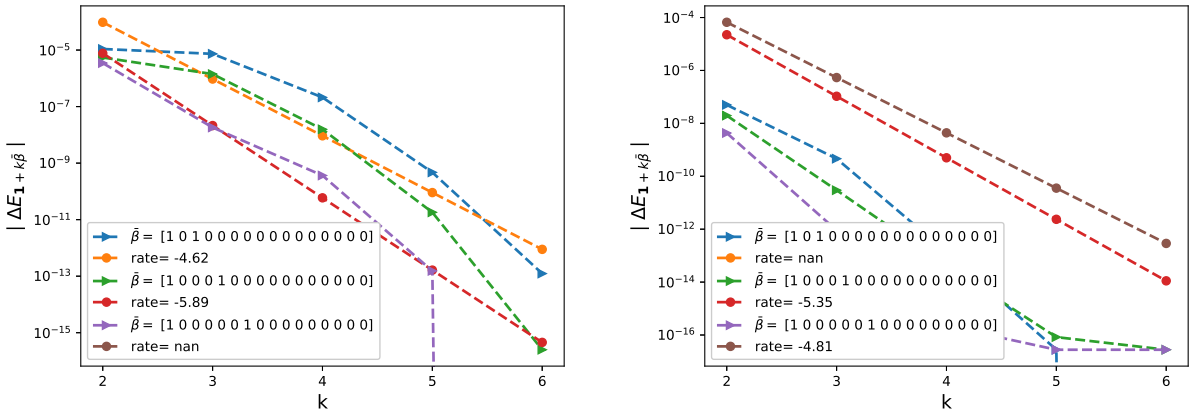

(a) (b)

Figure 52: The rate of convergence of mixed order differences $|\Delta E_\beta|$ $(\beta = \mathbf{1} + k\bar{\beta})$): a) $\rho = -0.9$ b) $\rho = 0$.

N=4, K=0.8

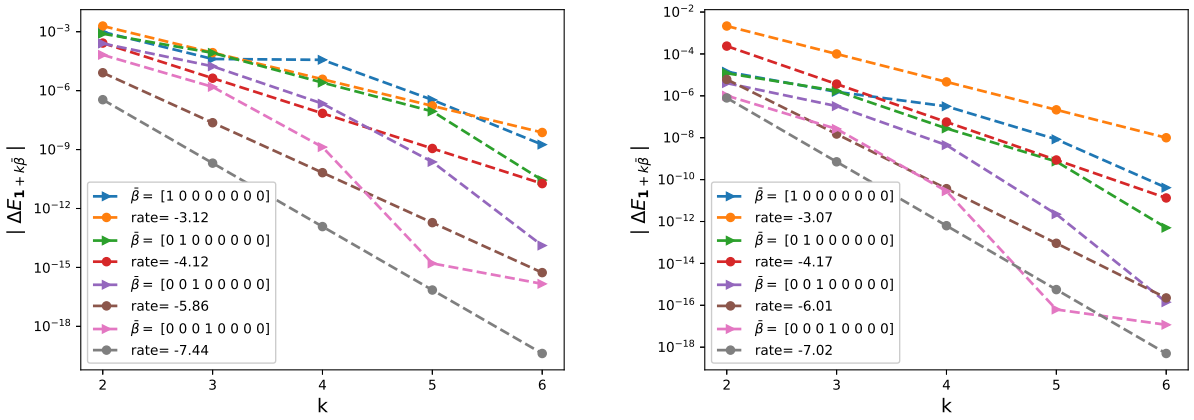

(a) (b)

Figure 53: The rate of convergence of first order differences $|\Delta E_\beta|$ ($\beta = \mathbf{1} + k\bar{\beta}$)): a) $\xi = 0.235^2$ b) $\xi = 10^{-5}$

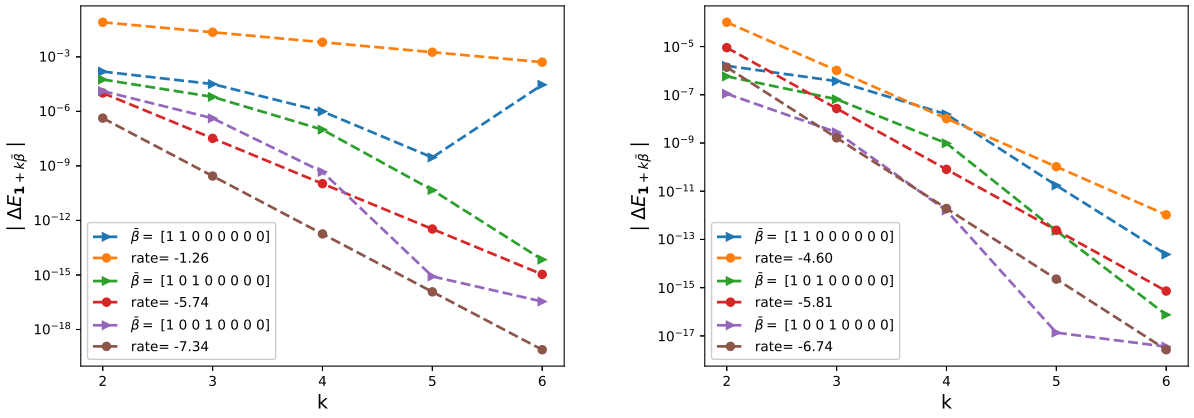

(a) (b)

Figure 54: The rate of convergence of mixed order differences $|\Delta E_\beta|$ ($\beta = \mathbf{1} + k\bar{\beta}$)): a) $\xi = 0.235^2$ b) $\xi = 10^{-5}$

N=8, K=0.8

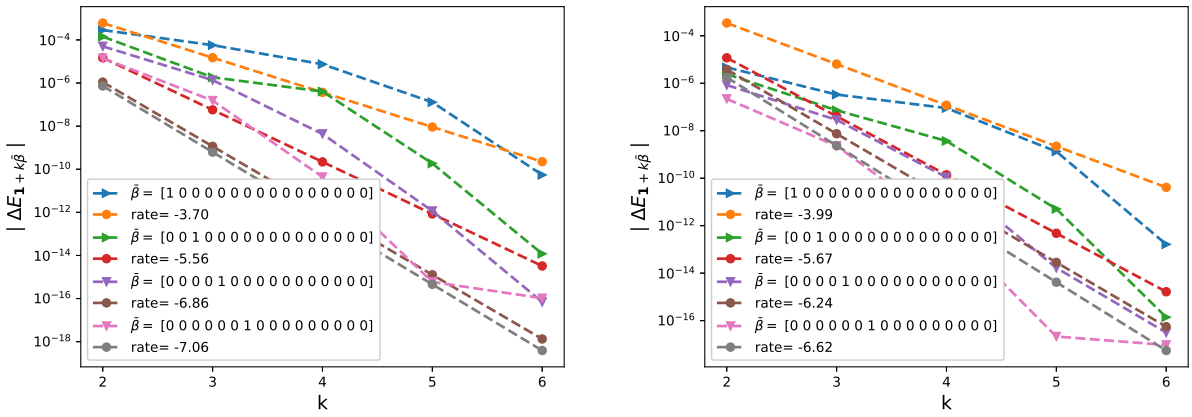

(a) (b)

Figure 55: The rate of convergence of first order differences $|\Delta E_\beta|$ $(\beta = \mathbf{1} + k\bar{\beta})$): a) $\xi = 0.235^2$ b) $\xi = 10^{-5}$

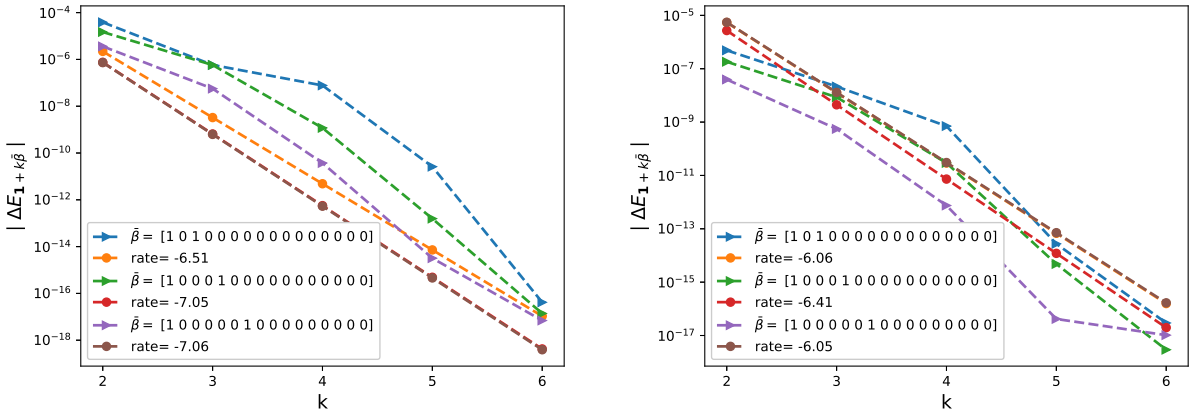

(a) (b)

Figure 56: The rate of convergence of mixed order differences $|\Delta E_\beta|$ $(\beta = \mathbf{1} + k\bar{\beta})$): a) $\xi = 0.235^2$ b) $\xi = 10^{-5}$

B.6 Investigating mixed differences wrt moneyness K

Case $H = 0.43$

$N = 8$

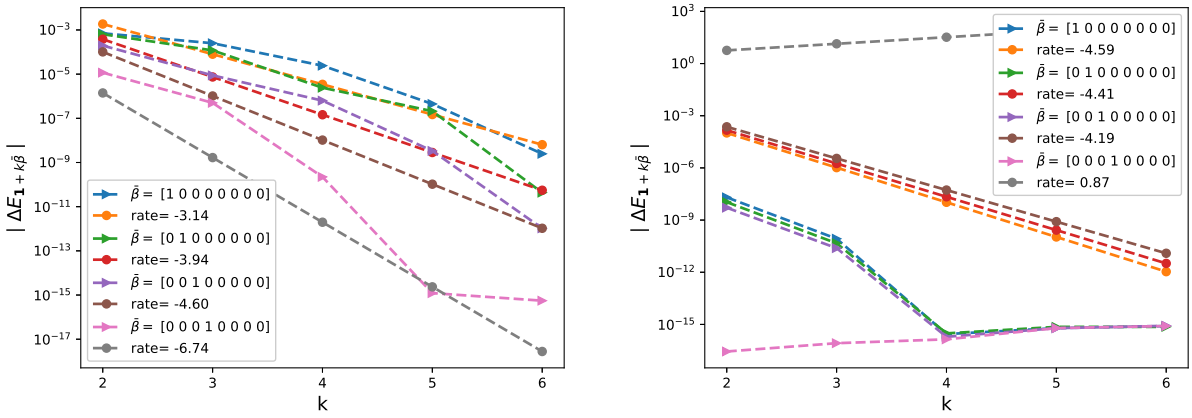

(a) (b)

Figure 57: The rate of convergence of first order differences $|\Delta E_\beta|$ ($\beta = \mathbf{1} + k\bar{\beta}$)): a) $\xi = 0.235^2$ b) $\xi = 10^{-5}$

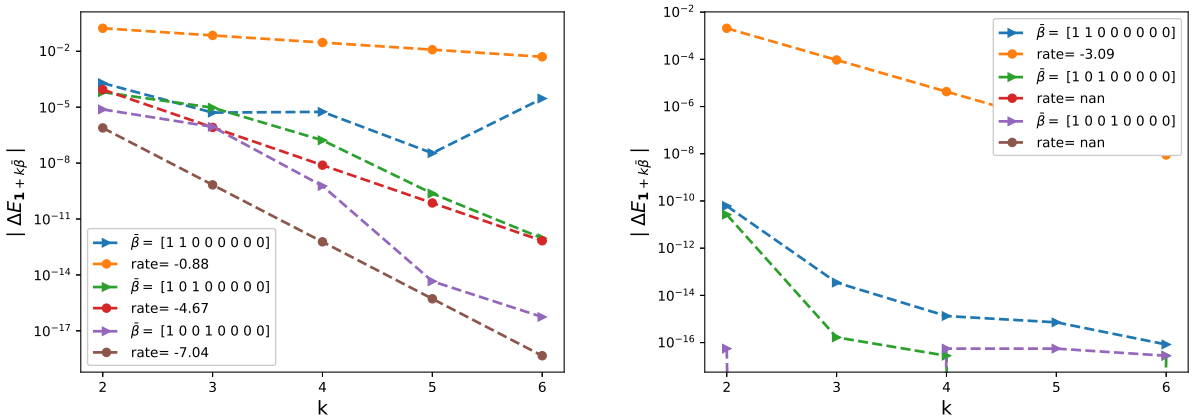

(a) (b)

Figure 58: The rate of convergence of mixed order differences $|\Delta E_\beta|$ ($\beta = \mathbf{1} + k\bar{\beta}$)): a) $\xi = 0.235^2$ b) $\xi = 10^{-5}$

$N = 16$

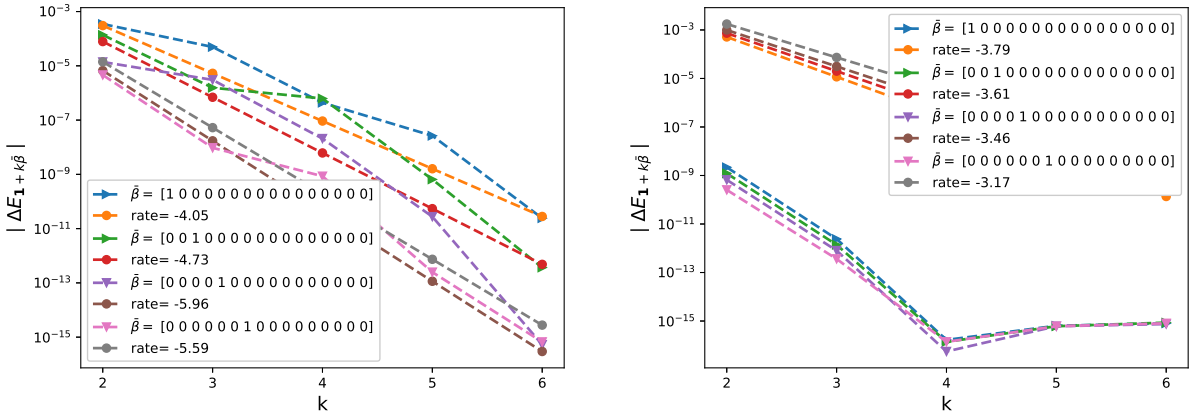

(a) (b)

Figure 59: The rate of convergence of first order differences $|\Delta E_\beta|$ $(\beta = \mathbf{1} + k\bar{\beta})$): a) $\xi = 0.235^2$ b) $\xi = 10^{-5}$

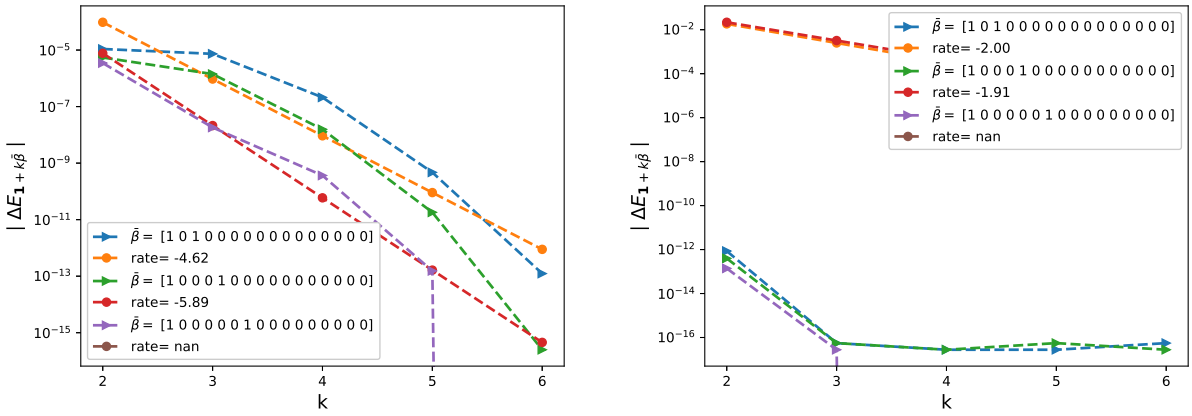

(a) (b)

Figure 60: The rate of convergence of mixed order differences $|\Delta E_\beta|$ $(\beta = \mathbf{1} + k\bar{\beta})$): a) $\xi = 0.235^2$ b) $\xi = 10^{-5}$

Case $H = 0.07$

$N = 8$

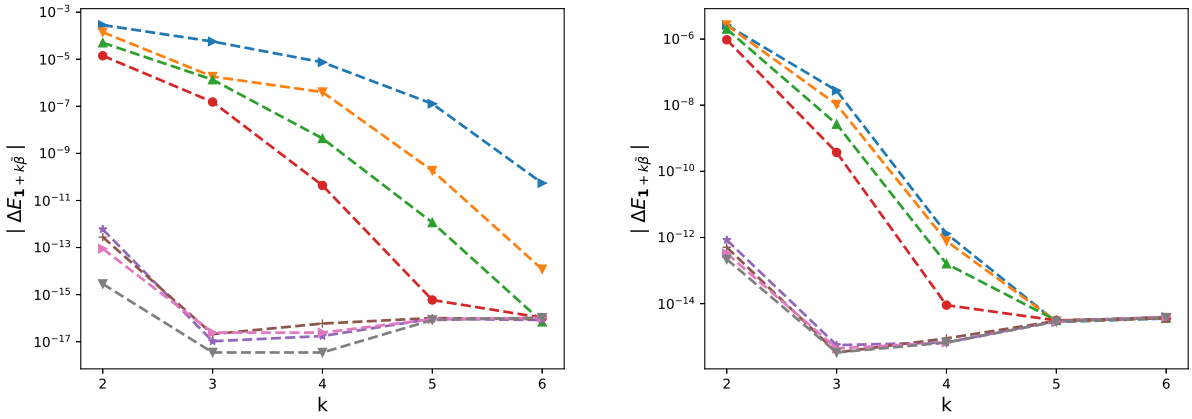

(a) (b)

Figure 61: The rate of convergence of first order differences $|\Delta E_\beta|$ ($\beta = \mathbf{1} + k\bar{\beta}$)): a) $K = 1$ b) $K = \exp(-4)$.

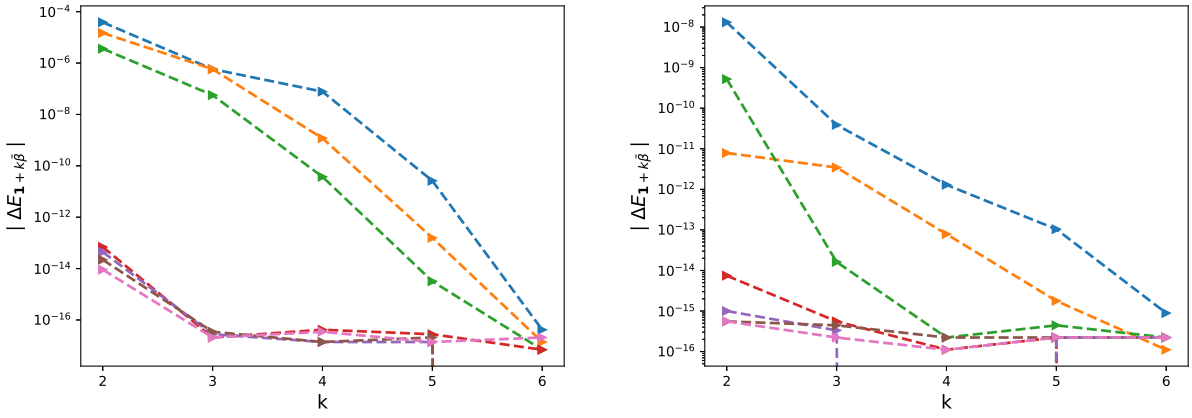

(a) (b)

Figure 62: The rate of convergence of second order differences $|\Delta E_\beta|$ ($\beta = \mathbf{1} + k\bar{\beta}$)): a) $K = 1$ b) $K = \exp(-4)$.

$N = 16$

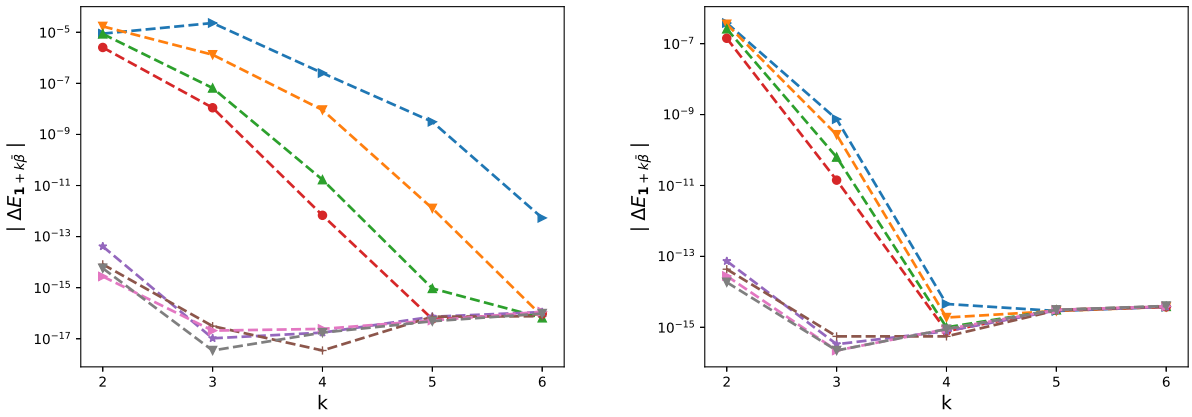

(a) (b)

Figure 63: The rate of convergence of first order differences $|\Delta E_\beta|$ ($\beta = \mathbf{1} + k\bar{\beta}$)): a) $K = 1$ b) $K = \exp(-4)$.

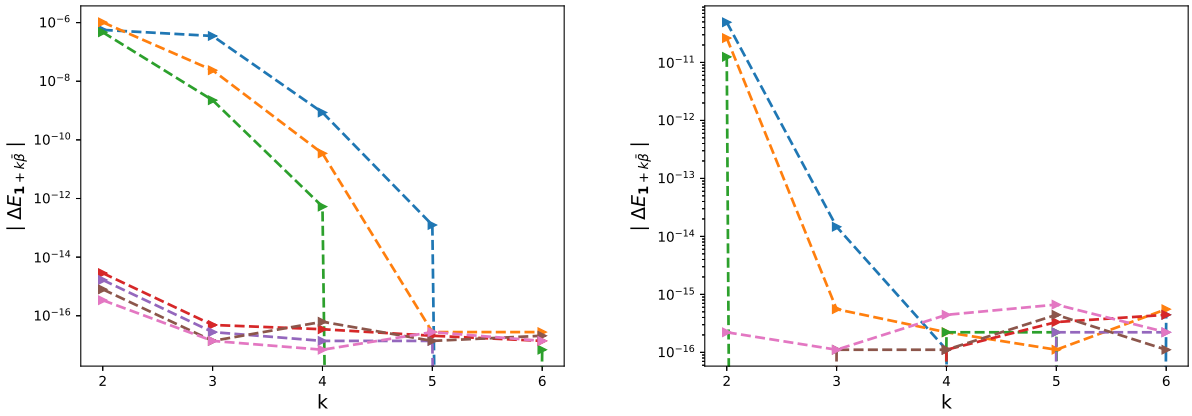

(a) (b)

Figure 64: The rate of convergence of second order differences $|\Delta E_\beta|$ ($\beta = \mathbf{1} + k\bar{\beta}$)): a) $K = 1$ b) $K = \exp(-4)$.

B.7 Convergence plots using MISC ($H = 0.43$)

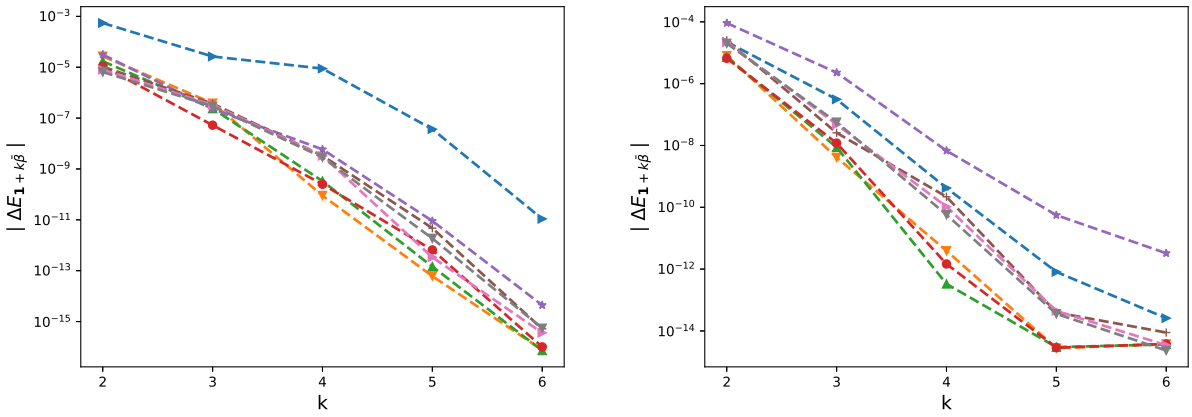

(a) (b)

Figure 65: The rate of convergence of first order differences $|\Delta E_\beta|$ ($\beta = \mathbf{1} + k\overline{\beta}$)): a) $K = 1$ b) $K = \exp(-4)$.

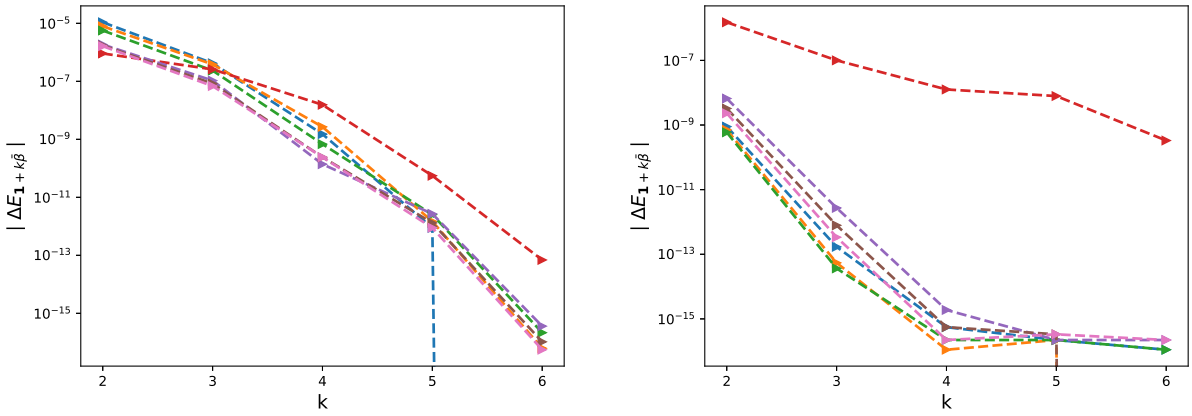

(a) (b)

Figure 66: The rate of convergence of second order differences $|\Delta E_\beta|$ ($\beta = \mathbf{1} + k\overline{\beta}$)): a) $K = 1$ b) $K = \exp(-4)$.

Case of 2 time steps, $K = e^{-4}$

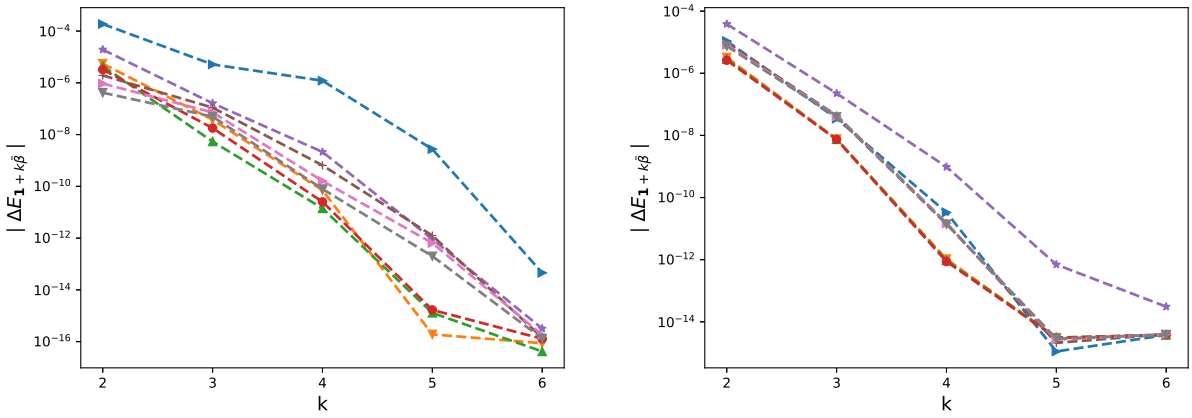

(a) (b)

Figure 67: The rate of convergence of first order differences $|\Delta E_\beta|$ ($\beta = \mathbf{1} + k\bar{\beta}$)): a) $K = 1$ b) $K = \exp(-4)$.

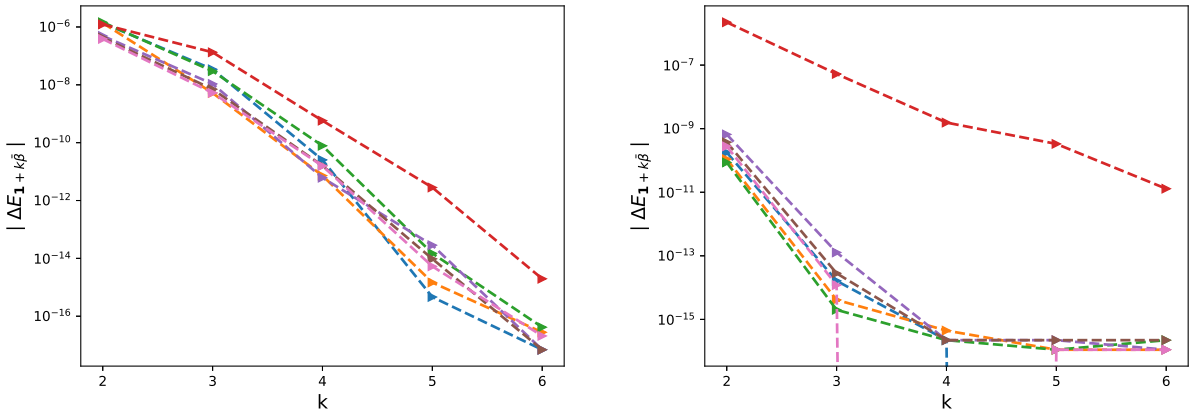

(a) (b)

Figure 68: The rate of convergence of second order differences $|\Delta E_\beta|$ ($\beta = \mathbf{1} + k\bar{\beta}$)): a) $K = 1$ b) $K = \exp(-4)$.

Case of 2 time steps, $K = 1.2$

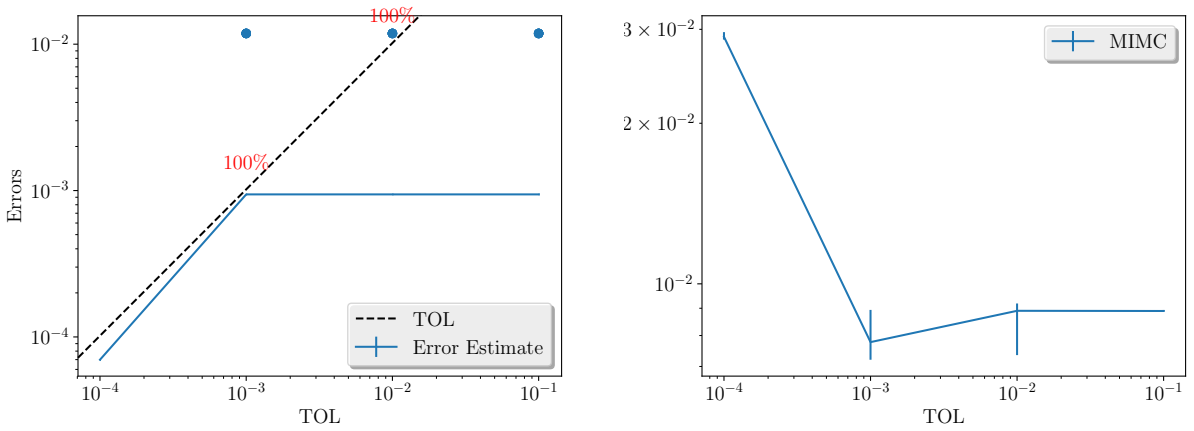

(a) Error estimate (b) Average running time as a function of TOL

Figure 69: Convergence and complexity results for the call payoff with rBergomi model.

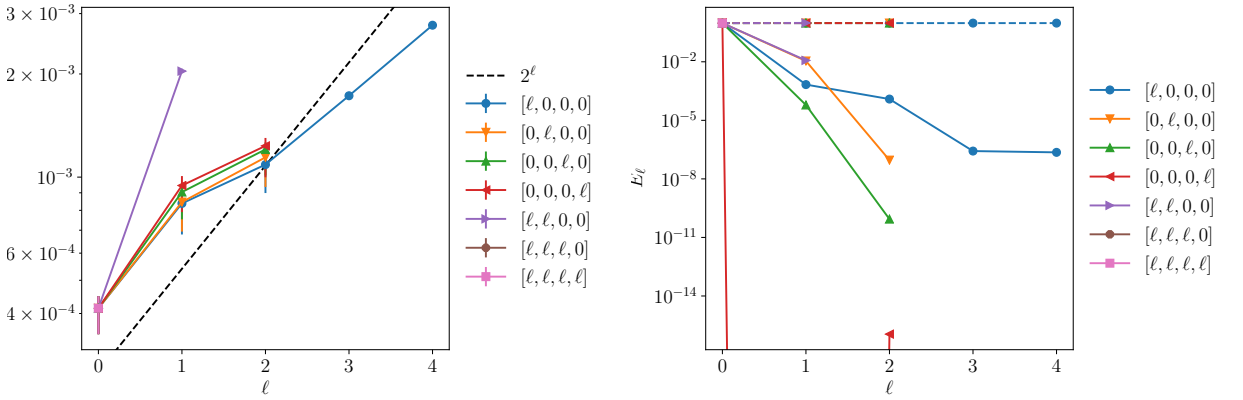

(a) Average Computational time per level (b) The convergence rate of mixed differences per level

Figure 70: Convergence and work rates for discretization levels the call payoff with rBergomi model.

Case of 4 time steps, $K = e^{-4}$

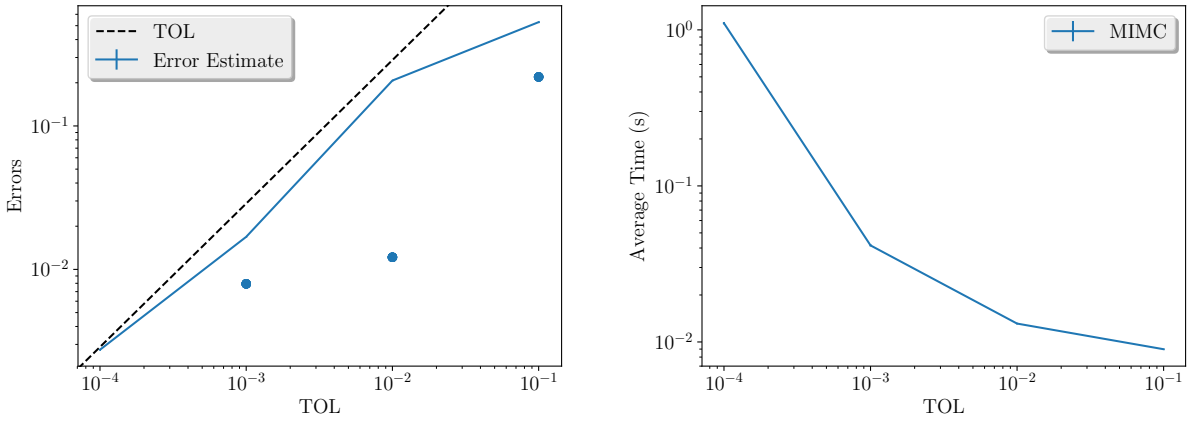

(a) Error estimate (b) Average running time as a function of TOL

Figure 71: Convergence and complexity results for the call payoff with rBergomi model.

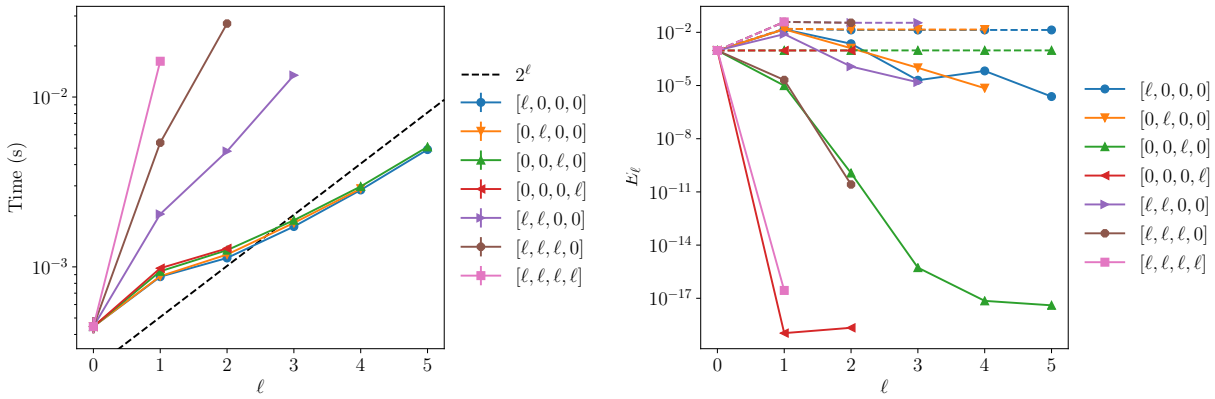

(a) Average Computational time per level (b) The convergence rate of mixed differences per level

Figure 72: Convergence and work rates for discretization levels the call payoff with rBergomi model.

Case of 4 time steps, $K = 1.2$

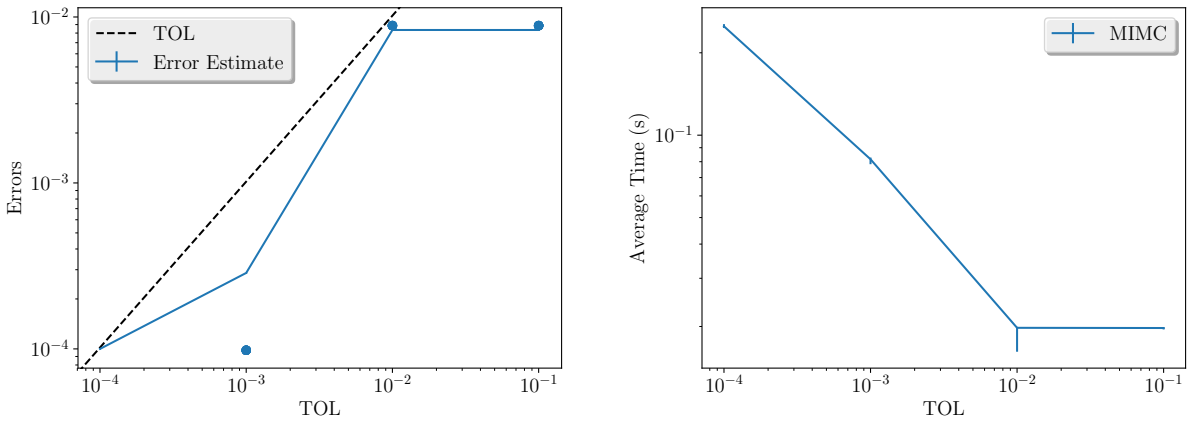

(a) Error estimate (b) Average running time as a function of TOL

Figure 73: Convergence and complexity results for the call payoff with rBergomi model.

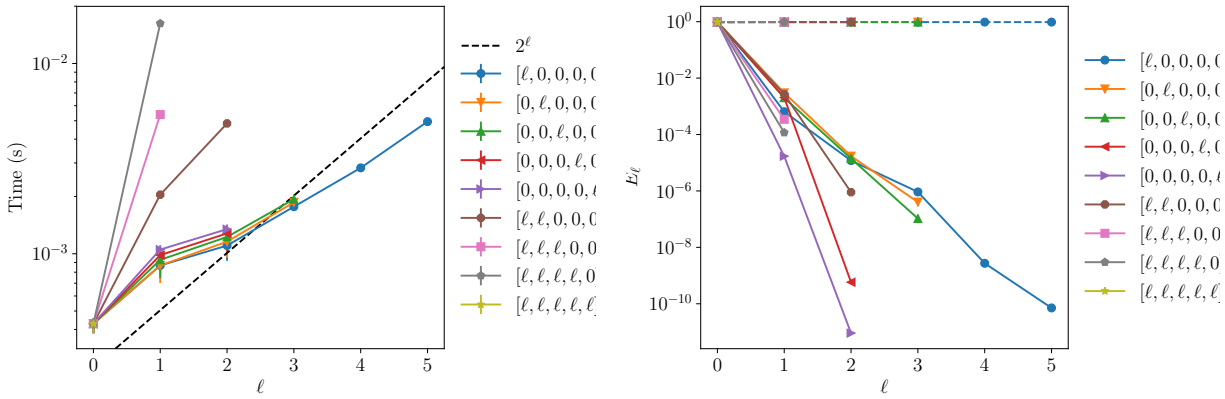

(a) Average Computational time per level (b) The convergence rate of mixed differences per level

Figure 74: Convergence and work rates for discretization levels the call payoff with rBergomi model.

Case of 8 time steps, $K = e^{-4}$

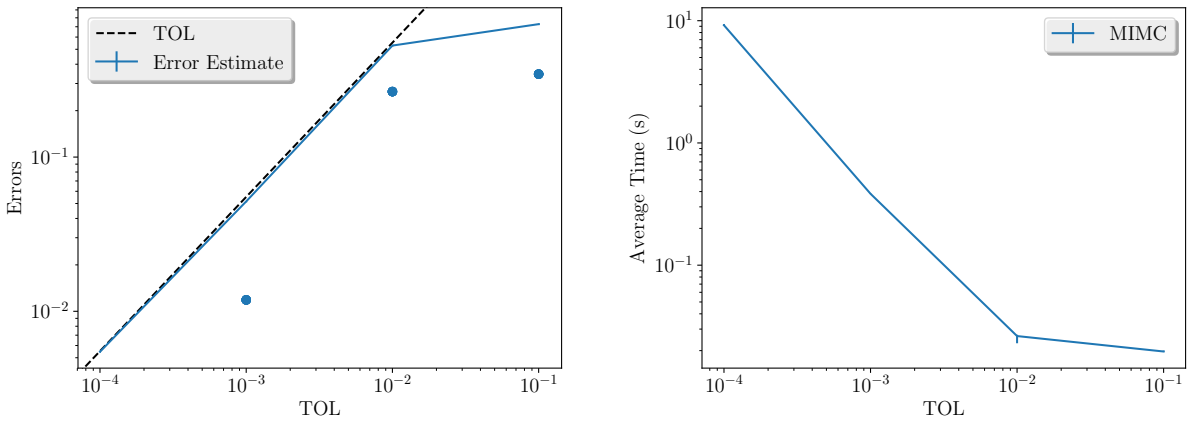

(a) Error estimate (b) Average running time as a function of TOL

Figure 75: Convergence and complexity results for the call payoff with rBergomi model.

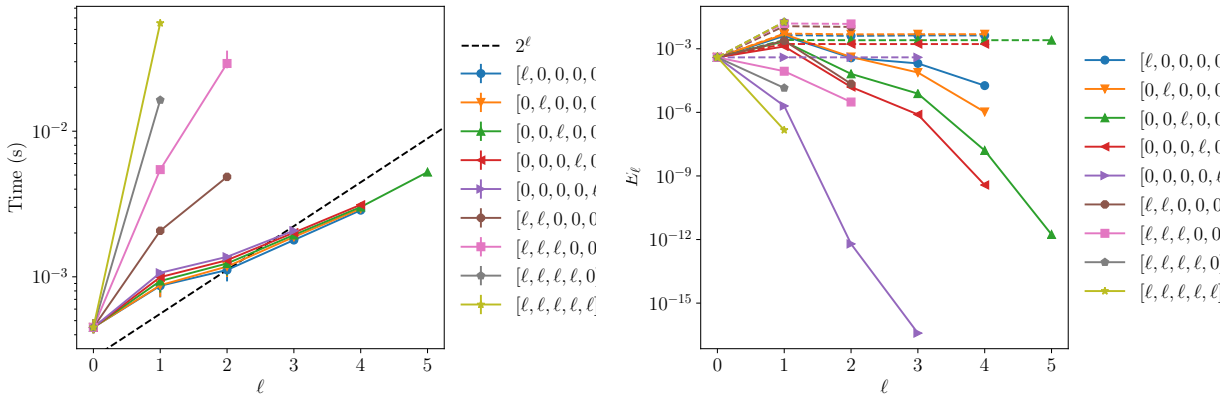

(a) Average Computational time per level (b) The convergence rate of mixed differences per level

Figure 76: Convergence and work rates for discretization levels the call payoff with rBergomi model.

Case of 8 **time steps,** $K = 1.2$

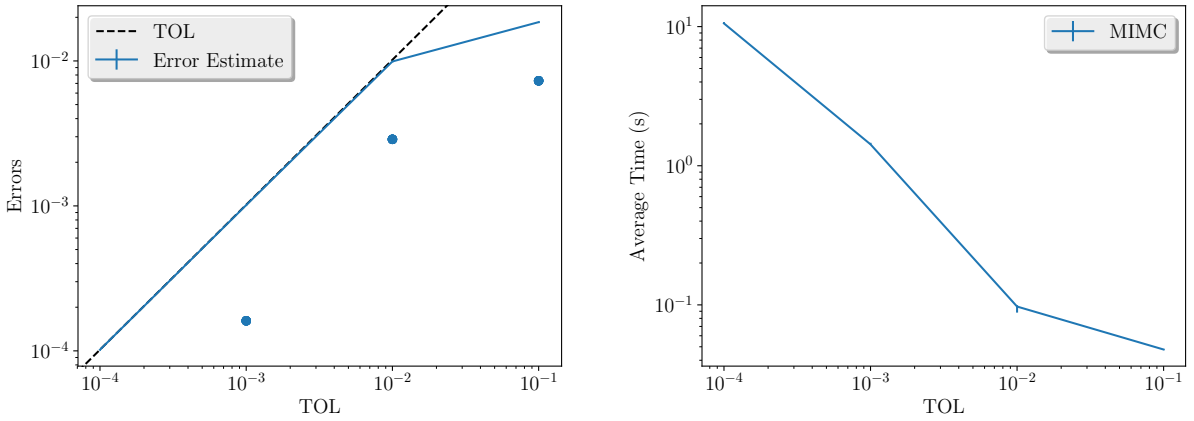

(a) Error estimate (b) Average running time as a function of TOL

Figure 77: Convergence and complexity results for the call payoff with rBergomi model.

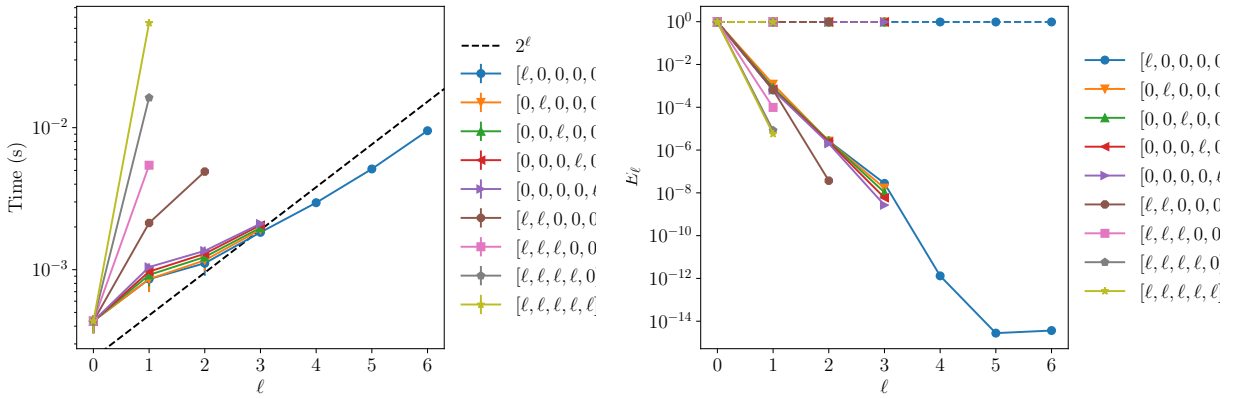

(a) Average Computational time per level (b) The convergence rate of mixed differences per level

Figure 78: Convergence and work rates for discretization levels the call payoff with rBergomi model.

Case of 16 **time steps,** $K = e^{-4}$

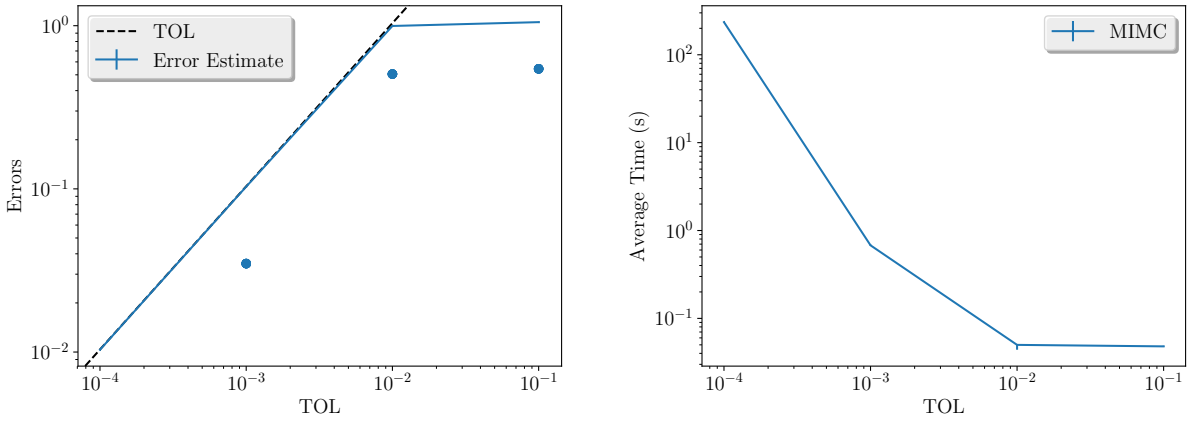

(a) Error estimate (b) Average running time as a function of TOL

Figure 79: Convergence and complexity results for the call payoff with rBergomi model.

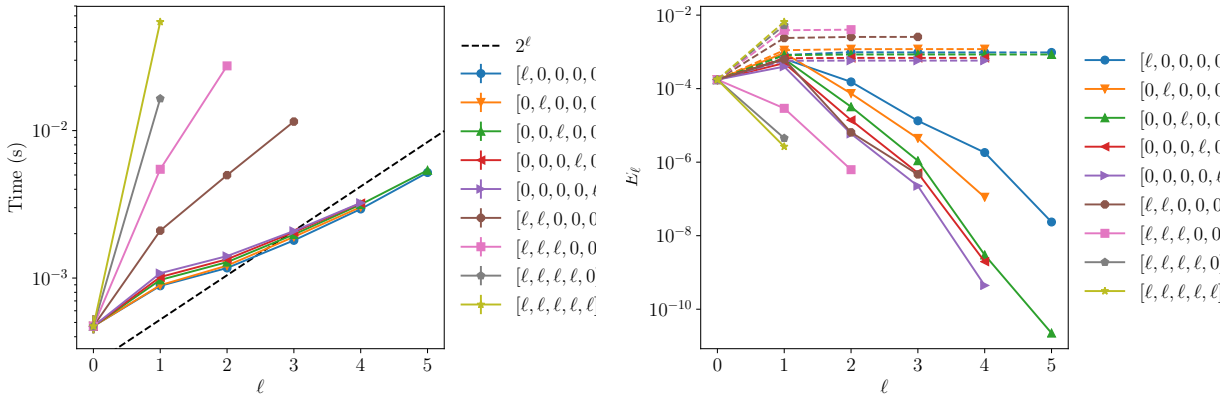

(a) Average Computational time per level (b) The convergence rate of mixed differences per level

Figure 80: Convergence and work rates for discretization levels the call payoff with rBergomi model.

Case of 16 time steps, $K = 1.2$

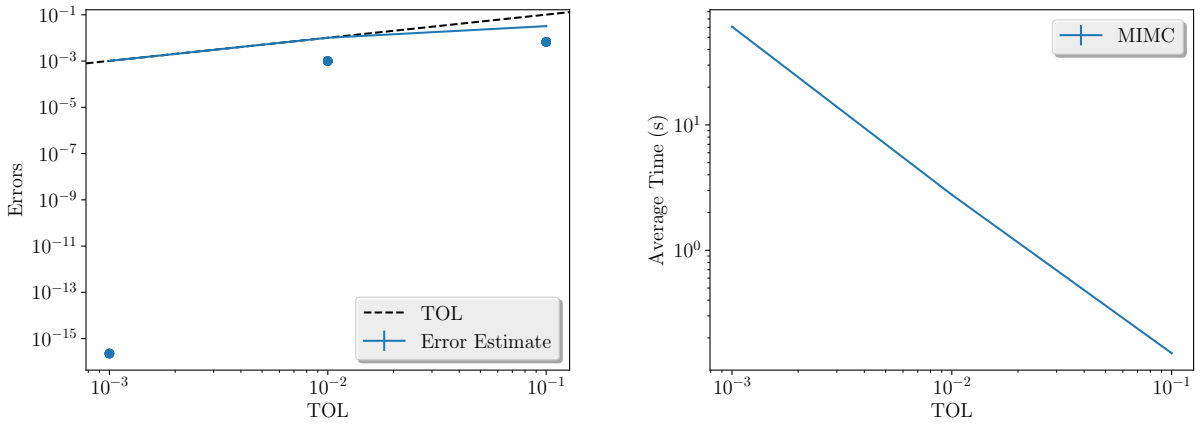

(a) Error estimate (b) Average running time as a function of TOL

Figure 81: Convergence and complexity results for the call payoff with rBergomi model.

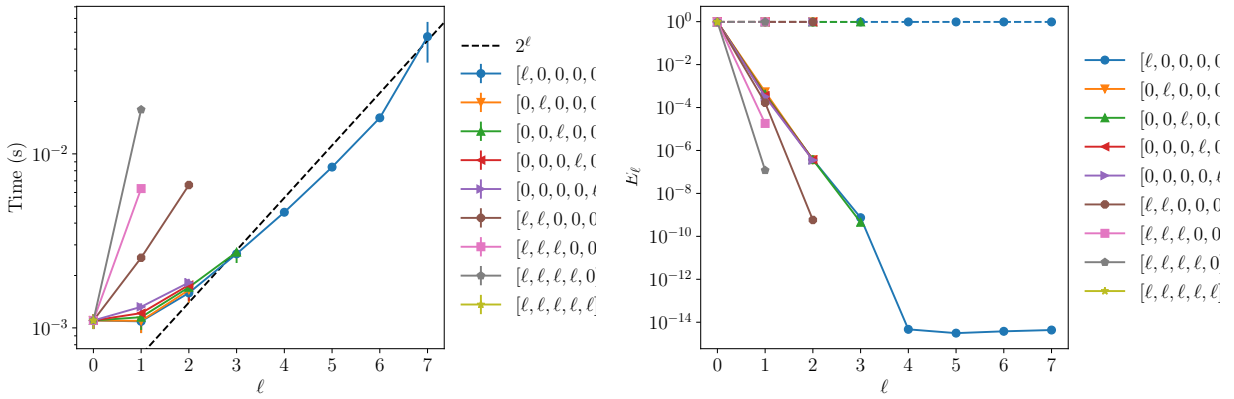

(a) Average Computational time per level (b) The convergence rate of mixed differences per level

Figure 82: Convergence and work rates for discretization levels the call payoff with rBergomi model.

B.8 MISC plots

B.9 Non Hierarchical

H=0.43

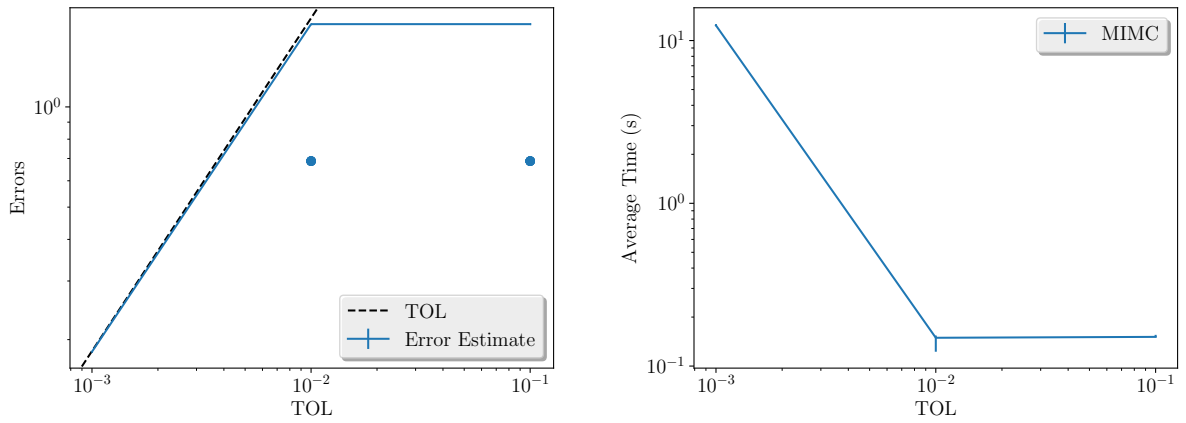

(a) Error estimate (b) Average running time as a function of TOL

Figure 83: Convergence and complexity results for the call payoff with rBergomi model.

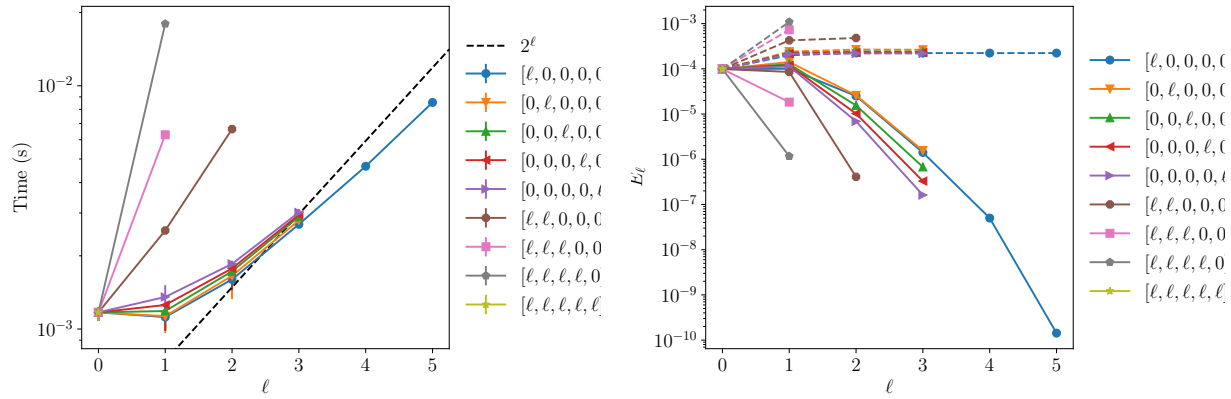

(a) Average Computational time per level (b) The convergence rate of mixed differences per level

Figure 84: Convergence and work rates for discretization levels the call payoff with rBergomi model.

Case of 8 time steps

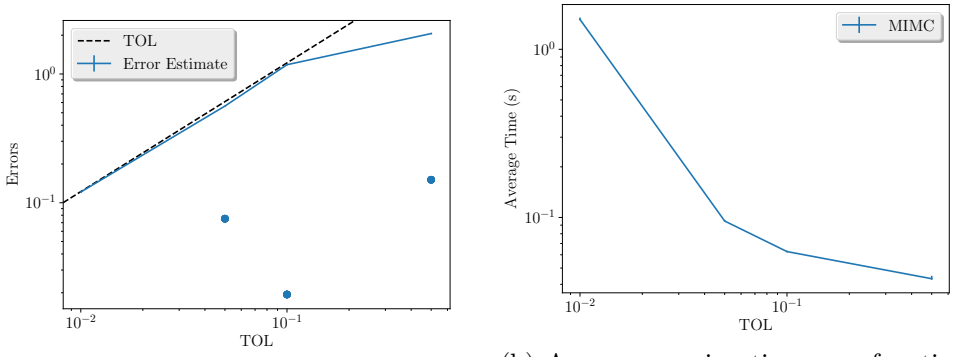

(a) Error estimate

(b) Average running time as a function of TOL

Figure 85: Convergence and complexity results for the call payoff with rBergomi model for $K = 1$, $H = 0.43$ and $N = 8$.

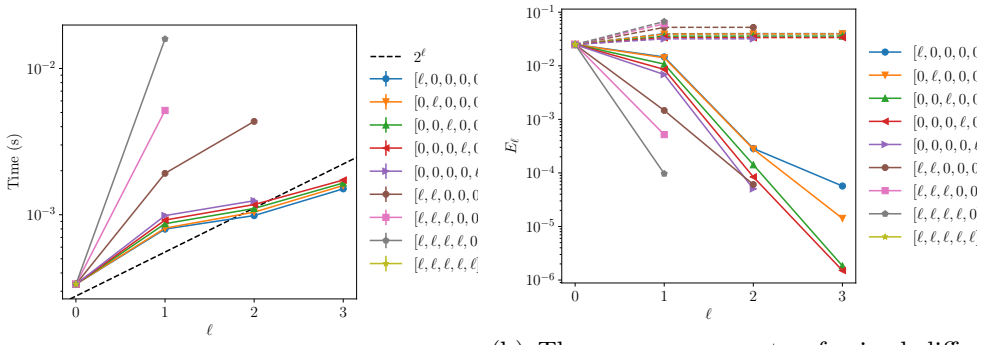

(a) Average Computational time per level

(b) The convergence rate of mixed differences per level

Figure 86: Convergence and work rates for discretization levels the call payoff with rBergomi model for $K = 1$, $H = 0.43$ and $N = 8$.

Case of 16 time steps

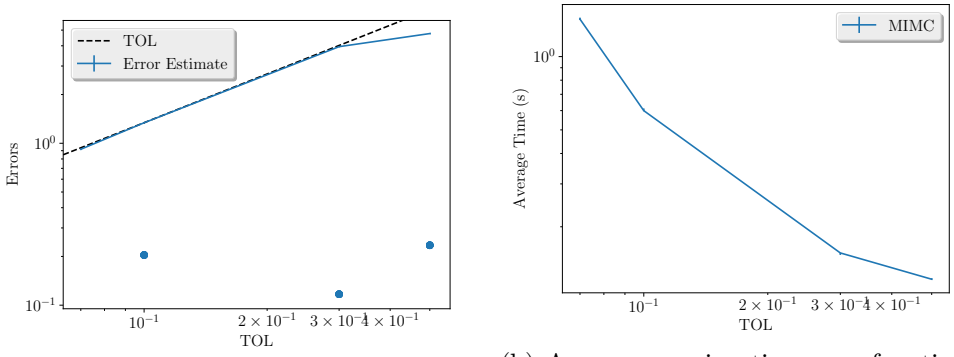

(a) Error estimate

(b) Average running time as a function of TOL

Figure 87: Convergence and complexity results for the call payoff with rBergomi model for $K = 1$, $H = 0.43$ and $N = 16$.

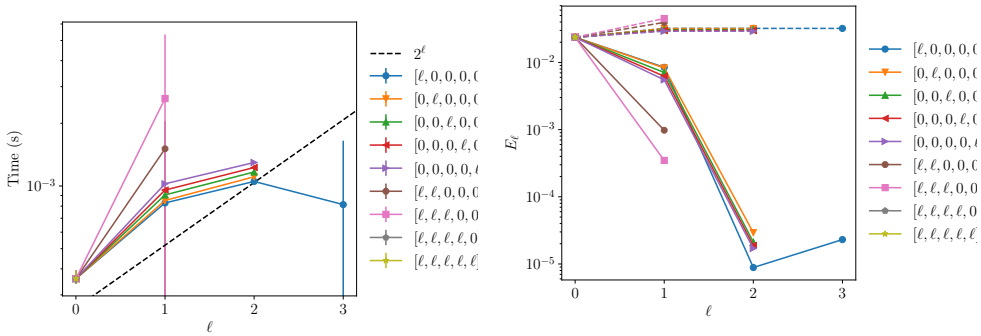

(a) Average Computational time per level

(b) The convergence rate of mixed differences per level

Figure 88: Convergence and work rates for discretization levels the call payoff with rBergomi model for $K = 1$, $H = 0.43$ and $N = 16$.

H=0.07

Case of 8 time steps

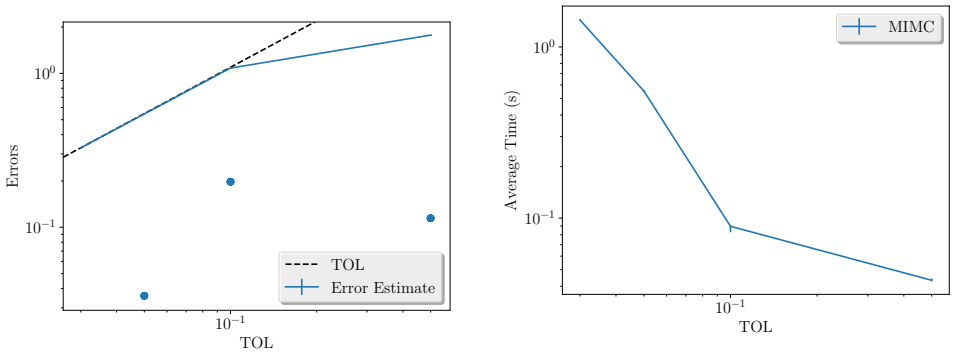

(a) Error estimate

(b) Average running time as a function of TOL

Figure 89: Convergence and complexity results for the call payoff with rBergomi model for $K = 1$, $H = 0.07$ and $N = 8$.

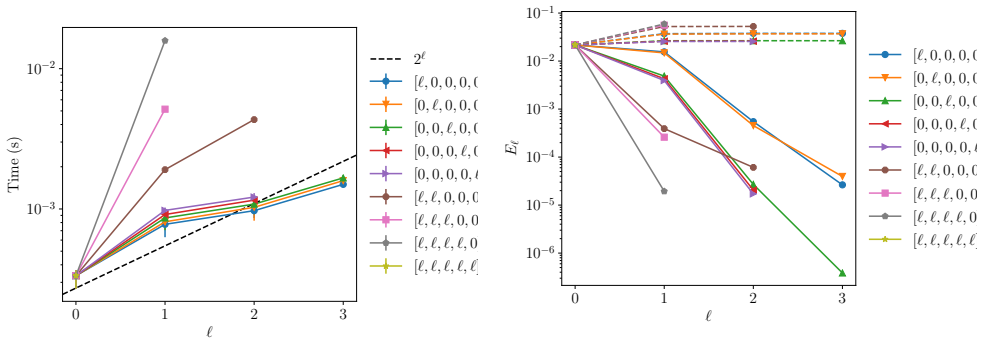

(a) Average Computational time per level

(b) The convergence rate of mixed differences per level

Figure 90: Convergence and work rates for discretization levels the call payoff with rBergomi model for $K = 1$, $H = 0.07$ and $N = 8$.

Case of 16 time steps

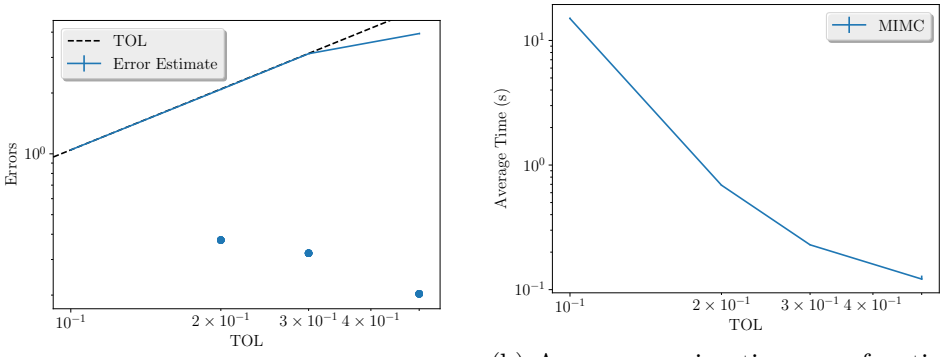

(a) Error estimate

(b) Average running time as a function of TOL

Figure 91: Convergence and complexity results for the call payoff with rBergomi model for $K = 1$, $H = 0.07$ and $N = 16$.

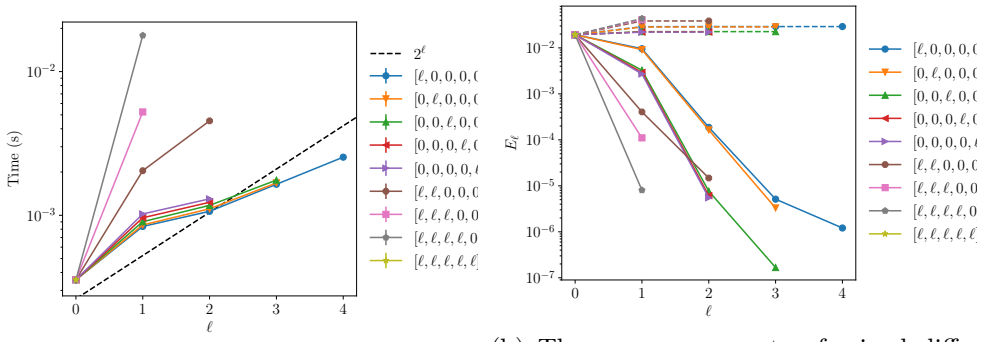

(a) Average Computational time per level

(b) The convergence rate of mixed differences per level

Figure 92: Convergence and work rates for discretization levels the call payoff with rBergomi model for $K = 1$, $H = 0.07$ and $N = 16$.

B.10 Hierarchical

H=0.43

Case of 8 time steps

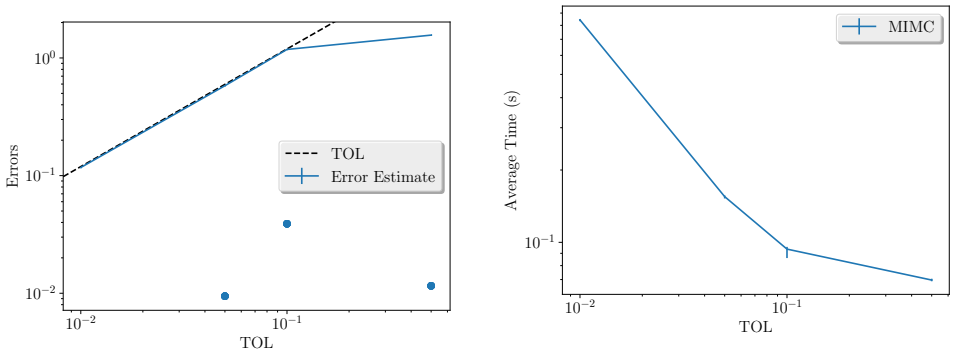

(a) Error estimate

(b) Average running time as a function of TOL

Figure 93: Convergence and complexity results for the call payoff with rBergomi model for $K = 1$, $H = 0.43$ and $N = 8$.

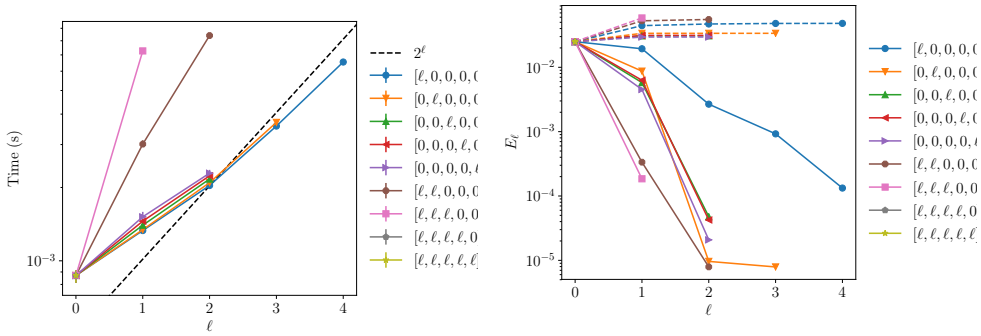

(a) Average Computational time per level

(b) The convergence rate of mixed differences per level

Figure 94: Convergence and work rates for discretization levels the call payoff with rBergomi model for $K = 1$, $H = 0.43$ and $N = 8$.

Case of 16 time steps

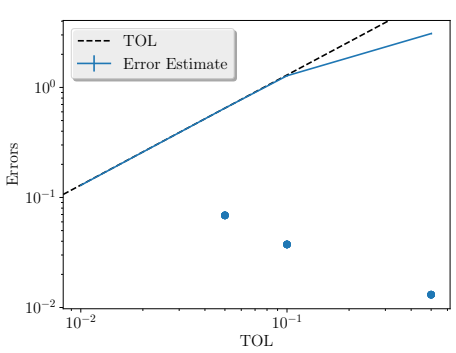

(a) Error estimate

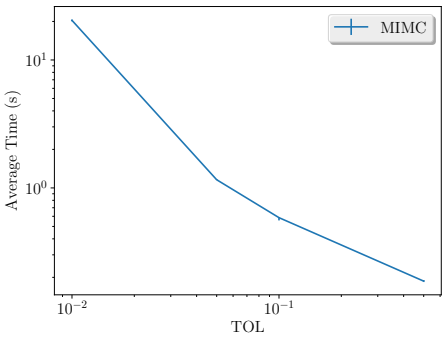

(b) Average running time as a function of TOL

Figure 95: Convergence and complexity results for the call payoff with rBergomi model for $K = 1$, $H = 0.43$ and $N = 16$.

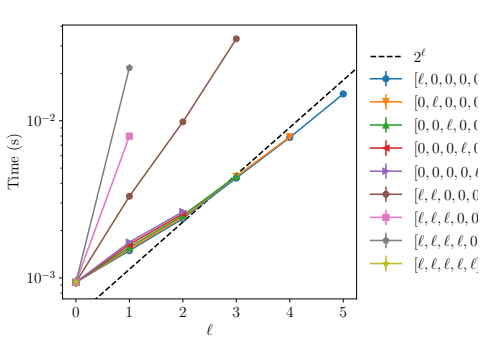

(a) Average Computational time per level

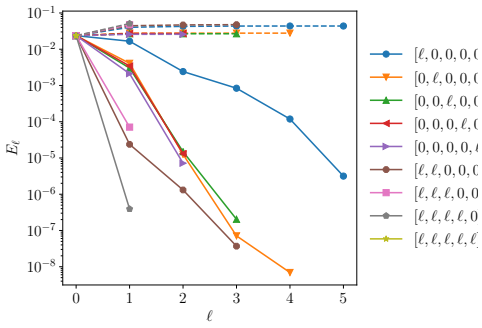

(b) The convergence rate of mixed differences per level

Figure 96: Convergence and work rates for discretization levels the call payoff with rBergomi model for $K = 1$, $H = 0.43$ and $N = 16$.

H=0.07

Case of 8 time steps

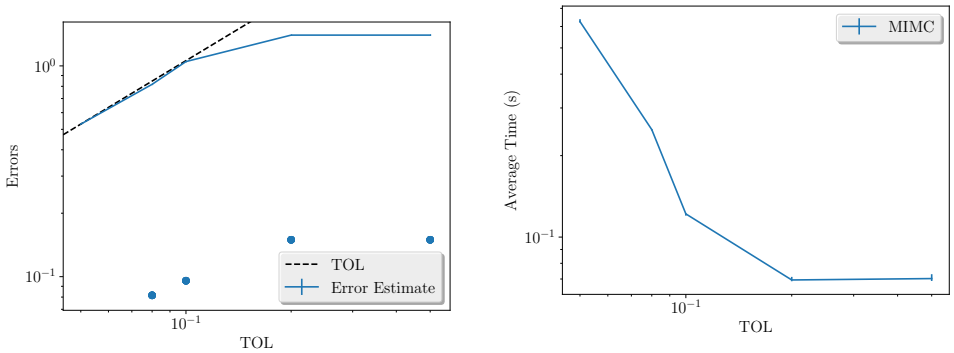

(a) Error estimate

(b) Average running time as a function of TOL

Figure 97: Convergence and complexity results for the call payoff with rBergomi model for $K = 1$, $H = 0.07$ and $N = 8$.

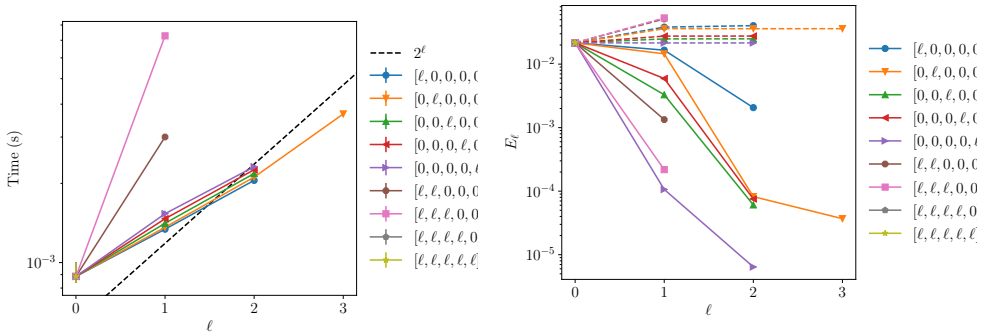

(a) Average Computational time per level

(b) The convergence rate of mixed differences per level

Figure 98: Convergence and work rates for discretization levels the call payoff with rBergomi model for $K = 1$, $H = 0.07$ and $N = 8$.

Case of 16 time steps

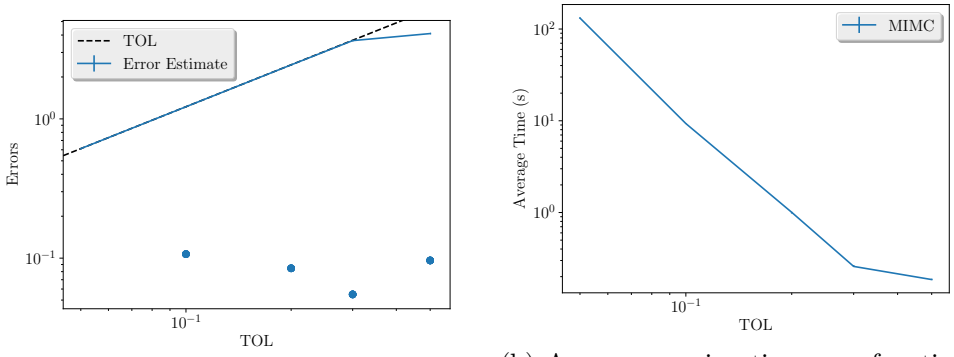

(a) Error estimate

(b) Average running time as a function of TOL

Figure 99: Convergence and complexity results for the call payoff with rBergomi model for $K = 1$, $H = 0.07$ and $N = 16$.

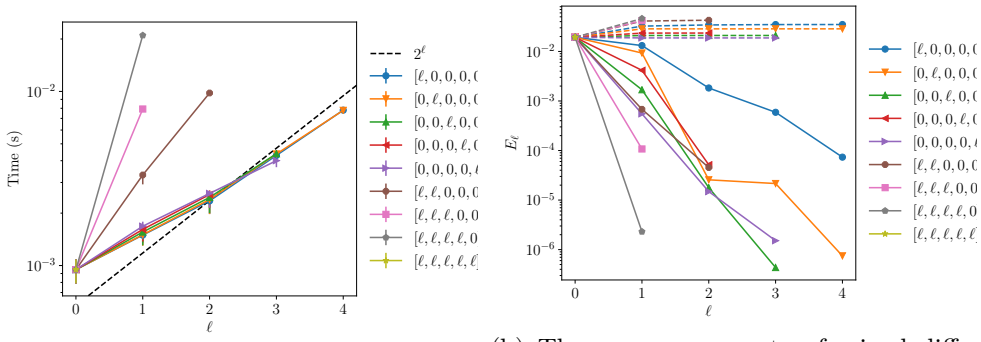

(a) Average Computational time per level

(b) The convergence rate of mixed differences per level

Figure 100: Convergence and work rates for discretization levels the call payoff with rBergomi model for $K = 1$, $H = 0.07$ and $N = 16$.

B.11 Comparing call options prices

B.11.1 Without Hierarchical representation

Case $H = 0.43$

Case $H = 0.07$

Method \Steps	2	4	8	16
MISC ($TOl = 5.10^{-1}$)	0.1057	0.0988	0.0944	0.0921
MISC ($TOl = 10^{-1}$)	0.1057	0.0988	0.0836	0.0594
MISC ($TOl = 5.10^{-2}$)	0.1057	0.0976	0.0758	0.0781
MISC ($TOl = 10^{-2}$)	0.1113	0.0940	0.0820	–
MC method ($M = 10^6$)	0.1079 (1.55e−04)	0.0921 (9.65e−05)	0.0822 (7.61e−05)	0.0769 (6.65e−05)

Table 18: Call option price of the different methods for different number of time steps. Case $K = 1$

Method \Steps	2	4	8	16
MISC ($TOl = 5.10^{-1}$)	0.1065	0.0900	0.0809	0.0762
MISC ($TOl = 10^{-1}$)	0.1065	0.0900	0.0733	0.0956
MISC ($TOl = 5.10^{-2}$)	0.1065	0.0898	0.0881	–
MISC ($TOl = 10^{-2}$)	0.1226	0.1022	0.0933	–
MC method ($M = 10^6$)	0.1216 (1.05e−03)	0.1020 (1.86e−04)	0.0912 (1.35e−04)	0.0854 (1.08e−04)

Table 19: Call option price of the different methods for different number of time steps. Case $K = 1$